Neuroprotective Role and Immunomodulatory Effects of Sialylation

Doctoral thesis

to obtain a doctorate (PhD)

from the Faculty of Medicine

of the University of Bonn

Tawfik Abou Assale

from Damascus, Syria

2025

Table of Contents

List of abbreviations

6SL	6'-Sialyllactose
ABR	Auditory brainstem response
AD	Alzheimer's disease
AMD	Age-related macular degeneration
C3	Complement component 3
C4	Complement component 4
CD33r	CD33-related Siglec
CD68	Cluster of differentiation 68
Cryab	Crystallin alpha b
Crybb1	Crystallin beta b1
DAP12	DNAX-activating protein of 12 kDa
GFAP	Glial fibrillary acidic protein
Gne	UDP-N-acetylglucosamine-2-epimerase/N-acetylmannosamine kinase
GSEA	Gene set enrichment analysis
Iba1	Ionized calcium-binding adapter molecule 1
IL-1β	Interleukin 1 beta
ITAM	Immunoreceptor tyrosine-based activation motif
ITIM	Immunoreceptor tyrosine-based inhibition motif
Pik3cd	Phosphatidylinositol-4,5-bisphosphate 3-kinase catalytic subunit delta
ROS	Reactive oxygen species
SIGLECs	Sialic acid-binding immunoglobulin-like lectins
SNHL	Sensorineural hearing loss
THP-1	Human monocytic cell line
TYROBP	TYRO protein tyrosine kinase binding protein
UV	Ultraviolet
WT	Wildtype
tg	Transgenic

1. Abstract

Sialic acids are terminal sugars on the cellular glycocalyx, crucial for modulating immune responses in the sialylated central nervous system. Sialylation acts as an inhibitory checkpoint, regulating inflammation and tissue damage. Sialic acid-binding immunoglobulin-type lectins (SIGLECs), expressed on immune cells, bind sialylated glycoproteins and glycolipids, thereby inhibiting pro-inflammatory responses and phagocytosis. In the first part of this thesis the therapeutic effects of 6'-sialyllactose (6SL), a human milk oligosaccharide, in preventing neomycin-induced hearing loss in postnatal mice were explored. Systemic 6SL injection improved hearing, reduced macrophage activation in the cochlear spiral ganglion, and reversed the expression of the pro-inflammatory *IL-1β* and apoptotic *Pik3cd* gene transcripts. *In vitro*, 6SL demonstrated anti-inflammatory, anti-phagocytic, and neuroprotective effects on lipopolysaccharide-challenged THP1-macrophages, highlighting its therapeutic potential in inflammatory-induced ototoxicity. In the second part the role of the human-specific SIGLEC-11 receptor in neurodegeneration and neuroinflammation in the aging brain was examined. Humanized Siglec-11 transgenic (tg) mice were studied at 6 and 24 months. Siglec-11 tg mice showed fewer Iba1-positive microglial cells, reduced lipid-laden microglia, and less neuronal loss compared to WT mice. Transcriptomic analysis revealed suppression of gene transcript pathways related to inflammatory and oxidative stress at 6 months, and complement and coagulation cascades at 24 months in Siglec-11 tg mice, suggesting a protective role for SIGLEC-11 in mitigating brain inflammation. In the third part the impact of age-related reduced sialylation on retinal inflammation and degeneration in Gne+/- mice with a heterozygous knock-out of the *Gne* gene was investigated. At 9 months, Gne+/- mice had lower polysialic and trisialic acid levels, higher CD68 expression, and at 12 months, fewer rod bipolar cells. Transcriptomic analysis revealed upregulated complement, inflammation, and apoptosis pathways, with increased pro-inflammatory and complement markers. Crossing Gne+/- mice with C3-deficient mice prevented CD68 elevation, rod bipolar cell loss, and increased *C4* expression, indicating that retinal inflammation and cell loss in hyposialylation are driven by complement activation. These findings highlight the relevance of sialylation in modulating immunity and reducing inflammation, thus offering new options for treatment of neurodegenerative diseases.

2. Introduction and aims with references

2.1 Sialic acids and their biological importance

Sialic acids are a family of monosaccharides with a nine-carbon backbone, typically found at the terminal ends of the mammalian cells glycocalyx. They are synthesized in the cytoplasm, where the rate-limiting bifunctional enzyme glucosamine (UDP-N-acetyl)-2-epimerase/N-acetylmannosamine kinase, encoded by the *Gne* gene, regulates and initiates their synthesis (Schwarzkopf et al., 2002). They are then incorporated into glycans in the Golgi apparatus by sialyltransferases, which produce different linkages based on substrate specificity (Harduin-Lepers et al., 2005; Rabouille et al., 1995; Wißfeld et al., 2024). Sialylation, the attachment of sialic acid to glycan chains, contributes to the cellular structural integrity and mediates several dynamic functions such as cell-cell communication, pathogen recognition, and immune modulation (Varki et al., 2017; Wißfeld et al., 2024). Sialylation plays a particularly important role in immune cells by modulating the recognition of self and non-self-entities, where the presence of the highly negatively charged sialic acid on immune cell surfaces contributes to the formation of hydrophilic shell around the cell, preventing non-specific cellular interactions and masking underlying molecules, thus preventing the premature immune activation(French et al., 2017; Varki et al., 2012). During inflammation or infection, sialic acids are often cleaved by neuraminidases, exposing epitopes that trigger immune responses such as toll-like receptors signaling and phagocytosis (Allendorf et al., 2020). For instance, sialylation has been shown to inhibit complement system activation and prevent the oxidative burst of microglia and macrophages (Klaus et al., 2021; Shahraz et al., 2015).

2.2 Sialic acid-binding immunoglobulin-type lectins (SIGLECS) role in immune regulation

Sialic acids on the cellular glycocalyx serve as ligands for sialic acid-binding immunoglobulin-type lectins (SIGLECs), a family of type-I lectins primarily expressed on immune cells that play a key role in immune regulation (Varki et al., 2006). SIGLECs are generally divided into two broad categories, the evolutionary-conserved and the rapidly evolving CD33-related (CD33r) SIGLECs (Bornhöfft et al., 2018). These receptors bind sialylated glycoproteins and glycolipids via their extracellular N-terminal domain. Once bound, SIGLECs transmit inhibitory signals via immunoreceptor tyrosine-based inhibition motifs (ITIMs) in their cytoplasmic tails. Less frequently, some SIGLECs may also engage

in activating signals through immunoreceptor tyrosine-based activatory motif (ITAM), recruiting adaptors proteins such as TYROBP (TYROBP)/DNAX-activation protein 12 (DAP12) (Angata et al., 2004; Cao et al., 2008; Linnartz et al., 2010). Through their ITIM signaling, SIGLECs participate in inhibiting phagocytosis from microglia and macrophages, preventing oxidative burst, and downregulating pro-inflammatory responses. These interactions thus resemble a safety mechanism by dampening inflammatory pathway activation and protecting healthy cells from damage (Duan et al., 2020). Being regarded as immune-checkpoints, SIGLECs play a key role in regulating innate immunity, orchestrating the prevention of pathological overactivation while allowing necessary immune defense (Wißfeld et al., 2024).

2.3 Therapeutic potential of sialylated compounds

Among the different bioactive sialylated molecules, the human milk oligosaccharide 6'-sialyllactose (6SL) has generated attention for its potential therapeutic benefits. 6SL has a wide therapeutic window, stemming from its non-glycemic and non-toxic properties (Phipps et al., 2019; Röhrig et al., 2016). The potential role of 6SL in treating inflammatory diseases is supported through multiple experimental findings. For instance, in response to inflammatory stimuli, 6SL treatment attenuated macrophages activation by inhibiting pro-inflammatory pathways, reactive oxygen species (ROS) production, and tissue damage markers expression (Yu et al., 2024). These immunomodulatory properties of 6SL allow it to be studied in different inflammatory diseases. Sensorineural hearing loss (SNHL) can be triggered by several factors such as antibiotics, aging, and noise exposure, and is characterized by auditory system and cochlear damage (Lee et al., 2018; Yang et al., 2015). The underlying mechanisms are shared among different types of SNHL and include immune inflammatory response, mitochondrial damage, oxidative stress, and cellular apoptosis (He et al., 2024). Thus, 6SL may represent a promising therapeutic candidate for the treatment of acquired sensorineural hearing loss.

2.4 SIGLEC-11 in neuroinflammation and neurodegeneration

As elucidated earlier, inhibitory microglial CD33r SIGLEC receptors are key players in preventing phagocytosis, inflammation, and oxidative burst. Specifically, SIGLEC-11 has been identified as a human-specific receptor, and key regulator of the brain immune responses (Angata et al., 2002; Hayakawa et al., 2005). In a study categorizing

Alzheimer's disease (AD) and dementia-associated genes according to their disease process relevance, SIGLEC11 was found to be the most relevant AD-associated microglial gene (Bellenguez et al., 2022). Moreover, recent studies have demonstrated that SIGLEC-11 plays a crucial role in microglial function, having both anti-inflammatory and neuroprotective effects (Karlstetter et al., 2017; Liao et al., 2021; Wang et al., 2010). When interactive with the oligo-/polysialylated glycocalyx of neighboring cells in culture, SIGLEC-11 demonstrated reduced microglial neurotoxicity properties (Wang et al., 2010). These findings suggest that SIGLEC-11 may represent a novel therapeutic target for modulating neuroinflammation and preventing age-related neurodegenerative diseases, such as Alzheimer's and Parkinson's disease.

2.5 Sialylation and retinal inflammation

The role of sialylation in retinal diseases, particularly age-related retinal inflammation, is emerging as an interesting area of research. Retinal degenerative diseases such as age-related macular degeneration (AMD) and diabetic retinopathy have been recently characterized as inflammatory in nature (Kaur et al., 2022). During aging, the human retina is especially vulnerable to complement-driven inflammatory processes (Gemenetzi et al., 2015). Polysialic acid, a polymer of α2,8-linked sialic acid monomers (Villanueva-Cabello et al., 2022), highly sialylated throughout all retinal layers (Karlstetter et al., 2017). Intravitreal soluble polysialic acid and polysialic acid-conjugated polyglycolic/polylactic acid were tested on two transgenic mouse models expressing the SIGLEC11 receptor and showed effective suppression of innate immune responses, including blocking mononuclear phagocyte activation, inhibiting complement activation, and protecting against vascular damage (Karlstetter et al., 2017; Krishnan et al., 2023). Moreover, brain analysis of mice deficient for one allele of the *Gne* gene (Gne+/-) have shown increased neuronal loss which was rescued by knocking-out complement factor *C3* (Klaus et al., 2020). Thus, restoring sialylation or enhancing sialic acid levels could offer a therapeutic strategy for preventing or slowing retinal degeneration associated with aging and complement activation.

2.6 Aims

This project aimed to investigate the neuroprotective role of sialylation and its impact on immune system modulation. In this project three distinct studies were performed. Firstly,

the protective effects of 6'-sialyllactose, a human milk oligosaccharide, in preventing sensorineural hearing loss and its anti-inflammatory mechanisms in the cochlea were evaluated. Secondly, the role of SIGLEC-11, a human lineage-specific microglial receptor, in alleviating neuroinflammation and neurodegeneration in the aging brain of a transgenic mouse model was examined. Thirdly, the consequences of reduced sialylation on retinal inflammation and degeneration, with a focus on complement activation were investigated. All animal experiments in the three publications were approved by the authors' institutional and governmental review boards and have complied with the Helsinki Declaration. Animal experiments approvals numbers for the first and second publication were Az. 84-02.04. 2017.A240 and Az. 81-02.04. 2024.A010, respectively. Killing of the mice in the third publication was carried for research according to the Animal Welfare Act (Tierschutzgesetz).

2.7 References

Allendorf, D. H., Puigdellívol, M., & Brown, G. C. (2020). Activated microglia desialylate their surface, stimulating complement receptor 3-mediated phagocytosis of neurons. *Glia*, *68*(5), 989–998. https://doi.org/10.1002/GLIA.23757

Angata, T., Kerr, S. C., Greaves, D. R., Varki, N. M., Crocker, P. R., & Varki, A. (2002). Cloning and characterization of human Siglec-11. A recently evolved signaling molecule that can interact with SHP-1 and SHP-2 and is expressed by tissue macrophages, including brain microglia. *The Journal of Biological Chemistry*, *277*(27), 24466–24474. https://doi.org/10.1074/JBC.M202833200

Angata, T., Margulies, E. H., Green, E. D., & Varki, A. (2004). Large-scale sequencing of the CD33-related Siglec gene cluster in five mammalian species reveals rapid evolution by multiple mechanisms. *Proceedings of the National Academy of Sciences of the United States of America*, *101*(36), 13251–13256. https://doi.org/10.1073/PNAS.0404833101

Bellenguez, C., Küçükali, F., Jansen, I. E., Kleineidam, L., Moreno-Grau, S., Amin, N., Naj, A. C., Campos-Martin, R., Grenier-Boley, B., Andrade, V., Holmans, P. A., Boland, A., Damotte, V., van der Lee, S. J., Costa, M. R., Kuulasmaa, T., Yang, Q., de Rojas, I., Bis, J. C., … Lambert, J. C. (2022). New insights into the genetic etiology of Alzheimer's disease and related dementias. *Nature Genetics*, *54*(4), 412.

https://doi.org/10.1038/S41588-022-01024-Z

Bornhöfft, K. F., Goldammer, T., Rebl, A., & Galuska, S. P. (2018). Siglecs: A journey through the evolution of sialic acid-binding immunoglobulin-type lectins. *Developmental and Comparative Immunology*, *86*, 219–231. https://doi.org/10.1016/j.dci.2018.05.008

Cao, H., Lakner, U., de Bono, B., Traherne, J. A., Trowsdale, J., & Barrow, A. D. (2008). SIGLEC16 encodes a DAP12-associated receptor expressed in macrophages that evolved from its inhibitory counterpart SIGLEC11 and has functional and non-functional alleles in humans. *European Journal of Immunology*, *38*(8), 2303–2315. https://doi.org/10.1002/EJI.200738078

Duan, S., & Paulson, J. C. (2020). Siglecs as Immune Cell Checkpoints in Disease. *Annual Review of Immunology*, *38*, 365–395. https://doi.org/10.1146/ANNUREV-IMMUNOL-102419-035900

French, B. M., Sendil, S., Pierson, R. N., & Azimzadeh, A. M. (2017). The role of sialic acids in the immune recognition of xenografts. *Xenotransplantation*, *24*(6), 10.1111/xen.12345. https://doi.org/10.1111/XEN.12345

Gemenetzi, M., & Lotery, A. J. (2015). Complement pathway biomarkers and age-related macular degeneration. *Eye*, *30*(1), 1. https://doi.org/10.1038/EYE.2015.203

Harduin-Lepers, A., Mollicone, R., Delannoy, P., & Oriol, R. (2005). The animal sialyltransferases and sialyltransferase-related genes: a phylogenetic approach. *Glycobiology*, *15*(8), 805–817. https://doi.org/10.1093/GLYCOB/CWI063

Hayakawa, T., Angata, T., Lewis, A. L., Mikkelsen, T. S., Varki, N. M., & Varki, A. (2005). A human-specific gene in microglia. *Science (New York, N.Y.)*, *309*(5741), 754–755. https://doi.org/10.1126/SCIENCE.1114321

He, C., Gai, H., Zhao, W., Zhang, H., Lai, L., Ding, C., Chen, L., & Ding, J. (2024). Advances in the Study of Etiology and Molecular Mechanisms of Sensorineural Hearing Loss. *Cell Biochemistry and Biophysics*, *82*(3). https://doi.org/10.1007/S12013-024-01344-3

Karlstetter, M., Kopatz, J., Aslanidis, A., Shahraz, A., Caramoy, A., Linnartz-Gerlach, B., Lin, Y., Lückoff, A., Fauser, S., Düker, K., Claude, J., Wang, Y., Ackermann, J., Schmidt, T., Hornung, V., Skerka, C., Langmann, T., & Neumann, H. (2017). Polysialic acid blocks mononuclear phagocyte reactivity, inhibits complement activation, and

protects from vascular damage in the retina. *EMBO Molecular Medicine*, *9*(2), 154–166. https://doi.org/10.15252/emmm.201606627

Kaur, G., & Singh, N. (2022). Inflammation and retinal degenerative diseases. *Neural Regeneration Research*, *18*(3), 513. https://doi.org/10.4103/1673-5374.350192

Klaus, C., Hansen, J. N., Ginolhac, A., Gérard, D., Gnanapragassam, V. S., Horstkorte, R., Rossdam, C., Buettner, F. F. R., Sauter, T., Sinkkonen, L., Neumann, H., & Linnartz-Gerlach, B. (2020). Reduced sialylation triggers homeostatic synapse and neuronal loss in middle-aged mice. *Neurobiology of Aging*, *88*, 91–107. https://doi.org/10.1016/J.NEUROBIOLAGING.2020.01.008

Klaus, C., Liao, H., Allendorf, D. H., Brown, G. C., & Neumann, H. (2021). Sialylation acts as a checkpoint for innate immune responses in the central nervous system. *Glia*, *69*(7), 1619–1636. https://doi.org/10.1002/GLIA.23945

Krishnan, A., Sendra, V. G., Patel, D., Lad, A., Greene, M. K., Smyth, P., Gallaher, S. A., Herron, Ú. M., Scott, C. J., Genead, M., & Tolentino, M. (2023). PolySialic acid-nanoparticles inhibit macrophage mediated inflammation through Siglec agonism: a potential treatment for age related macular degeneration. *Frontiers in Immunology*, *14*, 1237016. https://doi.org/10.3389/FIMMU.2023.1237016/FULL

Lee, M. Y., & Park, Y.-H. (2018). Potential of Gene and Cell Therapy for Inner Ear Hair Cells. *BioMed Research International*, *2018*, 1–11. https://doi.org/10.1155/2018/8137614

Liao, H., Winkler, J., Wißfeld, J., Shahraz, A., Klaus, C., & Neumann, H. (2021). Low molecular weight polysialic acid prevents lipopolysaccharide-induced inflammatory dopaminergic neurodegeneration in humanized SIGLEC11 transgenic mice. *Glia*, *69*(12), 2845–2862. https://doi.org/10.1002/GLIA.24073

Linnartz, B., Neumann, H., & Wang, Y. (2010). Microglial Immunoreceptor Tyrosine-Based Activation and Inhibition Motif Signaling in Neuroinflammation. *International Journal of Alzheimer's Disease*, *2010*, 587463. https://doi.org/10.4061/2010/587463

Phipps, K. R., Baldwin, N. J., Lynch, | Barry, Stannard, D. R., Šoltésová, A., Gilby, B., Mikš, M. H., & Röhrig, C. H. (2019). Toxicological safety evaluation of the human-identical milk oligosaccharide 6′-sialyllactose sodium salt. *J Appl Toxicol*, *39*, 10. https://doi.org/10.1002/jat.3830

Rabouille, C., Hui, N., Hunte, F., Kieckbusch, R., Berger, E. G., Warren, G., & Nilsson, T.

(1995). Mapping the distribution of Golgi enzymes involved in the construction of complex oligosaccharides. *Journal of Cell Science*, *108 (Pt 4)*(4), 1617–1627. https://doi.org/10.1242/JCS.108.4.1617

Röhrig, C. H., Choi, S. S. H., & Baldwin, N. (2016). The nutritional role of free sialic acid, a human milk monosaccharide, and its application as a functional food ingredient. *Https://Doi.Org/10.1080/10408398.2015.1040113*, *57*(5), 1017–1038. https://doi.org/10.1080/10408398.2015.1040113

Schwarzkopf, M., Knobeloch, K.-P., Rohde, E., Hinderlich, S., Wiechens, N., Lucka, L., Horak, I., Reutter, W., & Horstkorte, R. (2002). Sialylation is essential for early development in mice. *Proceedings of the National Academy of Sciences of the United States of America*, *99*(8), 5267–5270. https://doi.org/10.1073/pnas.072066199

Shahraz, A., Kopatz, J., Mathy, R., Kappler, J., Winter, D., Kapoor, S., Schütza, V., Scheper, T., Gieselmann, V., & Neumann, H. (2015). Anti-inflammatory activity of low molecular weight polysialic acid on human macrophages. *Scientific Reports*, *5*, 16800. https://doi.org/10.1038/srep16800

Varki, A., & Angata, T. (2006). Siglecs--the major subfamily of I-type lectins. *Glycobiology*, *16*(1). https://doi.org/10.1093/GLYCOB/CWJ008

Varki, A., & Gagneux, P. (2012). Multifarious roles of sialic acids in immunity. *Annals of the New York Academy of Sciences*, *1253*(1), 16–36. https://doi.org/10.1111/j.1749-6632.2012.06517.x

Varki, A., Schnaar, R. L., & Schauer, R. (2017). *Sialic Acids and Other Nonulosonic Acids*. https://doi.org/10.1101/glycobiology.3e.015

Villanueva-Cabello, T. M., Gutiérrez-Valenzuela, L. D., Salinas-Marín, R., López-Guerrero, D. V., & Martínez-Duncker, I. (2022). Polysialic Acid in the Immune System. *Frontiers in Immunology*, *12*. https://doi.org/10.3389/FIMMU.2021.823637

Wang, Y., & Neumann, H. (2010). Alleviation of neurotoxicity by microglial human Siglec-11. *The Journal of Neuroscience: The Official Journal of the Society for Neuroscience*, *30*(9), 3482–3488. https://doi.org/10.1523/JNEUROSCI.3940-09.2010

Wißfeld, J., Assale, T. A., Cuevas-Rios, G., Liao, H., & Neumann, H. (2024). Therapeutic potential to target sialylation and SIGLECs in neurodegenerative and psychiatric diseases. *Frontiers in Neurology*, *15*. https://doi.org/10.3389/FNEUR.2024.1330874

Yang, C.-H., Schrepfer, T., Schacht, J., Coffin, A. B., & Steyger, P. S. (2015). *Age-related hearing impairment and the triad of acquired hearing loss*. https://doi.org/10.3389/fncel.2015.00276

Yu, H., Jin, Y., Jeon, H., Kim, L., & Heo, K. S. (2024). Protective effect of 6′-Sialyllactose on LPS-induced macrophage inflammation via regulating Nrf2-mediated oxidative stress and inflammatory signaling pathways. *The Korean Journal of Physiology & Pharmacology : Official Journal of the Korean Physiological Society and the Korean Society of Pharmacology*, *28*(6), 503. https://doi.org/10.4196/KJPP.2024.28.6.503

3. Publications

3.1 Publication 1: 6'-sialyllactose ameliorates the ototoxic effects of the aminoglycoside antibiotic neomycin in susceptible mice

| Frontiers in Immunology

6'-sialyllactose ameliorates the ototoxic effects of the aminoglycoside antibiotic neomycin in susceptible mice

Tawfik Abou Assale[1], Thomas Kuenzel [2], Tamara Schink[1], Anahita Shahraz[1], Harald Neumann[1]* and Christine Klaus[1]

[1]Neural Regeneration, Institute of Reconstructive Neurobiology, Medical Faculty and University Hospital of Bonn, University of Bonn, Bonn, Germany, [2]Auditory Neurophysiology, Department of Chemosensation, Institute for Biology II, RWTH Aachen University, Aachen, Germany

Sialic acids are terminal sugars of the cellular glycocalyx and are highly abundant in the nervous tissue. Sialylation is sensed by the innate immune system and acts as an inhibitory immune checkpoint. Aminoglycoside antibiotics such as neomycin have been shown to activate tissue macrophages and induce ototoxicity. In this study, we investigated the systemic subcutaneous application of the human milk oligosaccharide 6'-sialyllactose (6SL) as a potential therapy for neomycin-induced ototoxicity in postnatal mice. Repeated systemic treatment of mice with 6SL ameliorated neomycin-induced hearing loss and attenuated neomycin-triggered macrophage activation in the cochlear spiral ganglion. In addition, 6SL reversed the neomycin-mediated increase in gene transcription of the pro-inflammatory cytokine interleukin-1β (*Il-1b*) and the apoptotic/inflammatory kinase *Pik3cd* in the inner ear. Interestingly, neomycin application also increased the transcription of desialylating enzyme neuraminidase 3 (*Neu3*) in the inner ear. *In vitro*, we confirmed that treatment with 6SL had anti-inflammatory, anti-phagocytic, and neuroprotective effects on cultured lipopolysaccharide-challenged human THP1-macrophages. Thus, our data demonstrated that treatment with 6SL has anti-inflammatory and protective effects against neomycin-mediated macrophage activation and ototoxicity.

KEYWORDS

neuroinflammation, sialylation, 6'-sialyllactose, neomycin, hearing loss, macrophages

1 Introduction

Hearing loss is a growing social and economic burden worldwide in an aging population ([1], [2]). The most common type of hearing loss is sensorineural. Hearing aids and cochlear implants can be used to improve the symptoms and quality of life of patients; however, the loss of auditory sensory neurons and hair cell degeneration remains a chronic, ongoing process. High variability in disease progression has been attributed to genetic

susceptibility and environmental factors, such as noise exposure, lifestyle, or diseases (3), which makes the development of a therapy difficult. Acquired sensorineural hearing loss can be caused by aging, drugs, or noise (4). The first signs of age-related acquired hearing loss may already occur at an age of 30 years–39 years in a minority of the population, but the disease is typically slowly progressive, and the prevalence increases to 55% at the age of 70 years–79 years (5). In contrast, drug- and noise-exposure-triggered hearing loss is less frequent but typically follows an acute event that induces acquired hearing loss. We focused on an animal model of aminoglycoside-induced hearing loss with a clear starting event and tested a therapeutic approach that might be relevant for other acquired sensorineural hearing loss events.

Aminoglycosides are important and potent anti-bacterial agents that have been widely used in previous times as antibiotic therapy, despite their severe side effects such as nephrotoxicity and ototoxicity. Although newer and safer antibiotic classes are now used in industrialized countries, aminoglycosides are still in use for local applications or systemically in several underdeveloped countries because of their low costs (6). Aminoglycosides have also been used in several animal models to induce acute hearing loss. Aminoglycoside exposure leads to auditory sensory neurons and hair cell loss in predictable base-to-apex progression, causing deafness (3). Furthermore, treatment with aminoglycosides leads to the activation of macrophages and the production of reactive oxygen species (ROS) in the inner ear of newborn mice (7). Interestingly, the ototoxic effects of neomycin treatment are reported to differ along the tonotopy axis (8).

Sialic acids (Sias) form the terminal ends of the glycocalyx as typical residues in glycoproteins and glycolipids of the cellular surface membrane. Sialylation is highly abundant in the central and peripheral nervous systems. It serves as a checkpoint for the immune system and controls oxidative stress and inflammation (9). Sialylation can be recognized by inhibitory sialic acid-binding immunoglobulin-type lectin (SIGLEC) receptors and complement modulators (e.g., complement factor H and properdin) (9–11), thus controlling innate immune activation. In addition to this anti-inflammatory potential, Sias are known to have anti-oxidative properties owing to their multiple hydroxyl groups. A high local concentration of Sias in the glycocalyx has the potential to scavenge free radical oxygen species (12). During an inflammatory reaction, they can be hydrolyzed by acidic pH, oxidation, or cleaved by cellular neuraminidases.

Milk is rich in Sia residues of oligosaccharides such as sialyllactose. Uptake of these oligosaccharides by breastfeeding helps newborns build up the sialylated glycocalyx of the central nervous tissue during early postnatal development (13). 6'-sialyllactose (6SL), the major form of sialyllactose in humans, possesses non-digestible and therefore non-glycemic properties (14) and can serve as an optimal external Sia source. Studies have shown that over 90% of orally administered sialyllactose can be absorbed in rat pubs, with 30% being retained in the body and 3%–4% in the brain (15). Furthermore, 6SL is tolerated at high concentrations without toxic effects (16), offering a wide therapeutic window. 6SL is a natural milk oligosaccharide that can be synthesized and produced in high amounts. Thus, 6SL is a

potent candidate for clinical applications that might act as a source for sialylation to counteract inflammatory processes.

In this study, we investigated the therapeutic properties of human milk oligosaccharide 6SL in an animal model of hearing loss. We treated postnatal mice challenged with neomycin to induce ototoxicity by systemic application of 6SL. We showed that 6SL treatment reversed the neomycin-induced increase in macrophages in the sensory spiral ganglion and partially prevented neomycin-induced hearing loss. We confirmed the anti-inflammatory, anti-phagocytic, and neuroprotective properties of 6SL *in vitro* in a human cell culture model.

2 Materials and methods

2.1 Experimental animals

All animal experiments were approved by the institutional and governmental review boards of the authors and complied with the Helsinki Declaration. C57BL/6J mice were obtained from the Charles River. All mice were maintained in a specific pathogen-free environment with free access to both water and food and a 12-hour day/night cycle. All efforts were made to minimize the number of animals used and their suffering. For *in vivo* experiments, the day of birth was defined as P0 and breedings were set in-house to obtain 8-day-old mouse pups (P8).

2.2 Induction of hearing loss

To induce hearing loss, male and female P8 mouse pubs were injected subcutaneously with either 50 μl 180 mg/kg body weight (bw) neomycin (Sigma, N5285, Germany) in PBS or with 50 μl 180 mg/kg bw neomycin + 60 mg/kg bw of purified 6'-sialyllactose (6SL) in PBS for five consecutive days (P8–P13). This method was modified from that described by Sun et al. (7). As a control, littermates were injected with 50 μl PBS alone. After six days of hearing loss induction, three subcutaneous injections of either 50 μl PBS (for PBS and Neo groups) or 60 mg/kg bw 6SL in PBS were administered (6SL group; P14–P16). The mice were monitored until P28–P30.

2.3 Auditory brainstem response test

Auditory Brainstem Response (ABR) test is a minimally invasive approach that measures the electrical activity generated within the auditory nerve and pathways in response to sound (17). We adapted the methods of Rüttiger et al. (18) for this study. In all physiological experiments, the experimenters were blinded to the treatment groups. On days P28–P30, mice were anesthetized and immediately placed in a sound-attenuation chamber on a controlled heating pad (38°C; Fine Science Tools GmbH, Germany) to maintain body temperature. Stainless steel disposable needle electrodes (0.35 mm diameter; Neuro.Dart, SIGMA Medizin Technik GmbH, Germany) were placed subcutaneously at the

vertex of the skull and ventral to the pinna of the left ear. The needle electrodes were connected to an extracellular amplifier (WPI DAM-70, World Precision Instruments GmbH, Germany) in the AC power differential mode. A reference needle electrode was subcutaneously placed at the root of the tail. The heart rates of the animals were monitored using electrocardiography throughout the experiment. Auditory stimulation was performed using a speaker (Visaton F 8 SC; driven by a Pioneer A-109 Stereo Amplifier; Pioneer & Onkyo Europe GmbH, Germany) placed 10 cm from the left ear of the animal. The acoustic output of the speaker was measured using a free-field microphone (Bruel & Kjaer Type 4190, Denmark) at the head position of the animal and subsequently compensated in custom recording software to obtain a flat frequency response between 0.5 kHz and 24 kHz up to 100 dB SPL. Acoustic stimuli (100 µs clicks or 1 ms pure tones with 0.2 ms cosine ramps) of alternating polarity were generated at a resolution of 10 µs using custom recording software (MATLAB, R2019a, The MathWorks, Germany) and converted to analog signals (National Instrument PCI-6281, Germany). Each stimulus was presented at least 256 times at a presentation rate of 30 Hz and differential voltage responses (vertex minus ear electrode) were amplified 10,000×, digitized at 10 µs resolution and stored using custom recording software. For analysis, voltage responses were digitally filtered (100 Hz–3,000 Hz band pass filter), and traces containing any signal exceeding 30 µV were rejected as artifacts. The remaining signals were averaged and analyzed between 0 ms and 7 ms post-stimulus onset. Tone or click auditory brainstem response (ABR) thresholds were visually determined by a trained observer blinded to the experimental conditions. The thresholds were objectively validated using the method described by Suthakar and Liberman [19]. Furthermore, ABR wave components were algorithmically detected and analyzed for amplitude and delay using a custom software. ABR waveforms were averaged within each treatment group and are presented as the mean wave ± standard deviation.

2.4 Tissue collection and preparation

After the ABR test, the mice were directly intracardially perfused with ice-cold PBS while still under deep anesthesia, and the cochleae were immediately dissected on ice as described by Montgomery and Cox [20] for RNA isolation or further immunohistochemistry experiments. For RNA isolation, eight mice per group were used, and for immunohistochemistry, at least five mice per group were analyzed. In summary, the skull was opened quickly and cut in half (sagittal). The forebrain, cerebellum, and brainstem were removed via blunt dissection. Extraneous bones and tissues were carefully dissected from the cochlea, and the cochlea was isolated from the temporal bone. Additional tissues were removed. For immunohistochemistry, the apex was slightly punctured to perfuse the cochlea with 4% ice-cold paraformaldehyde (PFA) via round and oval windows. The cochleae were again post-fixed in 4% PFA overnight, washed for 2 h in PBS, and decalcified in 5% EDTA in PBS while rotating at 4°C. Decalcified cochleae were washed three times in PBS for 15 min and cryoprotected in 30% sucrose (Roth, Karlsruhe, Germany). The

left cochlea was then embedded and frozen in O.C.T.^{TM} Compound, Tissue Tek® (Sakura/Fisher Scientific, Schwerte, Germany) and cut into 20 µM sagittal sections using a cryostat Microm Cryo Star HM 560 (Thermo Scientific, Schwerte, Germany). Sections were collected on Superfrost Plus adhesion microscope slides to minimize potential tissue loss during staining (Thermo Scientific, Germany).

2.5 RNA isolation and semi-quantitative real-time polymerase chain reaction

For RNA isolation from dissected cochleae, tissue samples were prepared as previously described [21]. The tissue was homogenized in 1 ml QIAzol lysis reagent (Qiagen, Germany) with a 5 mm stainless steel bead (Qiagen, Germany) for 5 min at 50 Hz and stored at −80°C until use. For RNA isolation from cells, cultures were washed with PBS and scraped in 1 ml QIAzol Lysis reagent (Qiagen, Germany) for further use. RNA was then extracted similarly for tissue and cell samples by first incubating for 5 min at RT and then adding 200 µM chloroform (Roth, Germany). After incubation for 3 min at room temperature, samples were centrifuged at 12,000 rpm for 15 min at 4°C. The upper phase, containing the RNA, was transferred to a new tube. Isopropanol (Roth, Germany) was added in a 1:1 ratio, and the samples were vortexed well and incubated overnight at −20°C. The following day, the samples were centrifuged again at 12,000 rpm for 20 min at 4°C. The supernatant was discarded, and the samples were washed three times by adding 300 µl of 70% ethanol (Roth, Germany) in PBS, centrifuged at 12,000 rpm for 5 min at 4°C, and the supernatant was discarded. After the last wash, the supernatant was discarded, and the samples were left to dry for 10 min–20 min at room temperature. RNA was resuspended in 11 µl RNAse-free DEPC water (Invitrogen, USA). RNA concentration was measured using a Nanodrop spectrometer (Thermo Fisher Scientific, USA). Reverse transcription of RNA was performed using SuperScript III reverse transcriptase and hexamer random primers (both from Invitrogen, Germany) according to the manufacturer's protocol for SuperScript First-Strand Synthesis. Semi-quantitative real-time polymerase chain reaction (sqRT-PCR) with specific oligonucleotides (Supplementary Tables 3, 4) was performed according to the manufacturer's protocol using SYBR Green PCR Master Mix (Invitrogen, Germany) and Mastercycler epigradient S (Eppendorf, Wesseling-Berzdorf, Germany). Transcripts of the housekeeping gene *glyceraldehyde-3-phosphate dehydrogenase (GAPDH)* were used as internal RNA loading controls. Amplification specificity was confirmed by melting curve analysis. The results were analyzed using Mastercycler ep realplex software (Eppendorf, Germany) after establishing the reaction efficiency for each primer pair. The values were normalized to their respective *GAPDH* values and quantified using the delta delta-CT method. For each animal, the mean CT read-out value for *GAPDH* was calculated and subtracted from the mean CT value of each gene primer of interest, yielding the delta CT value. The mean delta CT value for the PBS control group was calculated. The delta delta-CT value of each gene primer for each animal was then calculated by

subtracting the mean delta CT value of the PBS control group from the delta CT value of the respective primer. The power of the negative delta delta-CT value for each gene primer for each animal was then calculated and used as the relative read-out value for each gene transcription.

2.6 Immunohistochemistry of cochlea tissue

For neuronal cell density analysis, cryosections were washed with PBS and incubated in a blocking solution (10% BSA + 0.2% Triton X-100 + 5% NGS) for 1 h at room temperature. Primary antibodies for neuronal nuclei (NeuN; 1:500; Millipore #MAB377, Germany) diluted in blocking solution were added and the sections were incubated for 2 h at room temperature. After washing the sections three times with saline, the secondary antibody Alexa Fluor 647 (1:250; Dianova #115-606-072, Germany) diluted in blocking solution was added and incubated for another 2 h at room temperature. The sections were washed again twice and stained with DAPI (1:10,000, Sigma, Germany) before mounting with Aqua-Polymount (Polysciences Inc., Germany). Images of the spiral ganglion were taken using a magnification of ×40 and at 2 μM intervals over five optical sections with an SP8 confocal microscope and LAS-X software (Leica, Wetzlar, Germany). For the quantification of macrophages, cryosections were washed initially with PBS and incubated in blocking solution (10% BSA + 0.2% Triton X-100 + 5% NGS in PBS) for 2 h at room temperature, followed by incubation in primary antibodies directed against Iba1 (1:500; IBA1 rabbit-anti, Wako #019-19741, Germany) and against Cd68 (1:500, rat-anti-mouse, AbD Serotec, MCA1957, UK) in blocking solution overnight at 4°C. After thorough washing with saline, the sections were stained with the corresponding secondary antibodies (Alexa Fluor® 647-conjugated goat anti-rabbit IgG, 1:500, Dianova #111-606-144, Germany and Cy3 goat anti-rat, 1:200, Dianova #112-166-072; Germany) in PBS for 2 h at room temperature. After washing with saline, the sections were stained for nuclei (DAPI, 1:10,000) for 30 s and then covered with Aqua-Polymount (Polysciences Inc.). Images of the spiral ganglion were taken at a magnification of ×40 and at 2 μM intervals over five optical sections using an SP8 confocal microscope and LAS-X software (Leica, Wetzlar, Germany).

2.7 Morphological analysis of macrophages

The maximum projections of the Iba1-/DAPI-double-positive z-stack images were generated and analyzed with ImageJ (v.1.52u) using custom-written plugins. Macrophage density was quantified by counting the Iba1-/DAPI-double-positive cells per area in each image and calculating the average for each mouse. To determine the overall Iba1 expression, the total fluorescence integrated density was measured for each image and analyzed by subtracting the background fluorescence integrated density measured in the primary antibody negative control. The mean fluorescence

intensity was calculated per mouse, and the mean for each experimental group was calculated and normalized to that of the control group.

2.8 Purification of sialyllactose

6'-sialyllactose (6SL) purchased from Carbosynth was further purified using an FPLC approach with a HiPrep Q XL 16/10 column. The HiPrep Q XL 16/10 column was washed with Ampuwa water before loading it with 50 mg of 6SL (Carboysynth) dissolved in 1 mL of Ampuwa water. The column was washed with Ampuwa water to remove impurities, followed by a linear gradient of 1 M ammonium bicarbonate to elute the 6SL. The eluate was collected, frozen to −80°C and freeze-dried using the ALPHA 1-2/LD Plus freeze dryer at a pressure of 0.1 mbar for 24 h. Lyophilized 6SL was then reconstituted under sterile conditions, and its concentration was determined using the Aminoff method (22).

2.9 Human THP1 macrophage cell culture

Human monocytes (THP1 cells, kindly provided by Prof. Hornung, Bonn, Germany) were cultured in RPMI medium supplemented with 1% heat-inactivated chicken serum (Gibco, Germany), 1% penicillin/streptomycin (Gibco, Germany), 1% L-glutamine (Gibco, Germany), 1% sodium pyruvate (Gibco, Germany), and 1% N2 (Gibco, Germany). For differentiation, floating THP1 monocytes were plated and incubated with 10 ng/ml Phorbol-12-Myristate-13-Acetate (PMA; Sigma, Germany) in a prewarmed medium for 48 h to allow adherence. Cells were washed three times with prewarmed medium to remove the remaining PMA and were incubated for 48 h at 37°C and 5% CO_2. After 18 h, the cells showed macrophage-like morphology and could be used for experiments (further described as macrophages).

2.10 Co-culture of human sensory neurons and human THP1 macrophages

Human sensory neurons were obtained from human induced pluripotent stem (iPS; WiCell foreskin-1) cells, as described by Chambers et al. (23). On day 0, the iPS colonies were detached by collagenase IV (Gibco, Germany), collected by sedimentation, and resuspended in DMEM/F12 medium (Gibco, Germany) supplemented by 20% knockout serum replacement (Gibco, Germany), 1% nonessential amino acids (Gibco, Germany), 10 μM SB431542 (inhibitor of transforming growth factor b1 and activin receptors; Axom Medchem, Netherlands), 1 μM dorsomorphin (Sigma, Germany), 3 μM CHIR99021 (inhibitor of glycogen synthase kinase [GSK] 3b and GSK-3a; Axom Medchem, Netherlands), and 0.5 μM purmorphamine (Sigma, Germany) for 2 days. On day 2, the medium was replaced by 50:50 DMEM/F12: neurobasal, 1:200 N2 supplement (Gibco, Germany), 1:100 B27

supplement (N2B27 medium, Gibco, Germany) supplemented with 10 μM SB431542, 1 μM dorsomorphin, 3 μM CHIR, and 0.5 μM purmorphamine for 2 days. On day 4, 150 μM ascorbic acid (Tocris, United Kingdom) was added to the N2B27 medium, but SB431542 and dorsomorphin were withdrawn. On day 6, embryonic bodies were triturated and seeded on plates coated with Geltrex (Thermo Fisher Scientific, Germany) at low density and expanded in N2B27 medium supplemented with CHIR99021, ascorbic acid, and purmorphamin for five passages. The neural stem cells (NSCs) were then ready for differentiation. For differentiation, NSCs were split using accutase (Sigma, Germany) and replated in Geltrex-coated plates. NSCs were treated for 2 days with N2B27 medium supplemented with 3 μM CHIR99021 and afterwards for one week with 10 ng/ml BMP4 (Novus Biologicals, Germany). Consequently, the premature neurons were split by accutase and replated at a density of 20,000 cells per well in Geltrex-coated chamber slides in N2B27 maturation medium containing 10 ng/ml brain-derived neurotrophic factor (BDNF; Prospect, Israel), 10 ng/ml glial cell line-derived neurotrophic factor (GDNF; Prospect, Israel), and 500 μM dbcAMP (Sigma, Germany) for 2 weeks. In parallel, the human THP1 monocyte cell line was maintained in RPMI medium, as described above. Cells were incubated with PMA for 48 h, washed twice with the medium, and then incubated for an additional 48 h without PMA. For the experiments, THP-1 macrophages were scraped, counted, and added to the sensory iPS cell-derived neurons in a 1:1 ratio of co-culture medium (N2B27 medium plus BDNF, GDNF, and dbcAMP) and treated with 100 μM 6SL or vehicle control for another 48 h.

2.11 Neurite lengths analysis after co-culture with macrophages

Human sensory neuron-macrophage co-cultures were washed once with 1× PBS and fixed with 4% paraformaldehyde (PFA) for 15 min at room temperature (RT). Then, non-specific binding sites of the fixed co-culture were blocked, and the co-culture was stained with antibodies against rabbit anti-neurofilament (1:1,000; Sigma, USA) and rat anti-CD11b (2 μg/mL; BD Biosciences #553307, Germany) overnight at 4°C. The following day, the fixed co-cultures were washed three times with blocking solution and incubated with secondary antibodies (1:500 Alexa488-conjugated anti-rabbit antibody, #A11008 Invitrogen, Germany and 1:500 Cy3-conjugated anti-rat antibody, #112-166-072 Dianova, Germany) for 2 h at RT. Cells were washed three times with 1× PBS and subsequently labeled with 4',6-diamidino-2-phenylindole (DAPI, 1:5,000, Sigma). Images were captured using a confocal laser-scanning microscope (Fluoview 1000, Olympus). For quantification of neurite length, a total of 10 pictures per condition were collected, maintaining the same settings, and analyzed using ImageJ/NeuronJ software (NIH, MBF) by a blinded investigator. Images were processed equally, and the mean length of the neurofilament-positive neurites was quantified. The mean length of the untreated control cells was set to 100%.

2.12 Bead phagocytosis of THP1

Human macrophages (THP-1) were seeded at 96 h (48 h with and 48 h without PMA) prior to stimulation as described above. The cells were stimulated with 3 μg/ml LPS (InvivoGen) and different concentrations of 6SL for 24 h. After 23.5 h Fluoresbrite® Polychromatic Red Microspheres 1.0 μm beads (Polysciences Inc., USA) were added and incubated for 30 min. The cells were then washed and collected in PBS for analysis using flow cytometry (Accuri; BD, Germany). The percentage of cells that took up two or more beads was determined and normalized to the untreated condition (UT). The untreated condition was set as 100%.

2.13 Radical oxygen species analysis

THP1 macrophages were cultured and seeded as described above (48 h with and 48 h without PMA). Cells were pre-incubated with 6SL (5 μM), SOD (60 U/ml; Sigma, Germany), or Trolox (40 μM; Merck, Germany) for 1 h before stimulation with LPS (3 μg/ml, InvivoGen, Germany) for 15 min at 37°C. Cells were washed and incubated in 30 μM DHE in Krebs-HEPES buffer for another 15 min at 37°C under dark light conditions. The cells were then washed three times in Krebs–Hepes buffer, scraped, centrifuged, and resuspended in PBS for direct flow cytometry analysis (Accuri; BD, Germany). The mean DHE intensity of the flow cytometry analysis was normalized to that of the untreated condition (UT). The untreated condition was set to 1.0.

2.14 Ethics

All animal experiments were conducted according to the authors' institutional guidelines by the local government and the principles expressed in the Declaration of Helsinki. Experiments were conducted in accordance with the European Directive (2010/63/EU) on the protection of animals used for experimental and other scientific purposes. The Animal Ethics Committee of the University of Bonn and the local government approved all procedures.

2.15 Statistical analysis

Data with two experimental groups were tested for normality and then analyzed by either Student's t-test or Mann–Whitney test, or if group number >2 by one-way ANOVA followed by Bonferroni *post hoc* test or Dunnett's T3 method comparing all columns using the IBM SPSS Statistics (v.22; IBM Corporation, Germany). Data were considered significantly different if *p ≤0.050, **p ≤0.010, or ***p ≤0.001. The absence of statistical notation indicates that there were no statistically different outcomes. Click ABR thresholds, wave I metrics per sound pressure level, and immunohistochemistry staining analysis were compared among the three treatment groups using one-way ANOVA. For tone ABR thresholds, two-

way ANOVA (treatment × frequency) was used. For all *post-hoc* pairwise t-tests, the significance levels were adjusted according to Tukey's honestly significant difference (HSD) procedure (MATLAB multcompare.m).

3 Results

3.1 6'-sialyllactose partially rescued the neomycin-induced hearing impairment in auditory brainstem responses

Aminoglycoside antibiotics, including neomycin, are ototoxic to both humans and mice. Neomycin has been applied repeatedly in postnatal mice to induce hearing loss associated with local activation of macrophages (7). Therefore, we performed repeated daily applications of neomycin and tested the therapeutic potential of the co-application of 6SL on auditory brainstem responses (ABR) in early postnatal mice (Figure 1A). For this therapeutic approach, bovine milk-derived 6SL was further purified prior to experimentation with a fast protein liquid chromatography (FPLC)-based anion-exchange chromatography (AEX)-chromatography approach to remove residual contaminants. Mice were injected daily for 6 days starting at postnatal age P8 with either vehicle as control (PBS), 180 mg/kg bw neomycin (Neo), or 180 mg/kg bw neomycin plus 60 mg/kg bw 6SL (Neo + 6SL). Subsequently, the respective animal groups received daily injections of PBS (PBS group and Neo group) or 6SL (Neo + 6SL group) over three additional days (Figure 1A). After 12 days–14 days the animals were subjected to electrophysiological ABR measurements and immediately analyzed using immunohistochemistry. No significant difference in body weight was observed among the distinct experimental groups at the day of analysis 13.5 g± 3.1 g (PBS group), 15.0 g ± 0.6 g (Neo group), 13.9 g ± 1.1 g (Neo + 6SL group) (see Supplementary Table 1).

Typical ABR waveforms were obtained from mice in all experimental groups (Figure 1B). In neomycin-treated mice (Neo group), ABR waveforms were only observed at higher sound pressure levels (SPL; 70 dB and 90 dB) and showed reduced ABR amplitudes and delayed wave components even at 90 dB SPL compared to the PBS group. For the Neo + 6SL treated animals, this was to a certain extent also the case with a reduction in amplitude, but ABR waveforms were still visible at higher sound pressure levels. Therefore, we quantified the ABR thresholds of animals in the three treatment groups (Figure 1C). Control animals treated with vehicle only (PBS) had a click ABR threshold of 35 dB ± 6 dB SPL. Neomycin treatment caused profoundly elevated click ABR thresholds (74 dB ± 14 dB SPL; p <0.001) in mice. Animals treated with Neo + 6SL showed reduced click ABR thresholds, from 74 dB ± 14 dB to 51 dB ± 9 dB SPL (p = 0.002, ANOVA *Post-hoc* pairwise testing Tukey's HSD). Thus, treatment with 6SL led to a significant reduction in click ABR thresholds (ANOVA F = 32.8, total df = 20, p <0.001).

Since ototoxic effects of neomycin treatment are reported to differ along the axis of tonotopy (8), we next measured tone ABR thresholds in the three experimental groups (Figure 1C). Control

mice (PBS) showed a normal audiogram (3 kHz: 46 dB ± 9 dB SPL; 6 kHz: 25 dB ± 5 dB SPL; 12 kHz: 24 dB ± 5 dB SPL; and 24 kHz: 22 dB ± 8 dB SPL). In the Neo-treated mice, tone ABR thresholds were elevated (3 kHz: 70 dB ± 7 dB SPL; 6 kHz: 60 dB ± 19 dB SPL; 12 kHz: 74 dB ± 5 dB SPL; 24 kHz: 72 dB ± 4 dB SPL), with the most severe effects evident for higher frequencies, where an average threshold elevation of +50 dB SPL was found. In the Neo + 6SL group, a mixed picture emerged: Tone ABR thresholds for frequencies of 12 kHz and below were less increased compared to the Neo group (3 kHz: 62 dB ± 11 dB SPL; 6 kHz: 36 dB ±9 dB SPL; 12 kHz: 48 dB ± 16 dB SPL; 24 kHz: 78 dB ± 5 dB SPL), while the tone ABR threshold for 24 kHz was severely elevated. Statistical analysis using two-way ANOVA revealed that both frequency (F = 17.9, df = 83, p <0.001) and treatment (F = 158, df = 83, p <0.001) had significant effects on tone ABR thresholds. Furthermore, a significant interaction (F = 11.2, df = 83, p <0.001) between the frequency and treatment groups supported the finding that both the outcome of neomycin treatment and rescue by 6SL differed depending on the tonotopic position. *Post-hoc* pairwise testing (Tukey's HSD; Supplementary Table 2) supported this conclusion. The most severe neomycin effects in the basal high-frequency region (24 kHz condition) were unaffected by 6SL but were rescued in the middle frequency regions (6 kHz and 12 kHz) (Supplementary Table 2). Thus, treatment with 6SL decreased the tone ABR thresholds compared to the Neo group, showing a significant amelioration of the neomycin-induced damage by 6SL in middle-frequency regions of the cochlea.

To better understand the outcome of the effect of 6SL, we next analyzed the peak amplitude (Figure 1D) and latency (Figure 1E) of the ABR wave I component in click-evoked ABR at varying sound pressure levels. Average wave I amplitudes in control animals (PBS) grew from the threshold with a sigmoidal function for the control (PBS) and 6SL-treated groups (Neo + 6SL), whereas the growth function of ABR wave I amplitude was much shallower in neomycin-treated animals. Wave I amplitude was affected by both the Neo and Neo + 6SL groups for all sound pressure levels above 55 dB SPL (ANOVA 55 dB SPL: F = 7.4, df = 15, p = 0.007). At high sound pressure levels (ANOVA 90 dB SPL: F = 20.1, df = 20, p <0.001), the PBS group differed from both the Neo (p <0.001) and 6SL (p <0.001) groups in *post-hoc* pairwise tests (Tukey's HSD). Thus, the amplitude of the ABR wave component generated by hair cells was not restored to normal levels by 6SL treatment. This finding could be explained by either a reduced number of the generators or by an uncoherent activation of generators of the ABR wave component. Therefore, we also analyzed ABR wave I latencies (Figure 1E). At high sound pressure levels, Wave I latencies were lower in the Neo + 6SL group than in the Neo group (p = 0.035, ANOVA *post-hoc* pairwise test). Thus, analysis of ABR Wave I amplitude suggests that in both the Neo and Neo + 6SL rescue conditions, the number of functional ABR generators was reduced compared to the PBS control group. Only for the ABR Wave I latency was a reduction observed at higher SPL in the Neo + 6SL group than in the Neo group.

In summary, the data showed that 6SL treatment rescued neomycin-induced hearing loss in mice, particularly in the middle frequency regions, and ameliorated the click ABR threshold.
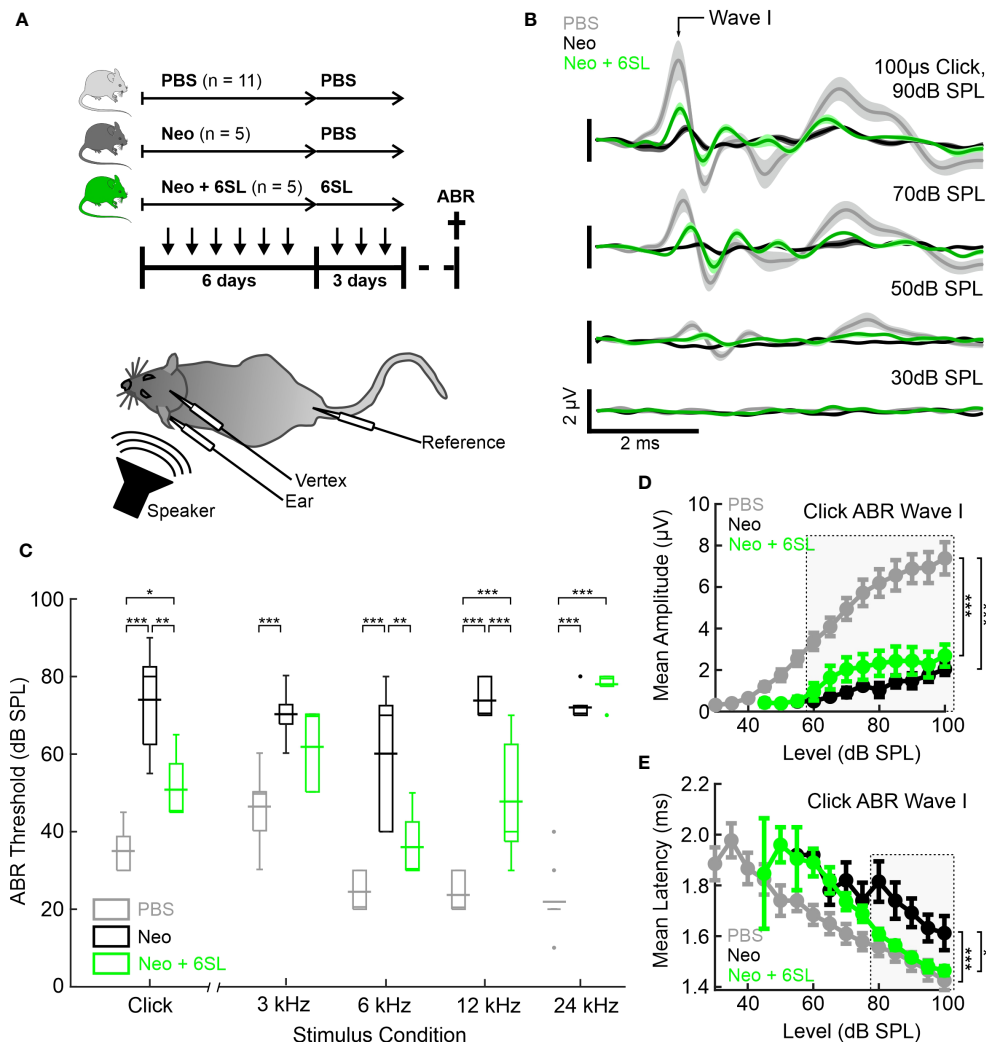
FIGURE 1

Systemic application of 6'-sialyllactose ameliorated the neomycin-induced hearing loss. **(A)** Auditory brain responses (ABR) were measured with electrodes (vertex, ear and reference) after noise exposure (speaker) in three experimental groups, namely control animals (vehicle control PBS, light gray), neomycin-treated animals (Neo, dark gray), and neomycin plus 6SL treated animals (Neo + 6SL, green). Mice received six repeated daily applications of either Neo, Neo + 6SL, or saline control, and subsequent repeated daily applications of 6SL or saline control, as indicated by the arrows on the timeline. Mice were sacrificed on days P28−P30 (cross on the timeline) after being subjected to ABR recordings. A schematic drawing of the mouse shows the electrode and speaker placement positions relative to the animal. **(B)** Click ABR waveforms at four sound pressure levels (30 dB, 50 dB, 70 dB, and 90 dB) are shown as mean (solid lines; n = 11/5/5 for PBS, Neo, and Neo + 6SL) $\pm$ standard deviation (shaded areas). Treatment with 6SL partially rescued the wave lost after neomycin application. One set of representative recordings was presented. **(C)** Box plots of auditory thresholds measured by ABR for different stimulus conditions. The auditory threshold increased in the Neo group and ameliorated in the Neo + 6SL group under distinct stimulus conditions. Thick horizontal lines crossing the boxplot indicate mean values and thin lines in the boxplots indicate median values. Asterisks indicate statistically significant differences between groups, marked by brackets: *p <0.05, **p <0.01, ***p <0.001. The absence of statistical notation indicates that there was no statistically significant difference. **(D, E)** Analysis of the click-evoked ABR Wave I component, shown as mean $\pm$ standard deviation amplitudes **(D)** and mean $\pm$ standard deviation peak latencies **(E)** vs. click sound pressure levels between 30 dB SPL and 100 dB SPL. At higher sound pressure levels (SPL), 6SL ameliorated the neomycin-induced increase in the ABR Wave I latency **(E)**. *p <0.05, **p <0.01, ***p <0.001 ANOVA. Brackets refer to the 90 dB SPL condition.

3.2 6'-sialyllactose prevented the strong increase in number of macrophages in the cochlear spiral ganglion

To understand what happened at the cellular level, we examined the macrophages in the inner ear. Neomycin treatment can increase the number and/or activation of macrophages in the inner ear (7). Therefore, we analyzed the number and expression levels of the macrophage marker Iba1 in the cochlear spiral ganglion, where the cell bodies of bipolar neurons innervate the hair cells (Figure 2A). We found only a low number of Iba1+ macrophages in the spiral cochlear ganglion of the PBS control group. Challenge of mice with neomycin increased the number of Iba1+ cells in the cochlear spiral ganglia, an effect that was reversed in the Neo + 6SL group (Figure 2A). We quantified the number and intensity of Iba1 staining (Figure 2B). Neomycin treatment increased the relative number of Iba1+ macrophages from 100% ± 18.3% to 221% ± 71.3% (p <0.001) (Figure 2B). This increase in Iba1+ macrophages
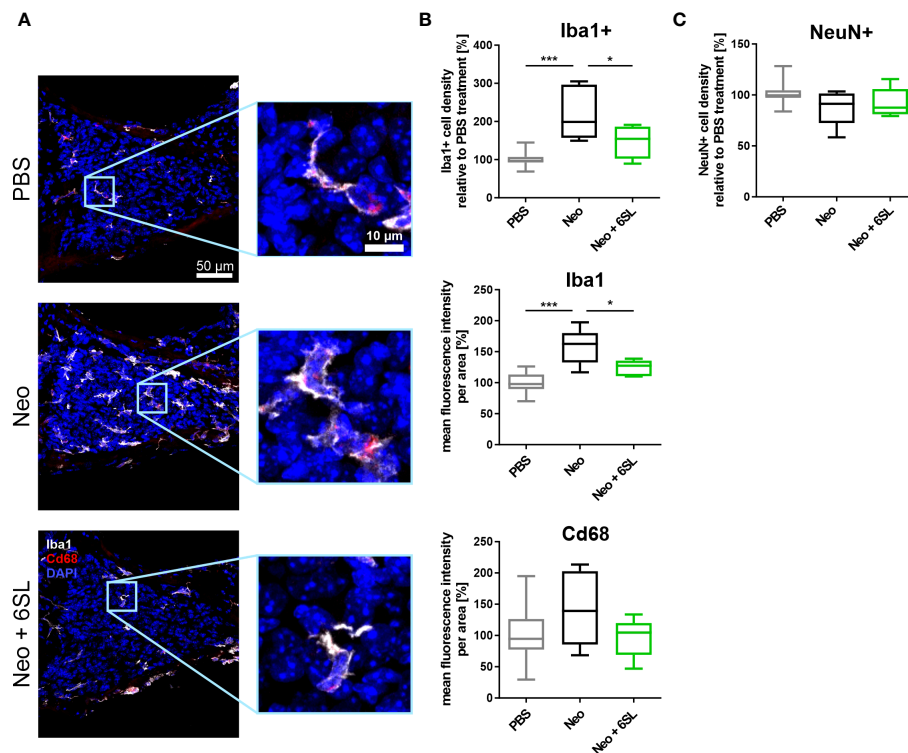
FIGURE 2

Treatment with 6'-sialyllactose prevented the increase in number of macrophages in the cochlear spiral ganglion. **(A)** Cryosections of the cochlear spiral ganglion were stained with an antibody against the macrophage marker ionized calcium binding adaptor molecule 1 (Iba1; white), lysosome-related protein Cd68 (red), and nuclear marker 4',6-diamidino-2-phenylindole (DAPI, blue). An increased number of macrophages was visible in the neomycin-treated spiral ganglia compared to that in the PBS- and Neo + 6SL-treated groups. Representative z-stack images of the cochlear spiral ganglion of mice treated with PBS, neomycin (Neo), or neomycin with 6'-siallylactose (Neo + 6SL) are shown. Scale bar: 50 µM; higher magnification: 10 µM. **(B)** The number of Iba1-positive macrophages and intensities of Iba1 and Cd68 were quantified in the cochlear spiral ganglia. Quantification of Iba1-positive cell density revealed significantly more macrophages in the Neo group than in the PBS or Neo + 6SL groups. The Iba1 fluorescence intensity was strongly upregulated after neomycin treatment compared to that in the PBS group. This upregulation was attenuated after simultaneous 6SL treatment of the neomycin-challenged mice. The Cd68 intensity showed no change among the groups. Data are shown as a min to max box + whisker plot; n = 5−11. **(C)** Quantification of the relative cell density of neuronal nuclei (NeuN)-positive cells in cochlear spiral ganglia. No difference was observed; however, the number of NeuN-positive cells was slightly decreased in the Neo group. Data shown as min to max box + whiskers plot; n = 5−11. All data were analyzed by one-way ANOVA and Tukey's multiple comparison test, *p <0.05, ***p <0.001.

was reversed from 221% ± 71.3% to 147% ± 43.3% (p = 0.028, Neo vs. Neo + 6SL group) after treatment with 6SL.

We also quantified the overall intensity of Iba1 and lysosomal activation marker Cd68 in the spiral ganglion. The overall intensity of Iba1 per area increased in the Neo group (from 100% ± 17.1% in PBS to 158% ± 29.1% in the Neo group; p ≤0.001), which was reversed in the Neo + 6SL group (124% ± 12.8%; p = 0.038 vs. Neo group), confirming the increased amount or activation of macrophages in the cochlear spiral ganglia (Figure 2B). The Cd68 intensity per unit area did not change among the groups.

Next, we analyzed neuronal density in the spiral ganglion by staining with the neuronal nuclei marker (NeuN). No significant difference in neuronal density between the three experimental groups was visible, although slightly fewer neurons were observed in the Neo group (PBS: 101% ± 10.6%; Neo: 87.8% ± 17.7%; 92.2% ± 14.4%, Figure 2C).

Thus, the data showed an increased number of Iba1+ macrophages as a sign of immune system activation in the spiral

ganglia after treatment with Neo, which was reversed by the application of 6SL.

3.3 6'sialyllactose ameliorated the neomycin-induced increase of the inflammation-related *Aif1* and *Pik3cd* gene transcription

To examine the increased immune activation at the gene transcription level, we analyzed gene transcripts of pro-inflammatory, oxidative, and apoptotic/necroptotic pathways in the whole inner ear. We found elevated transcription levels of the macrophage marker *Aif1 (Iba1)* in the Neo-treated compared to the PBS control group (Figure 3A). Specifically, *Aif1* gene transcription was increased from 0.927 ± 0.4-fold change (FC) to 2.37 ± 1.5 FC (p = 0.026), which was reversed by 6SL to 0.664 ± 0.4 FC (p = 0.008). Transcription of the macrophage lysosomal marker *Cd68* was not
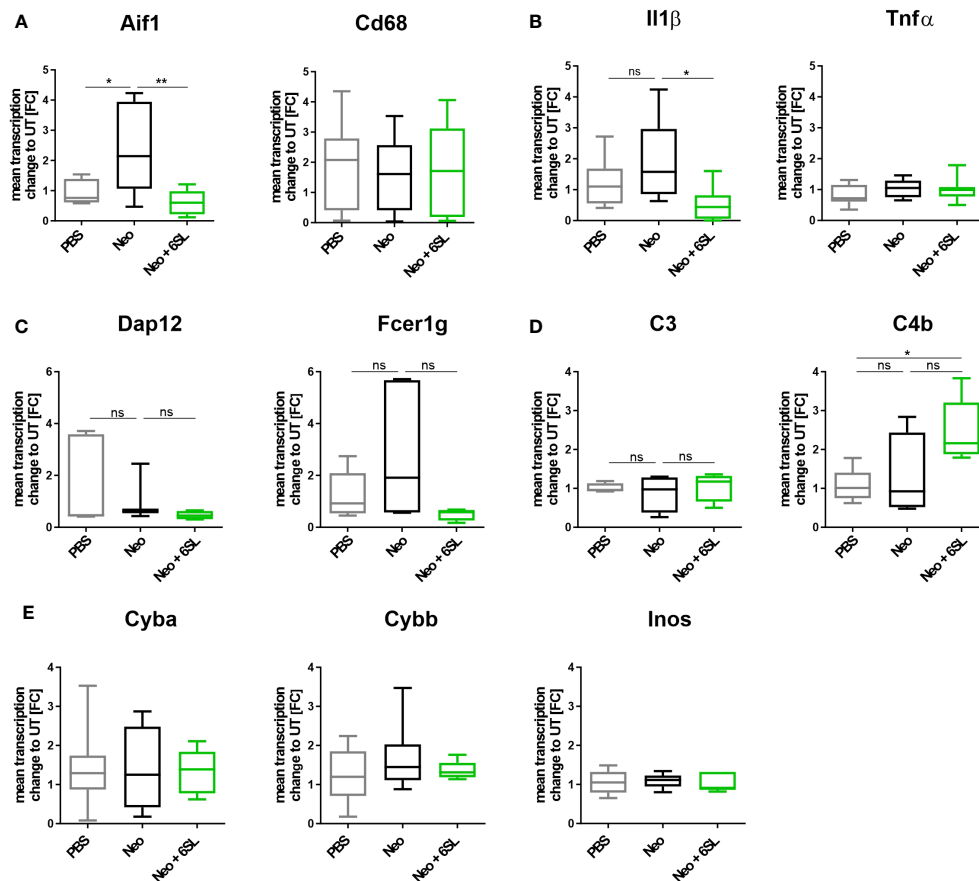
FIGURE 3

Treatment with 6′-sialyllactose ameliorated the neomycin-induced increase of immune-related gene transcription. **(A)** Transcription levels of allograft inflammatory factor 1 (*Aif1*; gene of Iba1) and the CD68 antigen (*Cd68*) of whole cochlea homogenates from mice treated with PBS, neomycin (Neo), or neomycin with 6′-siallylactose (Neo + 6SL). The *Aif1* transcript levels were higher in the Neo group than in the PBS control group. This increase was not observed in the Neo + 6SL group. The *Aif1* transcript levels decreased after additional treatment with 6SL. *Cd68* transcript levels remained unchanged across all treatment groups. Data are shown as a min to max box + whisker plot; n = 7−8. **(B)** 6SL decreased the transcription of the proinflammatory cytokine interleukin 1β (*Il1b*) in whole cochlear homogenates from mice treated with 6SL (Neo + 6SL) compared to that in neomycin (Neo) treatment group. Transcription of tumor necrosis factor-α (*Tnfα*) did not change. Data are shown as a min to max box + whisker plot; n = 6−8. **(C)** Gene transcription of the tyrosine kinase-binding protein (*Tyrobp/Dap12*) was unchanged in the neomycin (Neo) and neomycin groups treated with 6′-sialyllactose (Neo + 6SL) compared to the control group (PBS). Likewise, gene transcription of the phagocytic marker Fc fragment of IgE, high affinity I receptor for gamma polypeptide (*Fcer1g*), was unchanged in the Neo and the Neo + 6SL groups compared to the control group. Data are shown as a min to max box + whisker plot; n = 3−5. **(D)** Gene transcription of complement marker C3 (*C3*) was unchanged in the neomycin (Neo) and neomycin groups treated with 6′-siallylactose (Neo + 6SL) compared to the control group (PBS). Transcription levels of complement marker C4b (*C4b*) were higher in the Neo + 6SL group than in the PBS control group. Data are shown as a min to max box + whisker plot; n = 4−5. **(E)** Transcription levels of *Cyba*, *Cybb*, and *Inos/Nos2* were analyzed in whole cochlear homogenates for the oxidative burst pathway. Neither neomycin nor 6SL treatment had any effect on these gene transcripts compared with the PBS control group. Data are shown as a min to max box + whisker plot; n = 5−7. All data were analyzed by one-way ANOVA, Tukey's multiple comparison test, *p <0.05, **p <0.01, ns, not significant.

affected by neomycin or 6SL. Next, we analyzed the proinflammatory cytokine gene transcripts of interleukin 1β (*Il1b*) and tumor necrosis factor-α (*Tnfα*). The transcript levels of *Il1β* were higher in the Neo group than in the Neo + 6SL group (Figure 3B). In detail, gene transcription of *Il1b* was increased from 1.22 ± 0.8 FC to 1.92 ± 1.36 FC (p = 0.366) by treatment with Neo, an effect that was reverted in the Neo + 6SL group (0.56 ± 0.2 FC, p = 0.043). In contrast, *Tnfα* transcript levels showed no change. We further checked for gene transcription of phagocytic markers, such as the DNAX activating protein 12 kDa (*Dap12*) and the immunoreceptor tyrosine-based activation motif (ITAM)-

signaling Fc fragment of IgE, high affinity I receptor for gamma polypeptide (*Fcer1g*). For both genes, no changes were observed between the groups (Figure 3C). Since it is known that the complement system is involved in certain phagocytic processes led by macrophages, we also examined two key complement factors. While the transcription of complement factor *C3* was not affected by neomycin treatment, we observed an upregulation in *C4b* transcript levels after Neo treatment, which was elevated in the Neo + 6SL group compared to that in the PBS control group (Figure 3D). To understand the mechanistic link between immune activation and toxicity, we checked the transcription levels of

markers of oxidative pathways. Neither the transcription levels of *Cyba* and *Cybb*, the genes encoding for the subunits of NADPH oxidase 2 (nicotinamide adenine dinucleotide phosphate oxidase) or *iNos/Nos2*, were changed in the whole inner ear two weeks after the end of treatment (Figure 3E).

Reduced hearing ability could be a result of an increased number of dying cells in the inner ear. Although morphologically dying cells are difficult to detect, we wondered whether certain markers were increased after neomycin treatment. Therefore, we examined the gene transcripts involved in apoptosis and necroptosis by analyzing the transcription of the apoptosis marker fas associated via death domain (*Fadd*), phosphatidylinositol-4,5-bisphosphate 3-kinase catalytic subunit delta (*Pik3cd*), and caspase 8 (*Casp8*) (Figure 4A), and the necroptosis markers mixed lineage kinase domain like pseudokinase (*Mlkl*) and receptor-interacting serine/threonine-protein kinase 1 (*Ripk1*) (Figure 4B), in the whole inner ear. *Pik3cd* showed an upregulation after neomycin treatment compared to the PBS group (from 1.17 ± 0.6 FC to 2.47 ± 0.5 FC, p = 0.004) that was completely prevented in the therapy Neo + 6SL group (0.988 ± 0.4 FC, p = 0.002). Interestingly, gene transcript of the necroptotic pathway for *Mlkl* (1.1 ± 0.5 FC to 2.93 ± 2.35 FC, p = 0.108) showed a tendency for decreased levels in the Neo + 6SL group compared to the Neo group, (0.85 ± 0.2 FC, p = 0.079; Figure 4B).

In summary, the data showed upregulation of *Aif1* and *Pik3cd* gene transcription in the inner ear in the Neo group, which was reversed in the Neo + 6SL therapy group.

3.4 Neomycin- and 6'-sialyllactose-induced changes in sialylation-related gene transcripts

Aminoglycoside treatment has been shown to downregulate enzymes involved in sialylation in human podocytes (24, 25). Therefore, we analyzed the transcript levels of several genes involved in de- and re-sialylation, including glucosamine-2-epimerase/N-acetylmannosamine kinase (*Gne*), neuraminidases 1 and 3 (*Neu1* and *Neu3*), sialyltransferases ST3 beta-galactoside alpha-2,3-sialyltransferase 5 (*St3gal5*), ST6 beta-galactoside alpha-2,6-sialyltransferase 1 (*St6gal1*), ST6 N-acetylgalactosaminide alpha-2,6-sialyltransferase 2 (*St6galnac2*), and polysialyltransferase ST8 alpha-N-acetyl-neuraminide alpha-2,8-sialyltransferase 1 (*St8sia1*). Transcription of *Gne*, the essential enzyme in sialic acid biosynthesis, and transcription of *Neu1* were not affected by neomycin treatment or therapy with 6SL. However, we found increased transcription of neuraminidase 3 (*Neu3*) in the neomycin-treated group compared with the PBS control group (Figure 5). In detail, gene transcription of *Neu3* was increased from 0.86 ± 0.4 FC to 2.43 ± 1.7 FC in the Neo
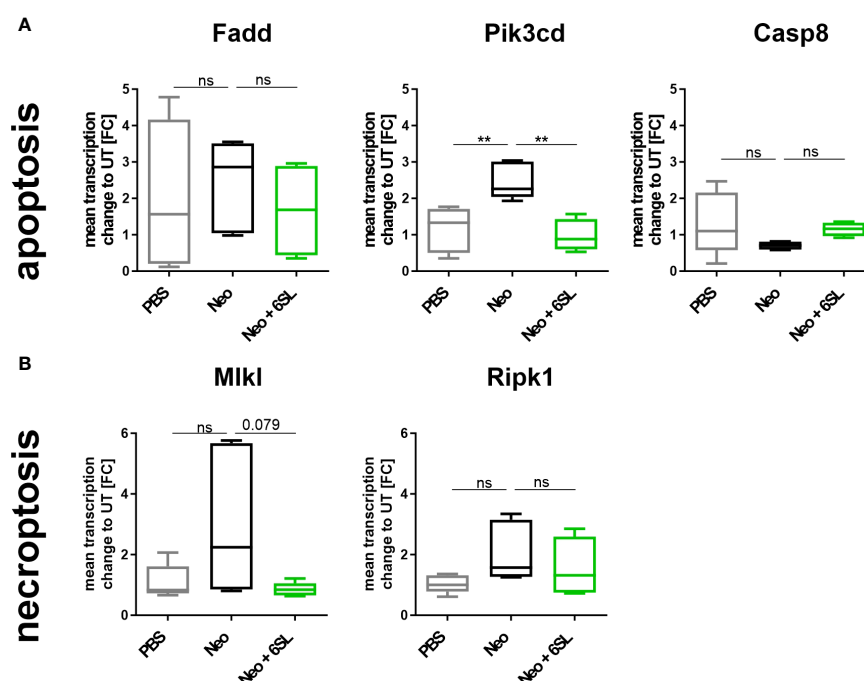

FIGURE 4
Effects of neomycin and 6'-sialyllactose on the apoptotic and necroptotic pathway-related gene transcription. **(A)** Transcription of the apoptosis pathway-related genes associated with the death domain (*Fadd*), phosphatidylinositol-4,5-bisphosphate 3-kinase catalytic subunit delta (*Pik3cd*), and caspase 8 (*Casp8*) were analyzed. Only the apoptosis/inflammation-related *Pik3cd* was elevated in whole cochlea homogenates of neomycin-treated mice (Neo) compared to the PBS control group and was reversed after additional treatment with 6'-sialyllactose (Neo + 6SL). Data are shown as a min to max box + whisker plot; n = 4−6. **(B)** Transcription of the necroptosis-related genes mixed lineage kinase domain like pseudokinase (*Mlkl*) and receptor-interacting serine/threonine-protein kinase 1 (*Ripk1*) showed no difference among the groups, although *Mlkl* tended to decrease in the Neo + 6SL group compared to the Neo group. Data are shown as a min to max box + whisker plot; n = 4−6. All data were analyzed by one-way ANOVA, Tukey's multiple comparison test, **p <0.01, ns, not significant.
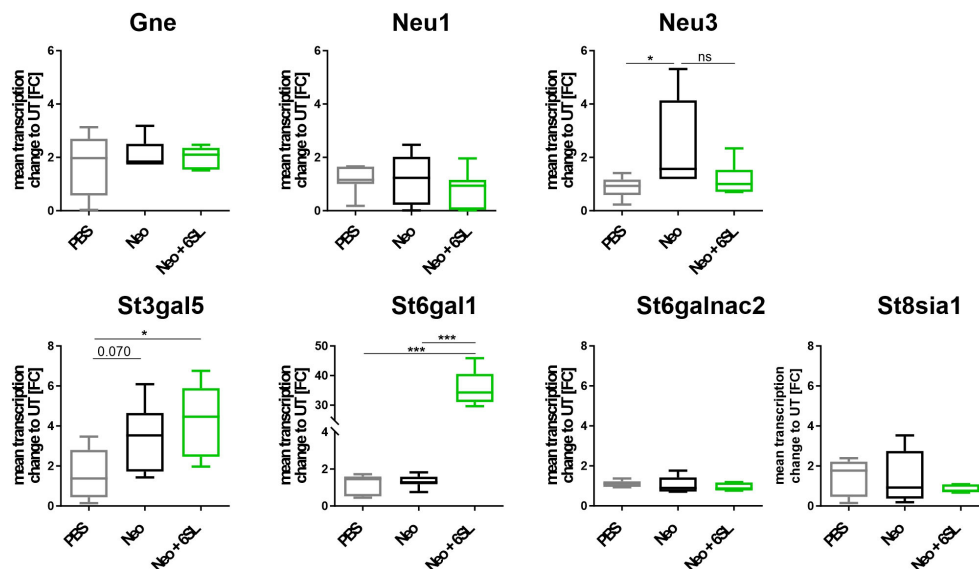
FIGURE 5
Neomycin and 6SL-induced changes of the sialylation-related genes transcript. The transcription levels of different genes in the sialylation regulation pathway were analyzed by qRT-PCR. Gene transcription of glucosamine-2-epimerase/N-acetylmannosamine kinase (*Gne*) and neuraminidase 1 (*Neu1*) in the cochlea were not affected by neomycin treatment, whereas the transcription level of neuraminidase 3 (*Neu3*) was upregulated in the neomycin group (Neo) compared to the PBS group. Gene transcription of the sialyltransferases *St3gal5* and *St6gal1* was upregulated in the Neo + 6SL group compared to that in the PBS control group. Transcription levels were not altered in the sialyltransferase *St6galnac* or polysialyltransferase *St8sia1*. Data are shown as a min to max box + whisker plot; n = 5–8. All data were analyzed using one-way ANOVA, Tukey's multiple comparison, *p <0.05, ***p <0.001, ns, not significant.

group compared to the control group (p = 0.041), while 6SL tended to revert this increase to 1.17 ± 0.6 FC in the Neo + 6SL group (p = 0.127 Neo + 6SL vs. Neo group). Interestingly, the gene transcripts of two sialyltransferases (*St3gal5* and *St6gal1*) were upregulated after Neo + 6SL treatment (Figure 5).

In summary, the data showed an increase after Neo treatment in the transcription of neuraminidase *Neu3*, an enzyme involved in desialylation, and a Neo+6SL-dependent increase in sialyltransferase *St3gal5* and *St6gal1* gene transcription.

3.5 6′-sialyllactose inhibited inflammatory and neurotoxic effects of human macrophages

As our data indicated an inflammation-related mechanism of 6SL, we analyzed the effect of 6SL on human THP1 macrophages *in vitro*. Upon inflammatory stimulation with lipopolysaccharides (LPS), phagocytic activity increases in macrophages. Accordingly, we analyzed the effect of 6SL on the phagocytosis of beads by human THP1 macrophages challenged with LPS. The THP1 cells were differentiated into macrophage-like cells and stimulated with LPS. Using a bead phagocytosis assay, the percentage of cells that phagocytosed two or more beads was determined by flow cytometry (Figure 6A). While 6SL alone did not affect baseline phagocytosis, 6SL was able to reduce the LPS-increased phagocytosis rate of human macrophages in a dose-dependent manner (Figure 6B). In detail, LPS stimulation increased the phagocytic uptake of THP1 cells from 100% in untreated cells to 199.07% ± 71.33% (p = 0.020),

whereas the addition of 5 µM 6SL alone (control) resulted in 122.79% ± 53.11% of phagocytosis rate. The LPS-induced increase in phagocytosis was reverted after treatment of macrophages with 0.05µM 6SL (189.41% ± 57.14%), with 0.15 µM 6SL (187.24% ± 49.27%), with 0.5µM 6SL (113.27% ± 43.64%), with 1.5µM 6SL (109.31% ± 33.76%; p = 0.059) or with 5µM 6SL (87.45% ± 8.68%; p = 0.008).

Another important defense mechanism of activated phagocytes is the release of reactive oxygen species (ROS), which is also triggered in macrophages cultured with LPS. In this study, 6SL was able to prevent the LPS-triggered oxidative burst of human macrophages, similar to the anti-oxidative enzyme superoxide dismutase 1 (SOD1) and the radical scavenger Trolox, a vitamin E analog (Figure 6C). In detail, the relative mean staining intensity of the superoxide marker dihydroethidium (DHE) was increased from 1.0 ± 0.3 in untreated THP1 cells to 1.64 ± 0.26 in cells stimulated with 3 µg/ml LPS (p = 0.008). The addition of 5 µM 6SL alone did not result in a change in the relative DHE staining intensity (1.02 ± 0.1). Treatment with 5 µM 6SL in LPS-stimulated cells reverted the relative DHE intensity to 1.14 ± 0.25 (vs. LPS; p = 0.051), similarly as the addition of the anti-oxidative enzyme SODs (1.07 ± 0.23; vs. LPS, p = 0.020) and the radical scavenger Trolox (1.18 ± 0.3; vs. LPS, p = 0.095).

Next, we analyzed the effect of 6SL on the transcription of inflammatory genes in human THP1 macrophages (Figure 6D). Transcription level of the pro-inflammatory cytokine interleukin 1β (*IL1B*) was increased after LPS stimulation to 3.12 ± 1.20 FC (p = 0.014) from 1.0 FC in untreated cells. Treatment with 6SL reduced the *IL1B* gene transcription from 3.12 ± 1.20 FC to 1.20 ± 0.55 FC (+
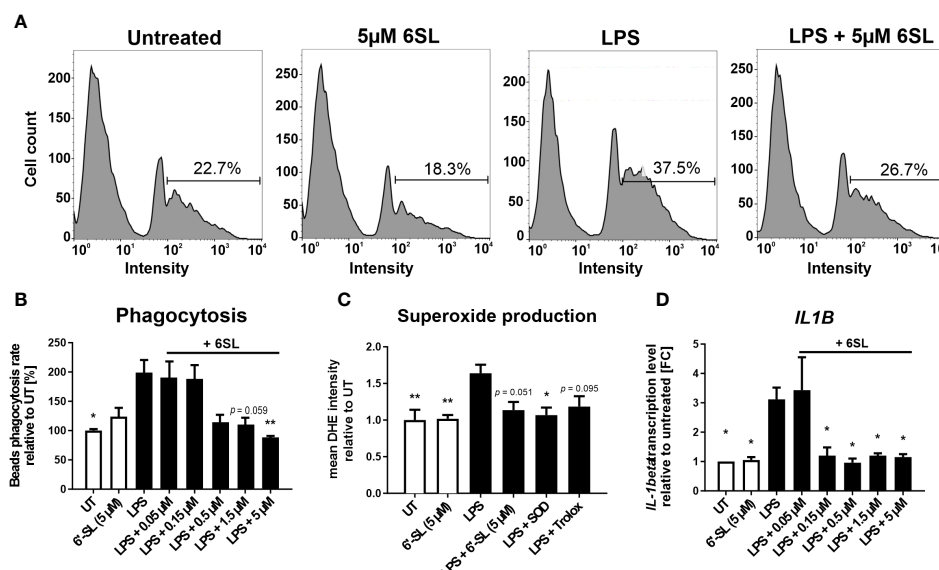
FIGURE 6

Anti-inflammatory and anti-oxidative effects of 6'-sialyllactose on cultured human THP1 macrophages. **(A)** Phagocytic uptake of microbeads by THP1 macrophages was analyzed using flow cytometry. A representative flow cytometric analysis of the four experimental groups is shown. The peak at the lowest intensity in each graph (intensity 1−10) represents the cells with no beads, and the peak at the next highest intensity (~40−80) represents the cells having taken up one bead. The percentage of cells with two or more beads was determined (percentage of cells showing an intensity of >90). LPS treatment was used to activate the phagocytic activity of THP1 macrophages. 6SL reduces the LPS-triggered phagocytic activity of THP1 macrophages. **(B)** Quantification of the phagocytic uptake of microbeads by THP1 macrophages was normalized to the untreated (UT) condition and revealed an increase after LPS treatment. Parallel treatment with 5 μM 6SL reduced LPS-induced increase in bead phagocytosis by human macrophages (THP1). Data are shown as mean $\pm$ SEM; n = 4−11; one-way ANOVA, Dunnett's T3 *post-hoc* comparison; *p $\leq$0.05, **p $\leq$0.01. **(C)** Superoxide production was determined using dihydroethidium (DHE). Flow cytometry of human macrophages (THP1) showed increased superoxide production after lipopolysaccharide (LPS) stimulation. Treatment with 6SL tended to prevent LPS-triggered superoxide production to a similar degree as the antioxidant superoxide dismutase 1 (SOD) and the vitamin E analog Trolox. Data are shown as the mean $\pm$ SEM; n = 5; one-way ANOVA, Tukey *post-hoc* comparison, *p $\leq$0.05, **p $\leq$0.01. **(D)** Human macrophages (THP1) were stimulated with lipopolysaccharide (LPS) for 24 h. Transcription of the proinflammatory marker interleukin 1β (*IL1B*) was upregulated after LPS treatment, whereas simultaneous 6SL treatment attenuated the LPS-induced inflammatory effect. Data are shown as the mean $\pm$ SEM; n = 3−9; one-way ANOVA, Dunnett's T3 *post-hoc* comparison, *p $\leq$0.05.

0.15 μM 6SL; p = 0.047), to 0.96 ± 0.32 FC (+ 0.5 μM 6SL; p = 0.011), to 1.20 ± 0.15 FC (+ 1.5 μM 6SL; p = 0.024) and to 1.15 ± 0.18 FC (+ 5 μM 6SL; p = 0.021).

Microglia and macrophages remove debris or dying cells from their environment, thus helping to maintain homeostasis in the tissue. In this study, we mimicked the interplay of macrophages in the peripheral nervous system using human induced pluripotent stem cell (iPSC)-derived peripheral sensory neurons to understand the anti-inflammatory effect of 6SL in a more complex *in vitro* environment. While co-culturing sensory neurons with macrophages resulted in reduced neural branch length, 6SL treatment of sensory neurons without macrophages did not affect the neurite length. However, treatment with 6SL prevented the neurotoxic effects of human macrophages in co-culture with human iPSC-derived peripheral sensory neurons (Figure 7). In detail, the relative neural branch length (1.0 ± 0.08) was decreased to 0.64 ± 0.14 when co-cultured with THP1 macrophages (p ≤0.001) but was not affected when neurons were incubated with 6SL (0.99 ± 0.12), or less reduced when simultaneously treated with 6SL (0.86 ± 0.08; p = 2.77).

In summary, 6SL exhibited anti-inflammatory and neuroprotective effects in human macrophages.

4 Discussion

Aminoglycosides are potent antibiotics with nephrotoxic and ototoxic effects. Although their use has declined in industrialized countries with the emergence of cephalosporins, aminoglycosides have re-emerged for widespread use after the rise of multidrug-resistant bacteria (6). Neomycin belongs to the class of aminoglycosides that are highly nephrotoxic and ototoxic (26). In this study, we analyzed 6SL as a potential treatment for preventing aminoglycoside-related ototoxicity in a neomycin-induced hearing loss mouse model.

We observed that consecutive subcutaneous injections of neomycin resulted in ototoxicity, as determined by the elevated ABR thresholds (Neo group). The mouse cochlea is susceptible to aminoglycoside ototoxicity in the sensitive postnatal period up to an age of 20 days (27). Typically, neomycin-induced ototoxicity mainly targets the structures of the organ of Corti, particularly the hair cells, including their sensory neural innervations, starting with the outer hair cells, followed by the inner hair cells (28). Damage first occurs in the basal turn of the cochlea and then progresses to the middle and apical regions (29). Thus, hearing loss first occurs at higher tone frequencies (located in the basal region) and then
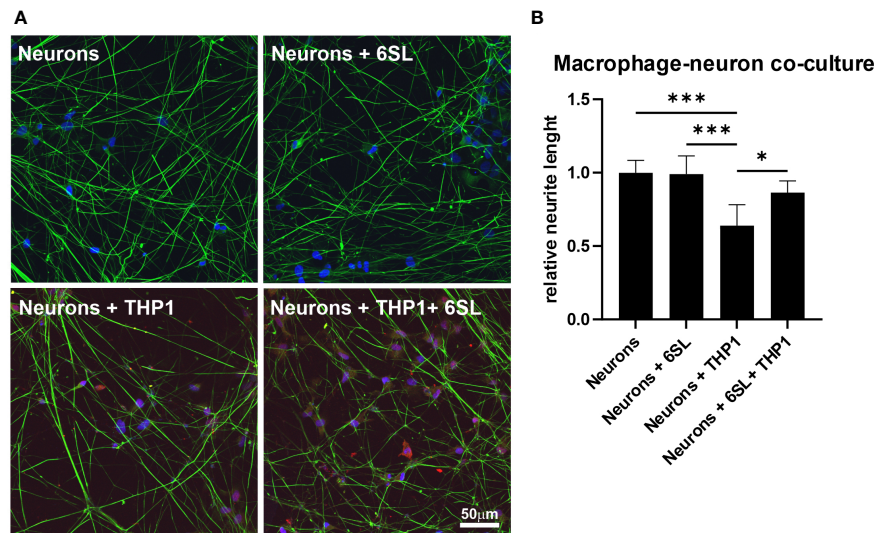
FIGURE 7
Neuroprotection of sensory neurons against macrophage-mediated neurite loss by 6'-sialyllactose. **(A)** Human sensory neurons (shown in green) were obtained from human induced pluripotent stems (iPSCs) and co-cultured with human macrophages (THP1, shown in red). Neurons or neurons co-cultured with THP1 macrophages were treated with 6'-Sialyllactose (6SL). The cellular nuclei were stained with DAPI (blue). The addition of THP1 macrophages to sensory neurons reduced overall neurite length. Scale bar: 50 µM. **(B)** Quantification of neurite length revealed no effect of 6SL treatment on the relative neurite length, while the addition of THP1 cells reduced the relative neurite length. Treatment with 6SL prevented the loss of neurite length in a co-culture of neurons and macrophages. Data are presented as mean $\pm$ SD, and data were collected from at least six images of repeated experiments; one-way ANOVA, Bonferroni *post-hoc* comparison, *p $\leq$0.05, ***p $\leq$0.001.

extends to lower tone frequencies (29). ABR testing is an objective method for evaluating auditory pathways. In our study, we confirmed in our study, that neomycin application had a detrimental effect on the auditory pathways, resulting in elevated hearing thresholds 14 days after the end of treatment for all frequencies tested.

The ABR thresholds were less impaired when 6SL was applied simultaneously with neomycin as therapy (Neo + 6SL group). In particular, hearing thresholds were less elevated in the Neo + 6SL therapy group, but this effect varied between tone frequencies. For the highest frequency tested, we could not see a difference between the Neo and the Neo + 6SL therapy groups; threshold levels for lower frequencies were decreased after 6SL treatment and reached almost baseline levels (6 kHz). Because aminoglycoside ototoxicity is thought to be related to an oxidative burst, basal cells operating at higher frequencies appear to be highly susceptible to damage (30). Thus, it is possible that the damage to higher-frequency regions of the cochlea was too severe to be rescued by the protective effects of 6SL. Accordingly, we performed a more detailed analysis of the ABR wave I components, which have been described to be similar in small mammals and humans, and to reflect the VIII cranial nerve activity (31). The ABR thresholds were less elevated (Figure 1C) and ABR wave I latency reached control values at stronger activation (Figure 1E), suggesting that the activity in the peripheral auditory nerve of the Neo + 6SL group was less affected than that of the Neo group. It has been shown in age-related cochlear synaptopathy in mice that ABR wave I amplitudes correlate with the number of inner hair cell ribbons, while inner hair cell counts remain consistent across different ages (32). Thus, we cannot fully interpret our ABR wave I amplitude data without the

quantification of hair cell numbers. Unfortunately, our histological analysis to quantify hair cell numbers in P28–P30 old mice failed because of insufficient preservation of the whole hair cell lining from the basal to the apical cochlea.

Macrophages are widely distributed in various sites of the cochlea, which are important for maintaining cochlear homeostasis (33, 34), similar to the homeostatic activity of microglia in the brain (35). Upon insult, cochlear macrophages become activated, changing their abundance, distribution, and morphology (35). Furthermore, macrophages also invade the cochlea from blood monocytes upon inner ear injury (36). Thus, the timely control of macrophage activation and/or invasion is necessary to limit inflammatory hair cell damage. There are different types of macrophages invading the inner ear, depending on the type of injury. In response to aminoglycoside ototoxicity, local CX3CR1 macrophages increase in number in the inner ear, while systemic LPS exposure increases the number of CCR2-expressing macrophages typically derived from blood monocytes (37). Studies have also shown that neomycin exposure leads to increased levels of inflammatory cytokines (7, 38).

Sialic acid-binding immunoglobulin-like lectin (Siglec) receptors sense sialylated glycostructures and are widely expressed in macrophages (39, 40). Most Siglec receptors mediate inhibitory signaling via their immunoreceptor tyrosine-based inhibition motif (ITIM) (41). Upon recognition of sialylation on neighboring cells by the Siglec receptors of mononuclear phagocytes, inhibitory Siglec-ITIM signaling leads to downregulation of the pro-inflammatory pathways in phagocytes (21, 42).

We demonstrated that 6SL dampened the cochlear macrophage immune response in neomycin-treated mice.

Immunohistochemical evaluation showed increased macrophage numbers in the Rosenthal's canal, the region where the cell bodies of the sensory neural innervations are located, in Neo-treated mice that were reverted to almost normal levels by 6SL (Neo + 6SL group). Data on inflammation-related *Aif1* and *Pik3cd* gene transcription in the whole cochlea supported the increased macrophage immune response observed in the spiral ganglion after Neo treatment, which was reversed by treatment with 6SL in the Neo + 6SL group. Several studies have elucidated the release of inflammatory mediators by activated macrophages associated with cochlear damage. Damaged tissues release damage-associated molecular patterns (DAMPs), which in turn act on pattern recognition receptors and result in a pro-inflammatory signature (34). Toll-like receptor 4 (TLR-4) is a pattern recognition receptor that is activated upon aseptic inflammation and leads to canonical activation of the NF-kB pathway, which subsequently promotes the release of pro-inflammatory cytokines such as Il-1β (34). In our study, the transcripts of the inflammatory marker *Aif1/Iba1* were elevated in the Neo group and returned to normal levels in the Neo + 6SL group. Likewise, transcripts of the pro-inflammatory cytokine Il-1β tended to increase in the Neo group, which was significantly returned to normal levels in the Neo + 6SL group, demonstrating the anti-inflammatory effect of 6SL.

An elevation in the ABR threshold in neomycin-treated mice, especially prominent at high frequencies, was described in a previous study (7). Sun et al. showed that in neomycin-treated mice, cochlear macrophages were recruited into the Organ of Corti, particularly in the middle and basal cochlear turns. Although treatment with the broad tetracycline antibiotic minocycline decreased the number of macrophages in the hair cell area and ABR thresholds in neomycin-treated mice, this treatment failed to rescue the outer and inner hair cell damage (7).

As a potential therapy, we tested whether the sialic acid carrier 6'-sialyllactose can ameliorate cochlear immune activation in neomycin-treated mice and protect against neomycin-induced hearing loss, as determined by measurement of ABR thresholds. In our study, we showed that 6SL therapy reverted the inner ear immune activation caused by neomycin insult, as reflected in the spiral ganglia by decreased macrophage number and/or activation, as well as lower pro-inflammatory gene transcription levels in the inner ear. We further showed that macrophage numbers reverted to normal levels in the therapy group (Neo + 6SL group), indicating a strong therapeutic effect similar to that of minocycline (7).

At the inner ear transcriptional level, we found an elevation in the apoptotic marker *Pik3cd* gene in the Neo-treated group, while the necroptotic markers showed no change between the different groups. In particular, apoptosis-related *Pik3cd* gene transcription was elevated in whole cochlea homogenates of neomycin-treated mice (Neo) compared to the PBS control group and was reversed after additional treatment with 6SL (Neo + 6SL). The *Pik3cd* gene contributes to the production of phosphatidylinositol 3-kinase (PI3K), which is expressed in macrophages and controls survival and apoptosis. While PI3K is undetectable in the resting state of cells, it substantially increases upon cellular stimulation (43). Furthermore, PI3K signaling was implicated in the promotion of hair cell survival after aminoglycoside exposure, and it has been shown that the inhibition of the PI3K signaling protein, PDK1, sensitized hair cells to gentamicin, but not to neomycin toxicity (44, 45). In line with our data, Ding et al. also reported that Fadd-mediated caspase-8 apoptosis does not play a role in aminoglycoside toxicity (46), which might explain why we have not observe an increase in other apoptotic markers such as Fadd and caspase-8.

To examine whether the complement system was involved in the Neo or the Neo + 6SL therapy group, we tested the transcription levels of different complement genes in the inner ear. Complement factor C3 is a critical node in all complement activation pathways. Complement factor C4b is only involved in the classical or lectin complement pathways (47). Interestingly, we found an elevation in the gene transcription of complement factor C4b in the Neo + 6SL therapy group, but there was no significant change in the C3 transcript among the three groups.

The mechanism underlying aminoglycoside-induced ototoxicity is not fully understood. The widely proposed mechanism involves the accumulation of reactive oxygen species (ROS) in the cochlea, which leads to apoptosis and cell death. Free radicals attack the cell membranes, proteins, and DNA, leading to lipid peroxidation, causing irreversible cell damage and cell death. Particularly, it has been shown that perivascular macrophage-like melanocytes in the lateral cochlear wall can produce radicals in response to injury, which in turn recruit blood monocytes (48). Thus, preventing oxidative stress might inhibit macrophage invasion from blood monocytes, and thereby could be helpful in preventing hearing loss, as elucidated earlier. Furthermore, the formation of iron-aminoglycoside complexes might be a possible factor leading to oxidative stress (49). Data from experimental and clinical studies have shown a positive effect of antioxidants, such as thymoquinone (50), aspirin (51), N-acetylcysteine, and vitamin A (52). In addition, flavonoids, such as naringenin, seem to reduce free radical formation after aminoglycoside treatment (53). However, to date, no agent has been approved for the clinical treatment of aminoglycoside-induced ototoxicity.

Sialic acid is known to scavenge free radicals locally (12, 54, 55). Sialic acid is a naturally occurring carbohydrate on our cellular glycocalyx, which is integrated in a terminal position in glycoproteins and glycolipids on the cell surface, acts as an immune checkpoint, and helps to maintain the immune system in a homeostatic state (10). Milk oligosaccharide 6'-sialyllactose is a natural sialic acid carrier that is already used in infants as a sialic acid source for early brain development, when an additional exogenous supply of sialic acid is needed to build up the glycocalyx of the brain (13).

To understand whether neomycin treatment or 6SL therapy interfered with the sialylation and desialylation process of the inner ear, we measured the transcriptional levels of different sialidases and sialyltransferases. While sialyltransferases add sialic acid residues to the carbohydrate chains of proteins and lipids in the endoplasmic reticulum, sialidases/neuraminidases remove sialic acids from glycoproteins and glycolipids (56). We observed increased neuraminidase 3 transcription in the Neo group, suggesting increased cleavage of sialic acids from gangliosides, which tended to revert in the Neo + 6SL treatment group. Interestingly,

transcription of the ST6GAL1 sialyltransferase, which is an enzyme that typically catalyzes α2,6-sialylated milk and has activity towards lactose (57), was also increased in the Neo + 6SL group compared to the wild-type control and Neo group, suggesting an indirect effect on sialylation via 6SL uptake. In line with this finding, transcription of the ST3GAL5 sialyltransferase, which contributes to the formation of GM3 ganglioside, a precursor of several gangliosides (58) was also elevated in the Neo + 6SL group, while it remained unchanged in the Neo group compared to the wild-type control. It has been shown that GM3 is expressed in all cochlear regions, but only distinctly in the stria vascularis, spiral ganglion, and organ of Corti. GM3 synthase-deficient mice had a deformed organ of Corti and complete hearing loss, while maintaining normal stria vascularis function and normal structure of other cochlear regions (59). These data suggest that 6SL supplementation can indeed alter the cellular sialylation process and might contribute to increased formation of gangliosides, possibly allowing resialylation and strengthening of sialic acid checkpoints for immune cells and maintaining the structure of the organ of Corti.

In human podocytes, treatment with the aminonucleoside puromycin resulted in the loss of sialic acid from proteins, which was accompanied by a reduction in the expression of sialyltransferases. Interestingly, sialic acid supplementation rescued the sialylation of podocyte proteins and partially restored the expression of sialyltransferases (24).

In vitro, we were also able to demonstrate the dose-dependent anti-inflammatory and anti-phagocytic effects of 6SL on cultured human macrophages stimulated with lipopolysaccharide (LPS), a typical pro-inflammatory stimulus. Increasing concentrations of 6SL reduced the transcription of the pro-inflammatory marker Il-1β and phagocytic activity in LPS-treated human macrophages to levels similar to those in untreated cells. In both cases, 6SL alone had no effect on human macrophages. Moreover, we also showed the anti-oxidative effects of 6SL on cultured human macrophages, where it had similar effects on macrophages as the antioxidants superoxide dismutase 1 (SOD) and the vitamin E analog Trolox. Interestingly, it has been shown that SOD1 deficient mice show premature age-related hearing loss, and antioxidants such as vitamins C and E have hearing preservative effects (60). Thus, we showed a clear hallmark of a therapeutic approach that focuses on macrophages. Furthermore, we directly demonstrated the neuronal protective effect of 6SL on macrophage toxicity by showing neurite length preservation in an *in vitro* model of human macrophage-neuronal co-culture. Similar neuroprotective effects have been described with polymers of sialic acids with an average degree of polymerization of 20 (61), demonstrating the general anti-inflammatory and antioxidative properties of sialylated oligo/polysaccharides on macrophages.

In summary, neomycin leads to an increased ABR threshold in mice as a sign of functional hearing loss as well as increased inflammation in the inner ear. The results obtained in this study show that 6SL treatment can partially restore impaired hearing function in neomycin-treated mice and reverse inner ear inflammation. Our study also demonstrated the *in vitro* anti-inflammatory effects of 6SL on human macrophages as well as its anti-phagocytic and anti-oxidative properties, along with its protective ability in human neurons.

Data availability statement

The original contributions presented in the study are included in the article/Supplementary Material. Further inquiries can be directed to the corresponding author.

Ethics statement

Ethical approval was not required for the studies on humans in accordance with the local legislation and institutional requirements because only commercially available established cell lines were used. The animal study was approved by Dr. Laura Gey, Universitätsklinikum Bonn, Haus für Experimentelle Medizin (HET), Venusberg-Campus 1, 53127 Bonn, Germany. The study was conducted in accordance with the local legislation and institutional requirements.

Author contributions

TA: Conceptualization, Investigation, Writing – original draft, Writing – review & editing, Methodology. TK: Methodology, Writing – original draft, Writing – review & editing, Investigation. TS: Investigation, Methodology, Writing – review & editing. AS: Investigation, Methodology, Writing – review & editing. HN: Writing – review & editing, Conceptualization, Funding acquisition, Project administration, Writing – original draft. CK: Conceptualization, Writing – original draft, Writing – review & editing, Data curation, Formal Analysis, Investigation, Project administration.

Conflict of interest

CK, AS, and HN are named inventors on a submitted patent patent family to WO2019115374 related to use of 6SL for hearing loss owned by the University of Bonn.

The remaining authors declare that the research was conducted in the absence of any commercial or financial relationships that could be construed as a potential conflict of interest.

Publisher's note

All claims expressed in this article are solely those of the authors and do not necessarily represent those of their affiliated organizations, or those of the publisher, the editors and the reviewers. Any product that may be evaluated in this article, or claim that may be made by its manufacturer, is not guaranteed or endorsed by the publisher.

Supplementary material

The Supplementary Material for this article can be found online at: https://www.frontiersin.org/articles/10.3389/fimmu.2023.1264060/full#supplementary-material

References

1. Wilson BS, Tucci DL, O'Donoghue GM, Merson MH, Frankish H. A Lancet Commission to address the global burden of hearing loss. *Lancet* (2019) 393 (10186):2106–8. doi: 10.1016/S0140-6736(19)30484-2

2. Bako P, Gerlinger I, Wolpert S, Müller M, Löwenheim H. The ototoxic effect of locally applied kanamycin and furosemide in Guinea pigs. *J Neurosci Methods* (2022) 372:109527. doi: 10.1016/J.JNEUMETH.2022.109527

3. Yang C-H, Schrepfer T, Schacht J, Coffin AB, Steyger PS. Age-related hearing impairment and the triad of acquired hearing loss. *Front Cell Neurosci* (2015) 9:276. doi: 10.3389/fncel.2015.00276

4. Lee MY, Park Y-H. Potential of gene and cell therapy for inner ear hair cells. *BioMed Res Int* (2018) 2018:1–11. doi: 10.1155/2018/8137614

5. Roth TN. Aging of the auditory system. *Handbook of Clinical Neurology. 129* (2015) 129:357–73. doi: 10.1016/B978-0-444-62630-1.00020-2

6. Krause KM, Serio AW, Kane TR, Connolly LE. Aminoglycosides: an overview. *Cold Spring Harbor Perspect Med* (2016) 6(6):a027029. doi: 10.1101/CSHPERSPECT.A027029

7. Sun S, Yu H, Yu H, Honglin M, Ni W, Zhang Y, et al. Inhibition of the activation and recruitment of microglia-like cells protects against neomycin-induced ototoxicity. *Mol Neurobiol* (2014) 51(1):252–67. doi: 10.1007/s12035-014-8712-y

8. Aran JM, Darrouzet J, Erre JP. Observation of click-evoked compound viii nerve responses before, during, and over seven months after kanamycin treatment in the Guinea pig. *Acta Oto-Laryngologica* (1975) 79:24–32. doi: 10.3109/00016487509124650

9. Klaus C, Liao H, Allendorf DH, Brown GC, Neumann H. Sialylation acts as a checkpoint for innate immune responses in the central nervous system. *Glia* (2021) 69 (7):1619–36. doi: 10.1002/GLIA.23945

10. Liao H, Klaus C, Neumann H. Control of innate immunity by sialic acids in the nervous tissue. *Int J Mol Sci* (2020) 21(15):5494. doi: 10.3390/IJMS21155494

11. Shahraz A, Lin Y, Mbroh J, Winkler J, Liao H, Lackmann M, et al. Low molecular weight polysialic acid binds to properdin and reduces the activity of the alternative complement pathway. *Sci Rep* (2022) 12(1):5815. doi: 10.1038/S41598-022-09407-2

12. Iijima R, Takahashi H, Namme R, Ikegami S, Yamazaki M. Novel biological function of sialic acid (N-acetylneuraminic acid) as a hydrogen peroxide scavenger. *FEBS Lett* (2004) 561(1–3):163–6. doi: 10.1016/S0014-5793(04)00164-4

13. Corona L, Lussu A, Bosco A, Pintus R, Marincola FC, Fanos V, et al. Human milk oligosaccharides: A comprehensive review towards metabolomics. *Children* (2021) 8(9):804. doi: 10.3390/CHILDREN8090804

14. Röhrig CH, Choi SSH, Baldwin N. The nutritional role of free sialic acid, a human milk monosaccharide, and its application as a functional food ingredient. *Critic Rev Food Sci Nutrit* (2017) 57(5):1017–38. doi: 10.1080/10408398.2015.1040113

15. Nöhle U, Schauer R. Metabolism of sialic acids from exogenously administered sialyllactose and mucin in mouse and rat. *Hoppe-Seyler's Z Fur Physiologische Chemie* (1984) 365(12):1457–68. doi: 10.1515/BCHM2.1984.365.2.1457

16. Phipps KR, Baldwin NJ, Stannard DR, Šoltésová A, Gilby B, Mikš MH, et al. Toxicological safety evaluation of the human-identical milk oligosaccharide 6′-sialyllactose sodium salt. *J Appl Toxicol* (2019) 39:10. doi: 10.1002/jat.3830

17. Strenzke N, Chakrabarti R, Al-Moyed H, Müller A, Hoch G, Pangrsic T, et al. Hair cell synaptic dysfunction, auditory fatigue and thermal sensitivity in otoferlin Ile515Thr mutants. *EMBO J* (2016) 35(23):2519–35. doi: 10.15252/EMBJ.201694564

18. Rüttiger L, Singer W, Panford-Walsh R, Matsumoto M, Lee SC, Zuccotti A, et al. The reduced cochlear output and the failure to adapt the central auditory response causes tinnitus in noise exposed rats. *PloS One* (2013) 8(3):e57247. doi: 10.1371/JOURNAL.PONE.0057247

19. Suthakar K, Liberman MC. A simple algorithm for objective threshold determination of auditory brainstem responses. *Hearing Res* (2019) 381:107782. doi: 10.1016/J.HEARES.2019.107782

20. Montgomery SC, Cox BC. Whole mount dissection and immunofluorescence of the adult mouse cochlea. *J Visualized Experiments: JoVE* (2016) 107:53561. doi: 10.3791/53561

21. Klaus C, Hansen JN, Ginolhac A, Gérard D, Gnanapragassam VS, Horstkorte R, et al. Reduced sialylation triggers homeostatic synapse and neuronal loss in middle-aged mice. *Neurobiol Aging* (2020) 88:91–107. doi: 10.1016/J.NEUROBIOLAGING.2020.01.008

22. Aminoff D. Methods for the quantitative estimation of N-acetylneuraminic acid and their application to hydrolysates of sialomucoids. *Biochem J* (1961) 81(2):384–92. doi: 10.1042/bj0810384

23. Chambers SM, Qi Y, Mica Y, Lee G, Zhang XJ, Niu L, et al. Combined small-molecule inhibition accelerates developmental timing and converts human pluripotent stem cells into nociceptors. *Nat Biotechnol* (2012) 30(7):715–20. doi: 10.1038/NBT.2249

24. Pawluczyk IZA, Ghaderi Najafabadi M, Patel S, Desai P, Vashi D, Saleem MA, et al. Sialic acid attenuates puromycin aminonucleoside-induced desialylation and oxidative stress in human podocytes. *Exp Cell Res* (2014) 320(2):258–68. doi: 10.1016/j.yexcr.2013.10.017

25. Pawluczyk IZA, Najafabadi MG, Brown JR, Bevington A, Topham PS. Sialic acid supplementation ameliorates puromycin aminonucleoside nephrosis in rats. *Lab Invest* (2015) 95(9):1019–28. doi: 10.1038/LABINVEST.2015.78

26. Macdonald RH, Beck M. Neomycin: a review with particular reference to dermatological usage. *Clin Exp Dermatol* (1983) 8(3):249–58. doi: 10.1111/J.1365-2230.1983.TB01777.X

27. Wu WJ, Sha SH, McLaren JD, Kawamoto K, Raphael Y, Schacht J. Aminoglycoside ototoxicity in adult CBA, C57BL and BALB mice and the Sprague–Dawley rat. *Hearing Res* (2001) 158(1–2):165–78. doi: 10.1016/S0378-5955(01)00303-3

28. Xie J, Talaska AE, Schacht J. New developments in aminoglycoside therapy and ototoxicity. *Hearing Res* (2011) 281(1–2):28–37. doi: 10.1016/J.HEARES.2011.05.008

29. Schacht J. Aminoglycoside ototoxicity: prevention in sight? *Otolaryngology–Head Neck Surg* (1998) 118(5):674–7. doi: 10.1177/019459989811800518

30. Huth ME, Ricci AJ, Cheng AG. Mechanisms of aminoglycoside ototoxicity and targets of hair cell protection. *Int J Otolaryngol* (2011) 2011:1–19. doi: 10.1155/2011/937861

31. Allen AR, Starr A. Auditory brain stem potentials in monkey (M. Mulatta) and man. *Electroencephalography Clin Neurophysiol* (1978) 45(1):53–63. doi: 10.1016/0013-4694(78)90341-3

32. Sergeyenko Y, Lall K, Charles Liberman M, Kujawa SG. Age-related cochlear synaptopathy: an early-onset contributor to auditory functional decline. *J Neurosci* (2013) 33(34):13686–94. doi: 10.1523/JNEUROSCI.1783-13.2013

33. Hu BH, Zhang C, Frye MD. Immune cells and non-immune cells with immune function in mammalian cochleae. *Hearing Res* (2018) 362:14–24. doi: 10.1016/J.HEARES.2017.12.009

34. Zhang Y, Li Y, Fu X, Wang P, Wang Q, Meng W, et al. The detrimental and beneficial functions of macrophages after cochlear injury. *Front Cell Dev Biol* (2021) 9:631904. doi: 10.3389/FCELL.2021.631904

35. Hough K, Verschuur CA, Cunningham C, Newman TA. Macrophages in the cochlea; an immunological link between risk factors and progressive hearing loss. *Glia* (2022) 70(2):219–38. doi: 10.1002/GLIA.24095

36. Sato E, Shick HE, Ransohoff RM, Hirose K. Expression of fractalkine receptor CX3CR1 on cochlear macrophages influences survival of hair cells following ototoxic injury. *JARO: J Assoc Res Otolaryngol* (2010) 11(2):223. doi: 10.1007/S10162-009-0198-3

37. Hirose K, Li SZ, Ohlemiller KK, Ransohoff RM. Systemic lipopolysaccharide induces cochlear inflammation and exacerbates the synergistic ototoxicity of kanamycin and furosemide. *JARO: J Assoc Res Otolaryngol* (2014) 15(4):555. doi: 10.1007/S10162-014-0458-8

38. Limatola C, Ransohoff RM. Modulating neurotoxicity through CX3CL1/ CX3CR1 signaling. *Front Cell Neurosci* (2014) 8:229(AUG). doi: 10.3389/ FNCEL.2014.00229

39. MacAuley MS, Crocker PR, Paulson JC. Siglec-mediated regulation of immune cell function in disease. *Nat Rev Immunol* (2014) 14(10):653–66. doi: 10.1038/NRI3737

40. Tateyama H, Murase Y, Higuchi H, Inasaka Y, Kaneoka H, Iijima S, et al. Siglec-F is induced by granulocyte-macrophage colony-stimulating factor and enhances interleukin-4-induced expression of arginase-1 in mouse macrophages. *Immunology* (2019) 158(4):340–52. doi: 10.1111/IMM.13121

41. Crocker PR, Paulson JC, Varki A. Siglecs and their roles in the immune system. *Nat Rev Immunol* (2007) 7(4):255–66. doi: 10.1038/NRI2056

42. Lübbers J, Rodríguez E, van Kooyk Y. Modulation of immune tolerance via siglec-sialic acid interactions. *Front Immunol* (2018) 9:2807. doi: 10.3389/ FIMMU.2018.02807

43. Rommel C, Camps M, Ji H. PI3K delta and PI3K gamma: partners in crime in inflammation in rheumatoid arthritis and beyond? *Nat Rev Immunol* (2007) 7(3):191–201. doi: 10.1038/NRI2036

44. Jadali A, Kwan KY. Activation of PI3K signaling prevents aminoglycoside-induced hair cell death in the murine cochlea. *Biol Open* (2016) 5(6):698–708. doi: 10.1242/BIO.016758

45. Wiedenhoft H, Hayashi L, Coffin AB. PI3K and inhibitor of apoptosis proteins modulate gentamicin- induced hair cell death in the zebrafish lateral line. *Front Cell Neurosci* (2017) 11:326. doi: 10.3389/FNCEL.2017.00326

46. Ding D, Zhang J, Jiang H, Xuan W, Qi W, Salvi R. Some ototoxic drugs destroy cochlear support cells before damaging sensory hair cells. *Neurotoxicity Res* (2020) 37 (3):743. doi: 10.1007/S12640-020-00170-8

47. Noris M, Remuzzi G. Overview of complement activation and regulation. *Semin Nephrol* (2013) 33(6):479–92. doi: 10.1016/J.SEMNEPHROL.2013.08.001

48. Dai M, Yang Y, Omelchenko I, Nuttall AL, Kachelmeier A, Xiu R, et al. Bone marrow cell recruitment mediated by inducible nitric oxide synthase/stromal cell-derived factor-1alpha signaling repairs the acoustically damaged cochlear blood-labyrinth barrier. *Am J Pathol* (2010) 177(6):3089–99. doi: 10.2353/ AJPATH.2010.100340

49. Sedó-Cabezón L, Boadas-Vaello P, Soler-Martín C, Llorens J. Vestibular damage in chronic ototoxicity: a mini-review. *Neurotoxicology* (2014) 43:21–7. doi: 10.1016/ J.NEURO.2013.11.009

50. Sagit M, Korkmaz F, Gürgen SG, Kaya M, Akcadag A, Ozcan I. The protective role of thymoquinone in the prevention of gentamicin ototoxicity. *Am J Otolaryngol* (2014) 35(5):603–9. doi: 10.1016/J.AMJOTO.2014.07.002

51. Sha S-H, Qiu J-H, Schacht J. Aspirin to prevent gentamicin-induced hearing loss. *New Engl J Med* (2006) 354(17):1856–7. doi: 10.1056/NEJMC053428

52. Aladag I, Guven M, Songu M. Prevention of gentamicin ototoxicity with N-acetylcysteine and vitamin A. *J Laryngology Otology* (2016) 130(5):440–6. doi: 10.1017/ S0022215116000992

53. Koçak S, Aydogan E, Şentürk E, Akakın D, Koroglu K, Özer F. Evaluation of the possible protective role of naringenin on gentamicin-induced ototoxicity: A preliminary study. *Int J Pediatr Otorhinolaryngology* (2017) 100:247–53. doi: 10.1016/J.IJPORL.2017.07.008

54. Eguchi H, Ikeda Y, Koyota S, Honke K, Suzuki K, Gutteridge JMC, et al. Oxidative damage due to copper ion and hydrogen peroxide induces GlcNAc-specific cleavage of an Asn-linked oligosaccharide. *J Biochem* (2002) 131(3):477–84. doi: 10.1093/OXFORDJOURNALS.JBCHEM.A003124

55. Goswami K, Nandakumar DN, Koner BC, Bobby Z, Sen SK. Oxidative changes and desialylation of serum proteins in hyperthyroidism. *Clinica Chimica Acta* (2003) 337(1–2):163–8. doi: 10.1016/j.cccn.2003.08.009

56. Rodriguez-Walker M, Daniotti JL. Human sialidase neu3 is S-acylated and behaves like an integral membrane protein. *Sci Rep* (2017) 7(1):4167. doi: 10.1038/ S41598-017-04488-W

57. Weiss GA, Hennet T. The role of milk sialyllactose in intestinal bacterial colonization. *Adv Nutr (Bethesda Md.)* (2012) 3(3):483S–488S. doi: 10.3945/ AN.111.001651

58. Gordon-Lipkin E, Cohen JS, Srivastava S, Soares BP, Levey E, Fatemi A. ST3GAL5-related disorders: A deficiency in ganglioside metabolism and a genetic cause of intellectual disability and choreoathetosis. *J Child Neurol* (2018) 33(13):825–31. doi: 10.1177/0883073818791099

59. Yoshikawa M, Go S, Takasaki K, Kakazu Y, Ohashi M, Nagafuku M, et al. Mice lacking ganglioside GM3 synthase exhibit complete hearing loss due to selective degeneration of the organ of Corti. *Proc Natl Acad Sci United States America* (2009) 106(23):9483–8. doi: 10.1073/PNAS.0903279106

60. Kishimoto-Urata M, Urata S, Fujimoto C, Yamasoba T. Role of oxidative stress and antioxidants in acquired inner ear disorders. *Antioxidants (Basel Switzerland)* (2022) 11(8):1469. doi: 10.3390/ANTIOX11081469

61. Shahraz A, Kopatz J, Mathy R, Kappler J, Winter D, Kapoor S, et al. Anti-inflammatory activity of low molecular weight polysialic acid on human macrophages. *Sci Rep* (2015) 5:16800. doi: 10.1038/srep16800

3.2 Publication 2: Neuroprotective role of sialic-acid-binding immunoglobulin-like lectin-11 in humanized transgenic mice

| Frontiers in Neuroscience

Check for updates

Neuroprotective role of sialic-acid-binding immunoglobulin-like lectin-11 in humanized transgenic mice

Tawfik Abou Assale[iD][†], Negin Afrang[†], Jannis Wissfeld[iD],
German Cuevas-Rios[iD], Christine Klaus,
Bettina Linnartz-Gerlach[iD][†] and Harald Neumann[iD]*[†]

Institute of Reconstructive Neurobiology, Medical Faculty and University Hospital of Bonn, University of Bonn, Bonn, Germany

Brain aging is a chronic process linked to inflammation, microglial activation, and oxidative damage, which can ultimately lead to neuronal loss. Sialic acid-binding immunoglobulin-like lectin-11 (SIGLEC-11) is a human lineage-specific microglial cell surface receptor that recognizes α-2-8-linked oligo−/polysialylated glycomolecules with inhibitory effects on the microglial inflammatory pathways. Recently, the *SIGLEC11* gene locus was prioritized as a top tier microglial gene with potential causality to Alzheimer's disease, although its role in inflammation and neurodegeneration remains poorly understood. In this study, aged Siglec-11 transgenic (tg) mice, which expressed the human SIGLEC-11 receptor on microglia and tissue macrophages, were investigated. The brains of the Siglec-11 tg mice were analyzed in 6-month-old mature mice and 24-month-old aged mice using immunohistochemistry and transcriptomics. Results showed decreased density and fewer clusters of ionized calcium binding adaptor molecule 1 (Iba1)-positive microglial cells in the hippocampus and substantia nigra, as well as less lipid-laden microglia in the Siglec-11 tg in comparison to wildtype (WT) controls. Additionally, Siglec-11 tg mice exhibited less age-related neuronal loss in the substantia nigra *pars compacta* in comparison to WT mice. Transcriptome analysis revealed suppression of oxidative phosphorylation and inflammatory pathways in Siglec-11 tg brains at 6 months, with further suppression of complement and coagulation cascades at 24 months of age in comparison to WT mice. Gene transcript levels of the pro-inflammatory cytokines *tumor necrosis factor alpha* (*Tnf*) and *interleukin 1 beta* (*Il-1β*) as well as the oxidative stress markers *cytochrome b-245 alpha* and *beta* (*Cyba* and *Cybb*) and the nitric oxide synthase 2 (*Nos2*), were reduced in the brains of 24-month-old Siglec-11 tg mice relative to WT controls. Brains of 24-month-old Siglec-11 tg mice also exhibited lower gene transcription of complement components 3, 4, and integrin alpha M (*C3, C4,* and *Itgam*), along with the complement C1q subcomponents a-c (*C1qa, C1qb,* and *C1qc*). In summary, aged Siglec-11 tg mice displayed reduced brain inflammation and oxidative stress, as well as protection against age-related neuronal loss in the substantia nigra.

KEYWORDS

Siglec-11, aging, microglia, neurodegeneration, neuroinflammation, oxidative stress

Introduction

Brain aging is a complex process that affects various functions and often leads to cognitive decline (Rodrigue and Kennedy, 2011). Common changes in the aging brain include neurodegeneration, accumulation of lipid-laden microglia, impaired synaptic neurotransmission, and a buildup of oxidative damage-related molecules (Lee and Kim, 2022). Microglia, the resident innate immune cells in the central nervous system (CNS), continuously monitor the microenvironment, detecting misfolded protein plaques, damaged or apoptotic cells, and other injured or degenerated materials. Chronic reactive microgliosis and the resulting neuroinflammation have been implicated in age-related neurodegeneration, which can lead to dementia (Luo et al., 2010).

Variants of several SIGLEC genes have been associated with either increased risk or protection against the development of Alzheimer's disease (AD) and dementia (Wißfeld et al., 2024). In addition to the *SIGLEC3/CD33* gene, the *SIGLEC11* gene locus has been identified as a key microglial gene with potential links to AD risk (Bellenguez et al., 2022). Bellenguez et al. (2022) prioritized AD/dementia-associated genes based on their relevance to disease processes, finding *SIGLEC11* to be the most significant microglial gene linked to AD.

Sialic acid-binding immunoglobulin-type lectins (SIGLECs) are recognition receptors that bind sialylated glycoproteins and glycolipids, primarily expressed on immune cells (Macauley et al., 2014). Most CD33-related (CD33r) SIGLECs, including SIGLEC-11, contain one or more immunoreceptor tyrosine-based inhibition motifs (ITIMs) in the cytoplasmic domain. When SIGLEC receptors bind to their sialylated ligands, they typically inhibit signals from immunoreceptor tyrosine-based activation motif (ITAM) receptors, leading to the downregulation of pro-inflammatory immune responses and phagocytosis in microglia and tissue macrophages (Klaus et al., 2021; Wang and Neumann, 2010).

Interestingly, SIGLEC-11 has been identified as a "human-specific microglial receptor," as it is not expressed on the microglia of non-human primates and is almost completely absent in rodents (Angata et al., 2002; Hayakawa et al., 2005; Khan et al., 2020; Wang et al., 2011, 2012). Previous *in vitro* studies showed that SIGLEC-11 preferentially binds to α2-8-linked sialic acid oligomers (oligoSia) and polymers (polySia) (Angata et al., 2002; Hayakawa et al., 2005; Shahraz et al., 2015). Furthermore, SIGLEC-11 reduces microglial neurotoxicity in culture by interacting with the intact oligo-/polysialylated glycocalyx of neighboring cells (Wang and Neumann, 2010).

In this study, we analyzed the effect of SIGLEC-11 on normal aging in 6-month-old mature and 24-month-old aged humanized Siglec-11 transgenic (tg) mice, which express the human SIGLEC-11 receptor on microglia and tissue macrophages (Karlstetter et al., 2017; Liao et al., 2021). We found that aged 24-month-old Siglec-11 tg mice exhibited reduced microglial density, fewer microglial clusters, and fewer lipid-laden microglia compared to the wildtype (WT) control mice. Additionally, Siglec-11 tg mice experienced less age-related neuronal loss in the substantia nigra at 24 months compared to WT mice. Furthermore, aged Siglec-11 tg mice demonstrated suppression of inflammatory, oxidative stress, and apoptotic pathways relative to WT mice.

Thus, SIGLEC-11 exerted anti-inflammatory effects that were neuroprotective in the aged brains of Siglec-11 tg mice.

Materials and methods

Animals and tissue collection

All animal experiments have been approved by the authors' institutional and governmental review boards and have complied with the Helsinki Declaration. C57BL/6J mice were obtained from Charles River. Siglec-11 transgenic (tg) mice (SIGLEC-11+/−) were generated by pro-nuclear injection of a macrophage/microglial-specific Iba1 mini-promotor as previously described (Karlstetter et al., 2017; Liao et al., 2021) and were backcrossed for at least 10 generations with C57BL/6J mice before performing experiments. REDExtract-N-Amp Tissue polymerase chain reaction (PCR) Kit (Sigma) was used to perform SIGLEC11 genotyping PCR for the Siglec-11 tg mice. All mice were maintained in specific pathogen free environment with free access to both water and food. In this study, we analyzed 1.5-, 6-, and 24-month-old male mice as juvenile, mature, and aged groups, respectively. We only investigated male mice, as their substantia nigra dopaminergic neurons are more susceptible to the effects of aging in comparison to female mice (Howell et al., 2020). For tissue collection, mice were euthanized and then transcardially perfused with ice-cold phosphate buffer saline (PBS). Brains were collected and cut into right and left hemispheres for immunohistochemistry and RNA isolation, respectively.

RNA sequencing, gene transcript pathway, and sqRT-PCR analyses

Left brain hemispheres of mice were collected as described above and homogenized in 1 mL QIAzol Lysis reagent (Qiagen, Germany) for 6 min at 50 Hz using a Tissue Lyser LT (Qiagen, Germany) and stainless-steel beads (Qiagen, Germany). Total RNA was extracted using the spin column protocol of the RNeasy® Mini Kit (Qiagen, Germany) according to the manufacturer's protocol. The RNA concentration was measured using a Nanodrop system (NanoDrop 200c, Thermo Fisher Scientific, Waltham, MA) and diluted to 100 ng/μl. RNA integrity was assessed using 2,100 Bioanalyzer (Agilent, Santa Clara, CA). For transcriptome analysis, library preparation (QuantSeq 3′ mRNA-Seq Library Prep Kit, Lexogen) with an input of 100 ng total RNA, quality control (Tapestation 2,200, Fa. Agilent), and RNA sequencing were performed at the Next Generation Sequencing (NGS) Core Facility (Medical Faculty, University Hospital of Bonn) with 2×10^7 single-end reads per sample on a NovaSeq 6,000 (Illumina). After performing quality control on raw reads using FastQC (v0.11.8) and MultiQC (v1.7), adapters were trimmed from the reads using Bbmerge/BBDUK (Bushnell et al., 2017). Reads were aligned to the mouse reference genome mm10 (GRCm38) with the ensemble gene annotation version 101 using STAR [v2.7.3a] (Dobin et al., 2013) with standard parameters. Read count generation was performed using featureCounts/Subread [v2.0.0] (Liao et al., 2014) ignoring multimapping reads. Then, differential expression analysis was performed with R [v4.3.1] in RStudio [v2023.6.2, build 531] (RStudio Team, 2020) using DESeq2 [v1.42.0] (Love et al., 2014). Transcript annotations were retrieved using the Bioconductor package org. Mm.eg.db [v3.11.4] (Carlson, 2019), and plots were created using ggplot2 [v3.3.3] (Wickham, 2016). Pathway enrichment analyses were

performed using clusterProfiler [v3.16.1] (Yu et al., 2012) and GSEA Desktop[v4.2.2] (Mootha et al., 2003; Subramanian et al., 2005) with log2FC ≥ 1 and adjusted *p*-value <0.05. Gene transcripts of each group within each age were contrasted and used for the differential analysis to extract the differentially expressed genes, enriched pathways, and hallmark gene sets. For reverse transcription (RT) of isolated RNA, Superscript® III Reverse Transcriptase (Invitrogen, Germany) and random hexamer oligonucleotides (Roche, Germany) were used following the manufacturers' protocol for SuperScript First-Strand Synthesis (Invitrogen, Germany). The cDNA concentration was measured with a Nanodrop system (NanoDrop 200c, Thermo Fisher Scientific). Semi-quantitative real-time polymerase chain reaction (sqRT-PCR) with specific oligonucleotides (for sequences see Supplementary Table S1) was performed with SYBR Green PCR Master Mix (Invitrogen, Germany) using the Eppendorf epigradient S Mastercycler® (Eppendorf, Wesseling-Berzdorf, Germany). Amplification specificity was confirmed by the analysis of the melting curves. Transcripts of the *glyceraldehyde-3-phosphate dehydrogenase* (*GAPDH*) housekeeping gene were used as internal controls. For sqRT-PCR gene transcription quantification, the values were adjusted relative to their corresponding *GAPDH* levels and assessed using the delta–delta CT approach. Initially, the average CT value for *GAPDH* was determined for each animal and deducted from the average CT value of each gene primer, resulting in the delta CT value. Subsequently, the mean delta CT value was calculated for the 6-month-old WT control group. The delta delta-CT value for each gene primer per animal was derived by subtracting the mean delta CT value of the control group from the delta CT value of the respective primer. The power of the negative delta delta-CT value for each gene primer per animal was then calculated and utilized as the relative measurement of gene transcription.

Immunohistochemistry

The right brain hemispheres were collected as described above and immersed in 4% paraformaldehyde (PFA, Sigma, Germany) for 24 h, followed by 30% sucrose (Sigma, Germany) supplemented with 0.1% sodium azide (Sigma, Germany) at 4°C until processed further. The hemispheres were embedded in O.C.T.™ Compound, Tissue Tek® (Sakura, Torrance, CA). Then, brains were sectioned in the rostral-caudal coronal plane with a thickness of 20 μm and mounted onto superfrost slides and stored at −20°C before staining. For SIGLEC-11 receptor staining, slides containing substantia nigra *pars reticulata* (SN*pr*) were blocked with PBS containing 10% bovine serum albumin (BSA; Roth), 0.2% triton X-100 (Sigma-Aldrich/Merck) and 5% normal goat serum (NGS; Sigma-Aldrich/Merck) for 2 h at room temperature (RT), followed by overnight incubation with anti-SIGLEC11 antibody (mouse anti-Siglec-11, clone 4C4, 1:100, BioLegend, #681702) and antibodies against the microglial marker ionized calcium binding adaptor molecule 1 (Iba1, 1:500, rabbit-anti, Synaptic Systems #234003) at 4°C. After three times washing with PBS, the slices were incubated with the corresponding secondary antibodies in blocking solution for 2 h at RT (Cy3-conjugated goat-anti-mouse IgG F[ab′]2 antibody, 1:200, Dianova #115–166-072 and Alexa-488-conjugated goat-anti-rabbit antibody, 1:400, Invitrogen #A11008). For neuronal quantifications, slides containing SN *pars compacta* (SN*pc*) matched levels (e.g., Bregma −3.20, −3.40 and −3.80 mm) per animal

were blocked with blocking solution for 1 h followed by 2 h incubation with primary antibodies against the dopaminergic neuron marker tyrosine hydroxylase (TH; 1:500, rabbit-anti, Sigma-Aldrich/Merck #T8700-1VL) and against neuronal nuclei marker NeuN (1:500, mouse-anti-human/mouse, Millipore #MAB377) in blocking solution. After washing three times with PBS, the slices were incubated with the corresponding secondary antibodies in blocking solution for 2 h at RT (Alexa-488-conjugated goat-anti-rabbit antibody, 1:500, Invitrogen #A11008 and Cy3-conjugated goat anti-mouse IgG F[ab′]2 antibody, 1:200, Dianova #115–166-072). For microglia evaluation, sections at Bregma level −3.18 mm were blocked with blocking solution (PBS containing 10% BSA, 0.25% triton X-100) for 2 h at RT followed by overnight incubation at 4°C with primary antibodies against microglial marker ionized calcium binding adaptor molecule1 (Iba1, 1:500, rabbit-anti, Synaptic Systems #234003) and lysosomal marker Cluster of Differentiation 68 (CD68, 1:500, rat-anti-mouse, BioRad #MCA1957) in incubation solution (PBS containing 5% BSA and 0.05% triton X-100). After five times washing with 1× PBS, the slices were incubated with corresponding secondary antibodies in blocking solution for 2 h at RT (Alexa-488-conjugated goat-anti-rabbit antibody, 1:400, Invitrogen #A11008 and Cy3-conjugated goat-anti-rat IgG F[ab′]2 antibody, 1:200, Dianova #112–166-072). For lipid-droplet accumulation in Iba1+ cells analysis, sections were blocked and permeabilized using 10% BSA and 0.25% TritonX-100 in PBS followed by the primary antibody rabbit-anti-ionized calcium-binding adapter molecule 1 (Iba1, 1:500; Wako, Japan) in incubation solution (IS; 5% BSA and 0.05% TritonX-100 in PBS) overnight at 4°C. After three washing steps in IS, the sections were incubated in the corresponding Alexa-488-coupled secondary antibodies (1:400, Jackson ImmunoResearch Laboratories, United Kingdom) in IS for 2 h at RT. All stainings were finalized by washing twice with PBS, staining with 4′,6-diamidino-2-phenylindole (DAPI, 1:10,000) for 30 s, followed by washing once with PBS. Finally, the slides were mounted with Aqua-poly/mount (Polysciences) and stored at 4°C until images were taken.

Microglial density, activation, and clustering analysis

To assess the microglial activation status, five z-stacks of Iba1 stained hippocampus and substantia nigra *pars reticulata* (SN*pr*) were acquired with an SP8 confocal microscope using a 40× objective lens and the LAS-X software (Leica, Germany). All number-coded images were analyzed by a blinded investigator, and the levels were defined according to the mouse brain atlas of Paxinos and Franklin. Images were exported as TIFF files and analyzed with ImageJ software (National Institute of Health). Microglial density was quantified by counting Iba1-/DAPI-double-positive cells per area in each image and calculating the average for each mouse. For microglial cluster analysis, three or more Iba1 positive cells in close proximity to each other (found within a 50 μm radius) were defined as a microglial cell cluster. The clusters were then counted in each image, and the average for each mouse was calculated. To measure the CD68 intensity per soma, the soma area of five Iba1/CD68-positive cells in each image was selected. CD68 fluorescence intensity was measured in each soma, and the background fluorescence intensity was substracted. The mean measured CD68 fluorescence intensity for the five somas was calculated per animal, and the mean for each group was calculated.

Neuronal density quantification

To quantify the neurons, TH- and NeuN-stained cells in the substantia nigra *pars compacta* (SN*pc*) or only NeuN-positive cells in the Cornu Ammonis 3 (CA3) area of the hippocampus were acquired and analyzed by a blinded investigator with an AxioObserver Z1 inverted microscope with Apotome (Carl Zeiss) via AxioCam Rm (AxioVision software) as described before (Bodea et al., 2014; Shahraz et al., 2021). Using ImageJ software (National Institute of Health), TH- and NeuN-positive cells were counted, and the area was measured. Neuronal density was calculated as number of counted cells per area, and the mean for each mouse was taken.

Lipid-laden microglia quantification

Images of Iba1-stained hippocampal and SN*pr* were acquired with an SP8 confocal microscope using a 40× objective lens and the LAS-X software (Leica, Germany). The autofluorescence emission of lipid droplets was imaged using the same detection settings as the Cy3 dye emission spectrum. All number-coded images were analyzed by a blinded investigator using the ImageJ software. The levels were defined according to the mouse brain atlas of Paxinos and Franklin. For microglial lipid accumulation analysis, z-stacks were taken at the Bregma level −2.7 to −2.8 mm. Iba1+ cells were quantified in each image and divided by the measured image area to calculate the number of cells per area. The mean number of Iba1+ cells/area was then calculated for each group. Next, lipid droplets- and Iba1-double-positive cells were also counted, and their ratio to total Iba1+ number was calculated. The ratio was then divided by the imaged area, and the mean for each group was calculated.

Statistical analysis

Data are presented as mean ± SEM (if not stated otherwise). The mean from at least three mice was collected and analyzed, and the n-number represents the number of investigated mice. Results were normalized to the mean of the adult (6-month-old) WT control mice. Outliers were identified with Grubbs' test and excluded. Data for 6- and 24-month-old age groups were analyzed with two-way analysis of variance (ANOVA) followed by Fisher's Least Significance Variance (LSD) *post hoc* test. For the 1.5-month-old age group, data were tested for normality using Shapiro–Wilk test and analyzed with Student's *t*-test. Statistical analysis was carried out using GraphPad Prism (v9.0.0). Only statistically significant comparisons were depicted in the figures as *$p \leq 0.05$, **$p \leq 0.01$, ***$p \leq 0.001$.

Results

Decreased microglial density and less microglial clusters in aged Siglec-11 tg mice

Humanized Siglec-11 transgenic (tg) mice, that express the human SIGLEC-11 receptor on microglia and macrophages (Karlstetter et al.,

2017; Liao et al., 2021), were used, since expression of SIGLEC-11 on microglia is human-lineage specific. First, we confirmed expression of Siglec-11 in the brain of this transgenic mouse line (Supplementary Figure S1). Immunohistochemistry showed expression of SIGLEC-11 on microglia in the brains of Siglec-11 tg mice co-stained with antibodies against the microglial marker protein ionized calcium-binding adaptor molecule 1 (Iba1). We analyzed microglial density, microglial expression of the phagolysosomal protein CD68, and microglial cluster formation in the brains of Siglec-11 tg mice at the 6- and 24-month age groups. Accordingly, we co-stained the hippocampus (Figure 1A) and substantia nigra pars reticulata (SN*pr*) (Figure 1C) with antibodies against Iba1 and CD68. In the hippocampus, the density of microglia, as determined by the number of Iba1-positive cells per selected area, was lower at 24 months of age in the Siglec-11 tg mice compared to WT control mice (Figure 1B). In detail, Siglec-11 tg mice showed substantially lower microglial density (84.05 ± 5.9%) at 24 months compared to WT mice (204.74 ± 12.7%; $p < 0.001$). We also analyzed Iba1 density in juvenile mice (1.5 months) to investigate whether the observed changes are possibly related to developmental abnormalities. However, there was no difference observed between WT and Siglec-11 tg mice in microglial density at 1.5 months of age (Supplementary Figure S2A). In addition, we studied the SN*pr* and found that the density of Iba1-positive cells was lower in the Siglec-11 tg mice compared to WT mice at 24 months of age (157.16 ± 31.5% vs. 227.19 ± 37%, $p = 0.006$) (Figure 1D). Again, analysis of 1.5-month-old mice showed no difference in the SN*pr* between the WT and Siglec-11 tg mice in microglial density (Supplementary Figure S2B).

Next, we analyzed the intensity of CD68 in the soma of microglia at different ages. Here, we found a lower microglial expression of CD68 in the hippocampus from 254 ± 44.2% in WT mice to 132.6 ± 20.8% in Siglec-11 tg mice ($p = 0.009$) at 24 months of age (Figure 1B), while no difference was observed in the substantia nigra (Figure 1D) at the same age.
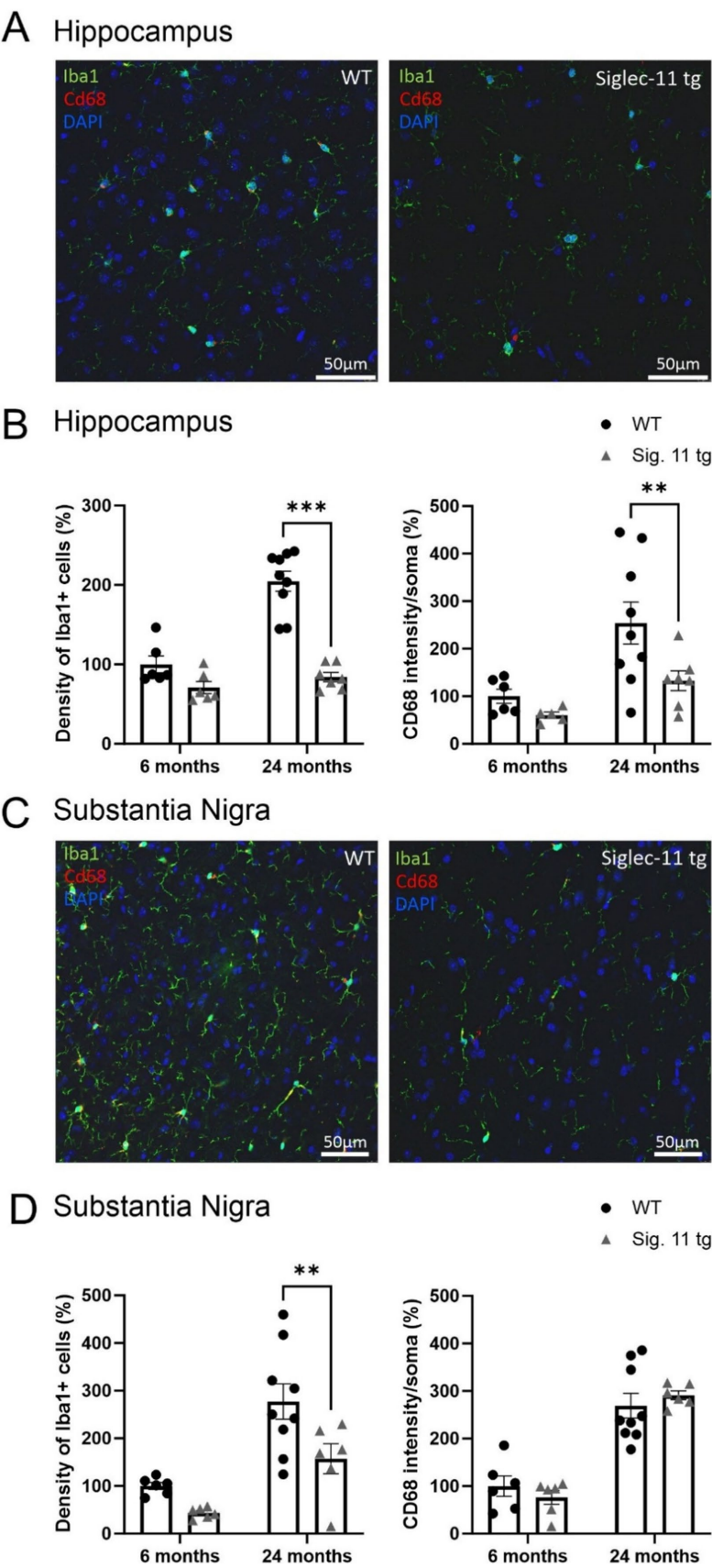
Finally, we analyzed the density of microglial cell clusters, which we defined as three or more microglial cell bodies in close proximity (within a radius of 50 μm) to each other (Figures 2A–D). While no difference was seen between both groups at 6 months of age, the density of microglial clusters was lower in Siglec-11 tg mice compared to WT mice at 24 months of age, both, in the hippocampus and the SN*pr*. In detail, at 24 months of age, hippocampal microglial cluster density was 96.73 ± 18% in Siglec-11 tg mice compared to 224.69 ± 42.6% in WT mice ($p = 0.010$) (Figure 2B), while in the SN*pr*, microglial cluster density was 108.41 ± 14.6% in Siglec-11 tg mice compared to 256.84 ± 27% in WT mice ($p < 0.001$) (Figure 2D).

Altogether, our data show lower microglial cell density and fewer microglial clusters in the hippocampus and SN*pr* at 24 months of age, and lower hippocampal lysosomal expression of CD68 in microglia at 24 months of age in Siglec-11 tg mice compared to WT mice.

Less microglial lipid accumulation in the substantia nigra of Siglec-11 tg mice

In addition, we investigated lipid accumulation in microglia as a hallmark of aging and oxidative stress in the brain (Fan et al., 2024). Therefore, we assessed the autofluorescence of lipid droplets in Iba1+ microglia in the hippocampus (Figure 3A) as well as in the SN*pr*
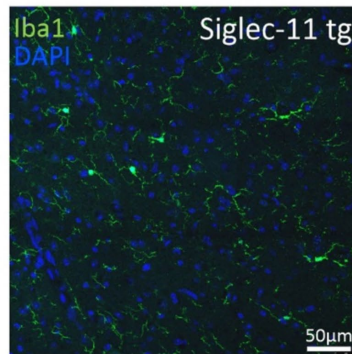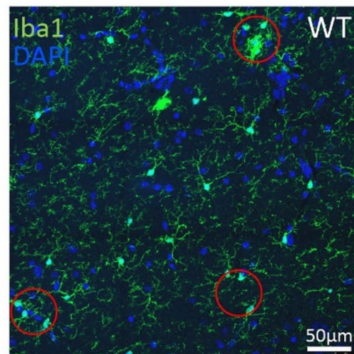
FIGURE 1

Less microglial density in aged Siglec-11 transgenic compared to wildtype mice. Hippocampal and substantia nigra tissue was co-stained with antibodies directed against the microglial transmembrane protein Iba1 and the phagolysosomal protein CD68. **(A)** Representative images of Iba1
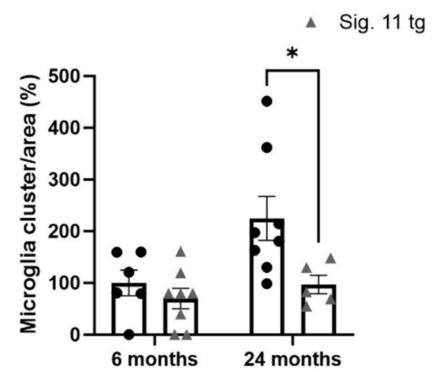
(Continued)

FIGURE 2
Less microglial cell clusters in aged Siglec-11 transgenic compared to wildtype mice. Hippocampal and substantia nigra tissue was stained with the antibody directed against the microglial transmembrane protein Iba1. Red circles measuring 50 μm in diameter elucidating the clustering of two or more microglial cells. **(A)** Representative images of Iba1 (green) and DAPI (blue) in the hippocampus of 24-month-old wildtype (WT) control and Siglec-11 transgenic (tg) mice are shown. **(B)** Quantification of hippocampal Iba1 cell clusters showed decreased levels at 24 months of age in Siglec-11 tg mice compared to WT mice. **(C)** Representative images of Iba1 (green) and DAPI (blue) in the substantia nigra *pars reticulata* of 24-month-old WT and Siglec-11 tg mice are shown. **(D)** Quantification in the substantia nigra *pars reticulata* showed decreased Iba1 cell clusters in Siglec-11 tg at 24 months of age compared to WT mice. Data were analyzed with two-way ANOVA and Fisher's LSD *post hoc* test and are shown as mean $\pm$ SEM. n = 5−8 mice per group. Scale bars 50 μm. *$p \leq 0.05$, ***$p \leq 0.001$.
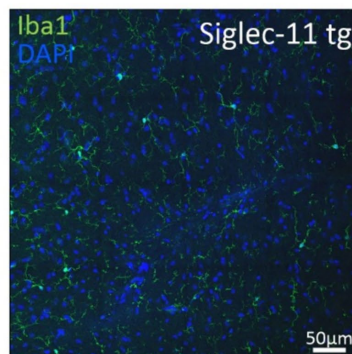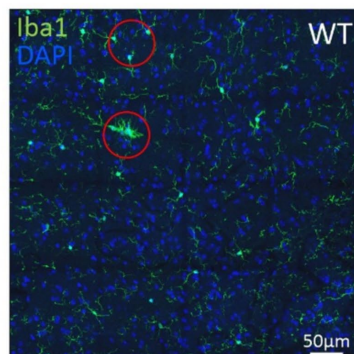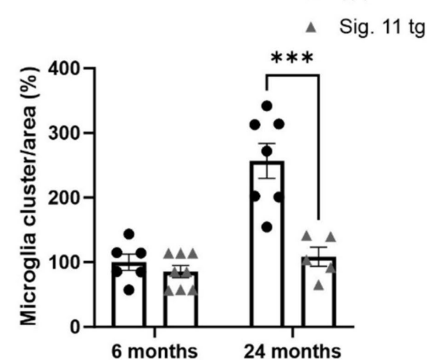
(Figure 3C). Our data showed a general decrease in the density of lipid-laden (lipid droplets plus Iba1-positive cells) microglia in the SN*pr* of both 6- and 24-month-old Siglec-11 tg compared to WT mice, while no difference was seen in the hippocampus (Figures 3B,D). In detail, at 6 months of age, relative density of lipid-laden microglia in the SN*pr* differed from 100 ± 15% in WT mice to 43.55 ± 9.9% (p = 0.002) in Siglec-11 tg mice, and at 24 months of age from 174.80 ± 11% in WT mice to 128.83 ± 8.4% in Siglec-11 tg mice (p = 0.012; Figure 3D).

In summary, our data showed lower density of lipid-laden microglia in the SN*pr* of 6- and 24-month old Siglec-11 tg compared to WT mice.

Higher neuronal density in the substantia nigra of aged Siglec-11 tg mice

To assess whether the decreased microglial activation observed in Siglec-11 tg mice has an impact on the neuronal numbers in the brain, neuronal density was quantified in the hippocampus and in the substantia nigra *pars compacta* (SN*pc*). Accordingly, we stained the hippocampal neurons with the neuronal nuclei marker (NeuN; Figure 4A), and in the SN*pc*, we used markers for NeuN and tyrosine hydroxylase (TH), a marker of dopaminergic neurons (Figure 4C). At 24 months of age, WT mice tended to have fewer numbers of
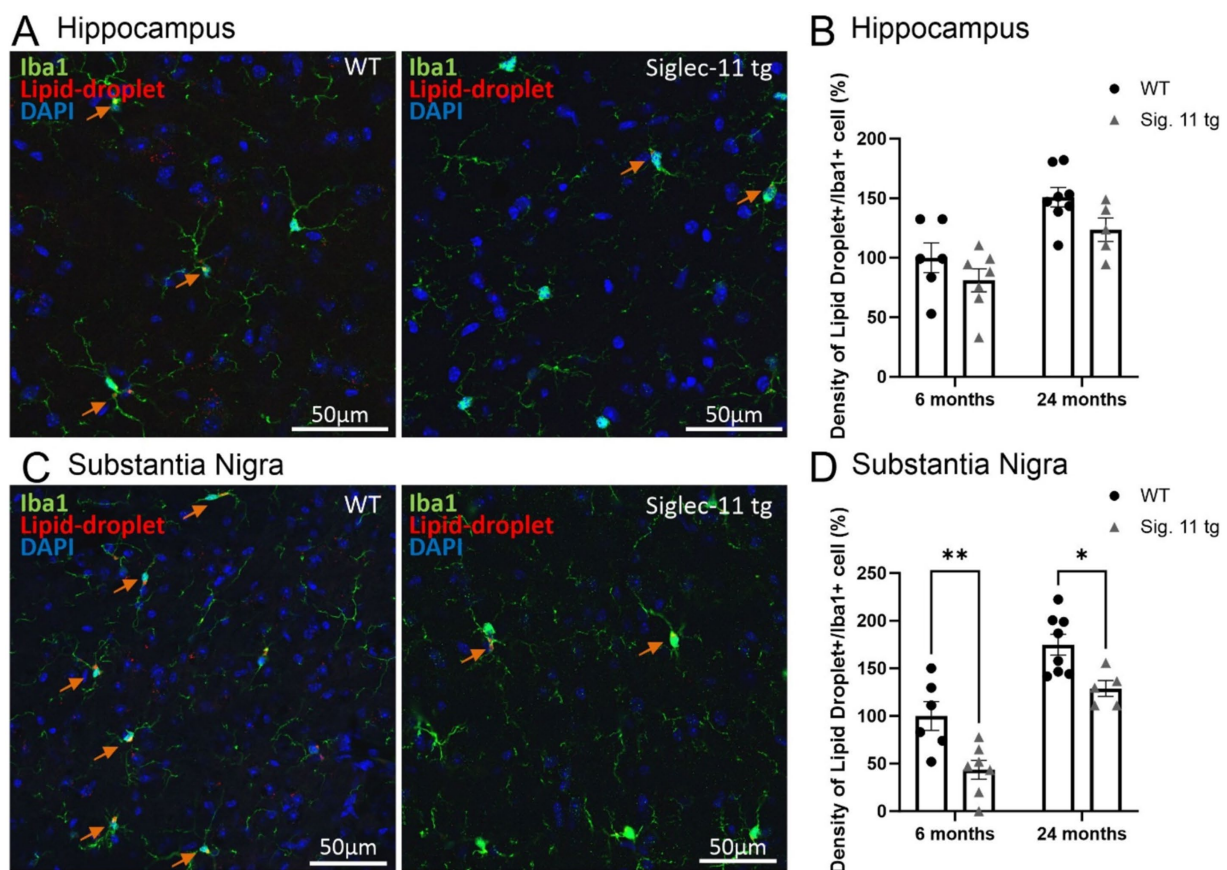
FIGURE 3
Decreased density of lipid-droplets containing microglia in the substantia nigra of Siglec-11 transgenic compared to wildtype mice. Hippocampal and substantia nigra tissue was stained with the antibody directed against the microglial transmembrane protein Iba1. **(A)** Representative images of lipid-droplets (red), Iba1 (green) and DAPI (blue) staining in the hippocampus at 24 months of age of wildtype (WT) and Siglec-11 transgenic (tg) mice. **(B)** Quantification of the number of lipid-droplets and Iba1 double-positive cells per area showed no significant change between Siglec-11 tg and WT control mice in the hippocampus. **(C)** Representative images of lipid-droplets (red), Iba1 (green), and DAPI (blue) staining in the substantia nigra *pars reticulata* (SN*pr*) at 24 months of age of WT and Siglec-11 tg mice. **(D)** Quantification of the number of lipid-droplets and Iba1 double-positive cells per area were decreased in the Siglec-11 tg mice at 6 and 24 months of age compared to WT control mice. Arrows pointing to microglial cells co-expressing lipid-droplet autofluorescence. Data were analyzed with two-way ANOVA and Fisher's LSD *post hoc* test and are shown as mean $\pm$ SEM; n = 5−8 mice per group. Scale bars 50 μm. *$p \leq 0.05$, ** $p \leq 0.01$.

hippocampal neurons in comparison to Siglec-11 tg mice, although it did not reach statistical significance ($p = 0.531$, Figure 4B). In the SN*pc*, we observed fewer NeuN-positive and TH-positive cells in WT mice compared to the Siglec-11 tg mice starting at 6 months of age, which became more prominently different for the TH-positive neurons at 24 months of age (Figure 4D). In detail, the relative NeuN-positive cells in the SN*pc* were lower in WT mice ($100 \pm 4.6\%$) compared to Siglec-11 tg mice ($140 \pm 9.2\%$, $p < 0.001$) at 6 months of age. Relative TH-positive cells were also fewer in WT ($100 \pm 7.7\%$) compared to Siglec-11 tg mice ($147.3 \pm 12.8\%$, $p = 0.003$) at 6 months of age, and between WT ($68 \pm 4\%$) and Siglec-11 tg mice ($119 \pm 14\%$, $p = 0.003$) at 24 months of age. We further quantified NeuN-positive cells in the hippocampus and NeuN-positive and TH-positive cells in the SN*pc* of 1.5-month-old juvenile mice to examine if the difference in neuronal numbers between both genotypes might already occur at an earlier time point. However, we found no significant differences in neuronal numbers at 1.5 months of age between WT and Siglec-11 tg mice (Supplementary Figures S3A,B).

Taken together, our results show more neuronal numbers in the SN*pc* of Siglec-11 tg compared to WT mice at 6 months of age, and

prominent dopaminergic neuronal preservation in Siglec-11 tg mice at 24 months of age.

Reduced oxidative phosphorylation and inflammatory gene transcript pathways in Siglec-11 tg mice

To better understand the underlying pathways related to the SIGLEC-11 receptor in the brain, and to unravel the mechanisms behind the observed changes in the Siglec-11 tg mice, we isolated RNA from the brain of 6- and 24-month-old Siglec-11 tg and WT mice and performed RNA-seq analysis. Principal component (PC) analysis showed a clear separation between the groups at both ages (Supplementary Figure S4A). For 6-month-old mice, PC1 accounted for 52% of the variance and PC2 accounted for 18% of the variance. We then performed a differentially expressed gene (DEG) analysis (Supplementary Figure S4B), which showed an increased expression of hemoglobin alpha and beta adult chain-related genes in the
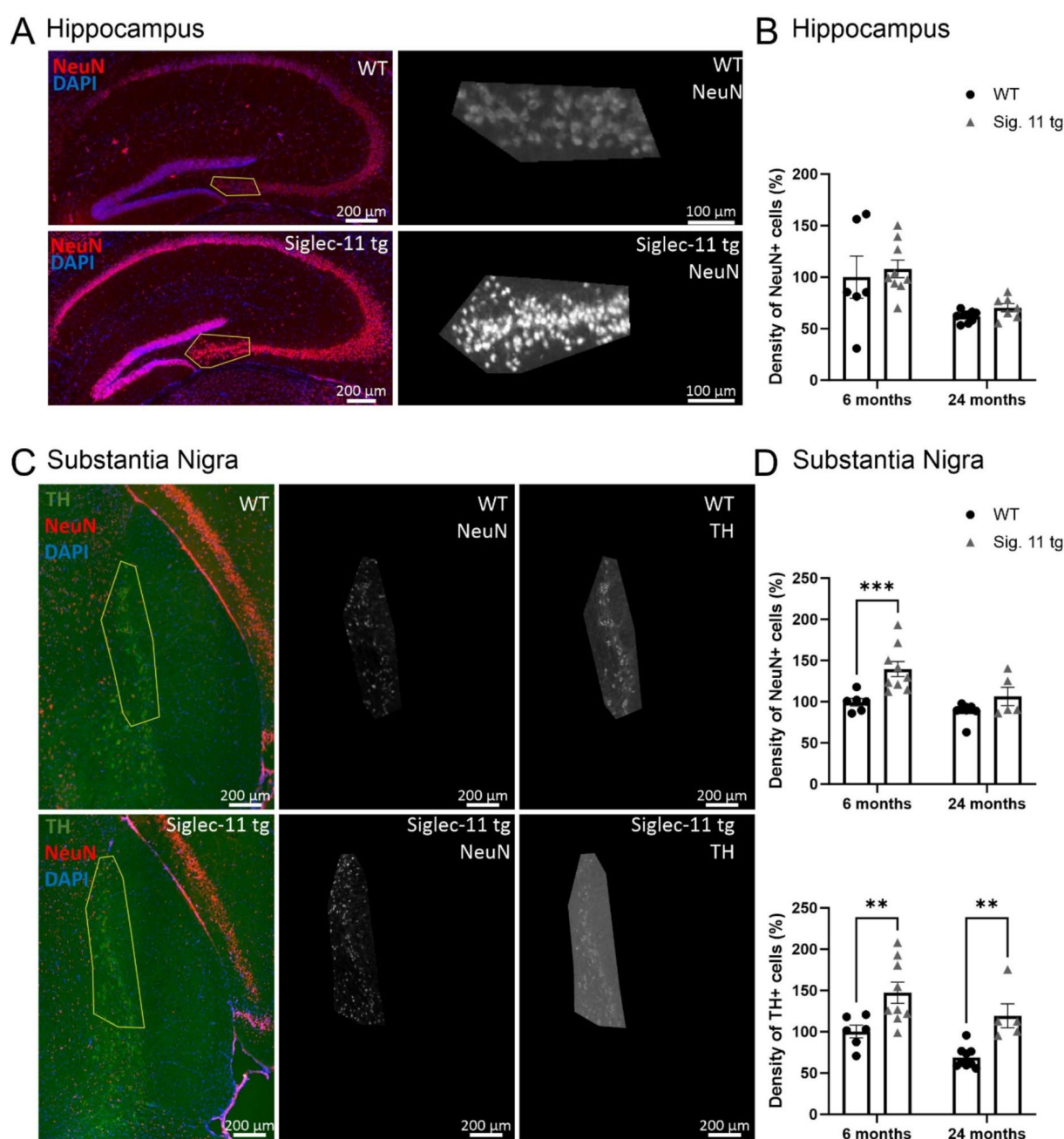
FIGURE 4

Higher number of dopaminergic neurons in the substantial nigra *pars compacta* in Siglec-11 transgenic compared to wildtype mice. Hippocampal tissue stained with the antibody directed against the neuronal nuclei (NeuN) and substantia nigra tissue stained with the antibodies directed against NeuN and the dopaminergic marker tyrosine hydroxylase (TH). **(A)** Representative images of NeuN (red) and DAPI (blue) staining in the hippocampus CA3 region of wildtype (WT) and Siglec-11 transgenic (tg) mice. **(B)** Quantification of NeuN-positive cell density in the hippocampal region showed no significant difference between WT and Siglec-11 tg mice. **(C)** Representative images of TH (green), NeuN (red), and DAPI (blue) staining in the substantia nigra *pars compacta* of 24-month-old WT and Siglec-11 tg mice. **(D)** Quantification of NeuN-positive cell density in the substantia nigra showed increased NeuN-positive cell density in Siglec-11 tg compared to WT mice at 6 months of age. Quantification of TH-positive cell density in the substantia nigra showed increased TH-positive cell density in Siglec-11 tg compared to WT mice at 6 and 24 months of age. Data were analyzed with two-way ANOVA and Fisher's LSD *post hoc* test and are shown as mean $\pm$ SEM; n = 5−9 mice per group. Scale bars as indicated in the figures. **$p \leq 0.01$, ***$p \leq 0.001$.

Siglec-11 tg mice compared to WT mice. On the other hand, mitochondrial ribosomal protein-related genes (*Mrps11* and *Mrpl46*), immune and inflammatory-related genes like S100 calcium-binding protein A9 (*S100a9*), cellular communication network factor 1 (*Ccn1*), ADAM metallopeptidase with thrombospondin type 1 motif 1 (*Adamts1*), and inhibitory synapses regulator gene neuronal PAS domain protein 4 (*Npas4*) were downregulated. We then performed a gene set enrichment analysis (GSEA) on Kyoto encyclopedia of genes and genomes (KEGG), which among hematopoietic cell lineage and inflammatory pathways, revealed the oxidative phosphorylation

pathway to be the top suppressed pathway in the Siglec-11 tg mice compared to WT mice (Figure 5A). GSEA of mouse hallmark gene sets showed enrichment of 10 hallmark gene sets at FDR less than 25% and a nominal *p*-value of less than 0.05 in the WT mice compared to Siglec-11 tg mice. Out of these, the top enriched hallmark gene sets were the oxidative phosphorylation (nominal $p < 0.02$), along with the reactive oxygen species pathway (nominal $p < 0.04$), and apoptosis pathway (nominal $p < 0.001$; Supplementary Figure S4C).

The 24-month-old mice showed 38% variance on PC1 and 19% variance on PC2 in the PC analysis (Supplementary Figure S5A). The DEG analysis revealed *Snca* coding the alpha-synuclein protein (*α*-synuclein) as the top downregulated gene in Siglec-11 tg mice compared to WT mice (Supplementary Figure S5B). As seen in the 6-month group, the *Mrpl46* and *Mrps11* genes were also downregulated at 24 months in the Siglec-11 tg mice. The Homeobox B8 (*Hoxb8*) gene was the only significantly upregulated gene in Siglec-11 tg mice at 24 months of age. Gene set enrichment analysis (GSEA) on KEGG showed the suppression of complement and coagulation cascades along with cytokine-cytokine receptor interaction in Siglec-11 tg mice compared to WT mice (Figure 5B). GSEA of hallmark gene sets showed three enriched gene sets at a nominal *p*-value of less than 0.05 in WT mice compared to Siglec-11 tg mice, which were angiogenesis, Kirsten rat sarcoma virus (KRAS) signaling, and epithelial-mesenchymal transition. Complement and inflammatory gene sets were also enriched in WT compared to Siglec-11 tg mice, although not reaching the significance threshold (Supplementary Figure S5C).

Taken together, the RNA-seq analysis showed suppressed oxidative stress and apoptotic pathways at 6 months of age and suppressed complement and inflammatory pathways at 24 months of age in Siglec-11 tg compared to WT mice.

Decreased gene transcription of microglial and astrocytic markers in aged Siglec-11 tg mice

Next, we measured the gene transcription levels of the macrophage/microglial markers allograft inflammatory factor 1 (*Aif1*) and transmembrane protein 119 (*Tmem119*), along with the macrophage lysosomal activation marker *Cd68,* in the whole-brain hemisphere homogenates of Siglec-11 tg mice and WT controls (Figure 6A). Siglec-11 tg mice showed lower gene transcription levels of all microglial markers in comparison to WT mice. In detail, at 24 months of age, the relative *Aif1* gene transcription differed from 4.15 ± 0.6 fold change (FC) in WT mice to 1.37 ± 0.2 FC ($p < 0.001$) in Siglec-11 tg mice, *Tmem119* differed from 4.10 ± 0.7 FC to 1.37 ± 0.2 FC ($p < 0.001$), and *Cd68* differed from 3.16 ± 0.3 FC to 0.86 ± 0.1 FC ($p < 0.001$), respectively.

We also tested the astrocytic markers glial fibrillary acidic protein (*Gfap*) and S100 calcium-binding protein B (*S100b*; Figure 6B). In comparison to WT at 24 months of age, Siglec-11 tg mice showed a lower *Gfap* gene transcription, differing from 5.36 ± 1.4 FC in WT mice to 2.21 ± 0.4 FC in Siglec-11 tg mice ($p = 0.009$), and *S100b* gene transcription, differed from 2.46 ± 0.5 FC in WT mice to 0.80 ± 0.1 FC in Siglec-11 tg mice ($p < 0.001$). We tested the microglial and astrocytic markers at the younger age of 1.5 months and found no difference between both genotype groups (Supplementary Figures S6A,B).

In summary, our data showed decreased gene transcription of microglial and astrocytic markers in 24-month-old Siglec-11 tg compared to WT mice.

Decreased inflammatory, oxidative burst, and complement gene transcripts in aged Siglec-11 tg mice

To affirm the results obtained from the RNA-seq analysis and to examine whether the reduced microglial activation in Siglec-11 tg mice also leads to reduced inflammatory/immune activated states in comparison to WT mice, we measured the gene expression levels of different pro-inflammatory, oxidative burst, and complement system markers via sqRT-PCR (Figures 7, 8). We investigated the transcription levels of the pro-inflammatory cytokines tumor necrosis factor alpha (*Tnf*) and interleukin-1ß (*Il-1ß*) (Figure 7A). In comparison to WT, Siglec-11 tg mice showed a lower gene transcription of *Tnf*, differing from 10.51 ± 2.3 FC in WT mice to 4.48 ± 0.8 FC in Siglec-11 tg mice ($p = 0.006$), and lower *Il-1ß* gene transcription, differing from 2.46 ± 0.5 FC in WT mice to 0.44 ± 0.1 FC in Siglec-11 tg mice ($p < 0.001$) at 24 months of age. We tested both markers at 1.5 months of age and found no difference between the groups (Supplementary Figure S6C).

To explore the effect of the SIGLEC-11 receptor on oxidative damage in the brain, we measured the gene transcript levels of the oxidative stress markers cytochrome b-245 alpha and beta (*Cyba* and *Cybb*) and the nitric oxide synthase 2 (*Nos2*) by sqRT-PCR (Figure 7B). Our results showed clearly lower gene transcription of these oxidative stress markers in the Siglec-11 tg mice compared to WT mice. In detail, at 24 months of age *Cyba*, *Cybb,* and *Nos2* were all higher in WT mice compared to Siglec-11 tg mice, differing from 4.87 ± 0.9 FC to 0.33 ± 0.1 FC ($p < 0.001$), from 6.2 ± 1.2 FC to 2.03 ± 0.2 FC ($p < 0.001$), and from 5.83 ± 1.5 FC to 0.87 ± 0.1 FC ($p < 0.001$), respectively. Analyzing all three markers at 1.5 months of age revealed a higher *Cyba* gene transcription in WT mice compared to Siglec-11 tg mice, differing from 0.44 ± 0.02 FC to 0.02 ($p < 0.001$), while both *Cybb* and *Nos2* were lower in WT mice compared to Siglec-11 tg mice, differing from 0.45 ± 0.03 FC to 0.98 ± 0.1 FC ($p < 0.001$) and from 1.7 ± 0.1 FC to 2.3 ± 0.1 FC ($p = 0.001$), respectively (Supplementary Figure S6D).

We then analyzed the gene transcript levels of complement components 3 and 4 (*C3* and *C4*) along with the integrin alpha M (*Itgam*) and the complement C1q subcomponent subunits a-c (*C1qa*, *C1qb*, *C1qc*) to unravel the effect of SIGLEC-11 receptor on the complement system activation (Figure 8). We observed a general decrease of complement system genes in Siglec-11 tg mice compared to WT mice. In detail, at 24 months of age *C3* differed from 3.48 ± 0.9 FC in WT mice to 1.33 ± 0.2 FC ($p < 0.018$) in Siglec-11 tg mice, *C4* differed from 7.73 ± 1.2 FC in WT mice to 2.85 ± 0.6 FC ($p < 0.001$) in Siglec-11 tg mice, and *Itgam* differed from 4.23 ± 0.7 FC in WT mice to 2.44 ± 0.4 FC in Siglec-11 tg mice ($p = 0.007$). The gene transcript levels of complement C1q subcomponents were lower in Siglec-11 transgenic mice compared to WT mice at 24 months of age, differing from 0.77 ± 0.1 FC to 3.31 ± 0.7 FC ($p < 0.001$) for *C1qa*, from 0.85 ± 0.2 FC to 2.93 ± 0.9 FC ($p = 0.014$) for *C1qb,* and from 0.36 ± 0.1 FC to 1.31 ± 0.1 FC ($p < 0.001$), respectively. *C1qc* was also lower in Siglec-11 tg mice compared to WT mice at 6 months of age, differing from 1.00 ± 0.4
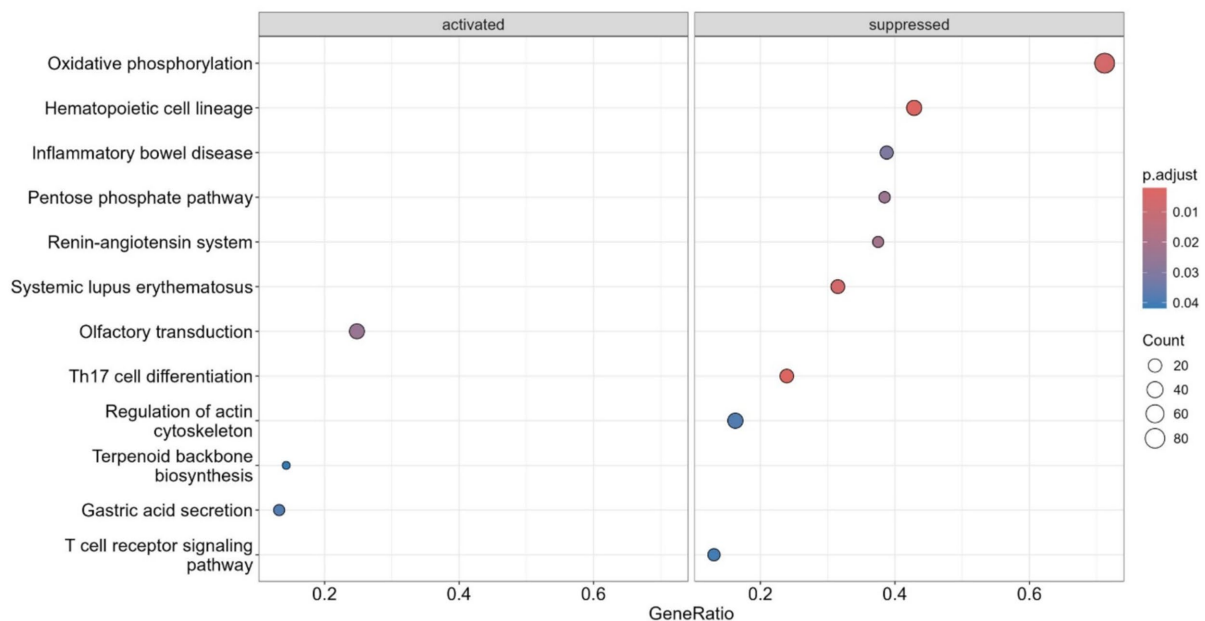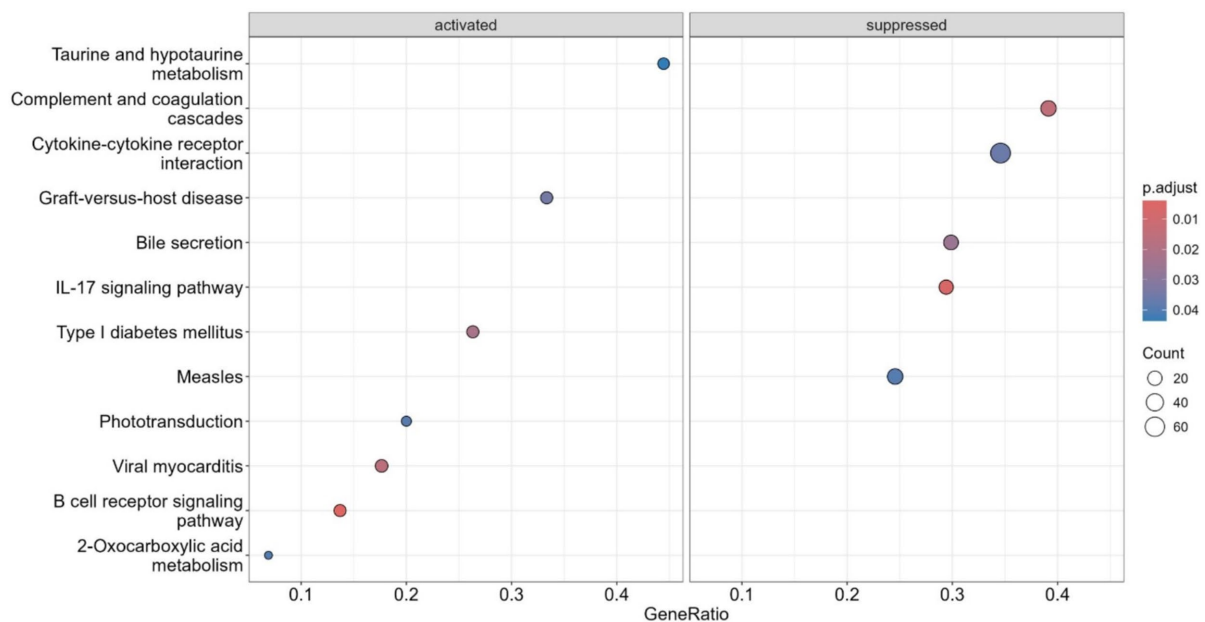
FIGURE 5
Suppressed oxidative phosphorylation, inflammatory, complement and coagulation transcriptome pathways in Siglec-11 transgenic compared to wildtype mice. Whole genome RNA sequencing of brain tissue was performed. Gene set enrichment on Kyoto encyclopedia of genes and genomes transcriptome pathway analysis was carried out with 6- and 24-month-old Siglec-11 transgenic (tg) in comparison to wildtype (WT) control mice of the same age. **(A)** At 6 months of age suppression of the oxidative phosphorylation and inflammatory pathways were observed in the Siglec-11 tg mice. **(B)** At 24 months of age suppression of complement and coagulation cascades, along with suppressed cytokine-cytokine receptor interaction pathways were found in the Siglec-11 tg mice. Data shown from n = 4–5 mice per group.

FC to 0.24 ± 0.03 FC ($p < 0.001$). Analysis of complement markers gene transcripts at 1.5 months of age revealed a lower *C4* and a higher *Itgam* transcript level in WT mice compared to Siglec-11 tg mice, differing from 0.06 ± 0.01 FC to 0.25 ± 0.04 FC ($p < 0.001$),

and from 2.29 ± 0.1 FC to 1.79 ± 0.08 FC ($p = 0.002$), respectively (Supplementary Figure S6E).

Overall, our results show a lower gene expression of inflammatory, oxidative stress, and complement system markers in 24-month-old
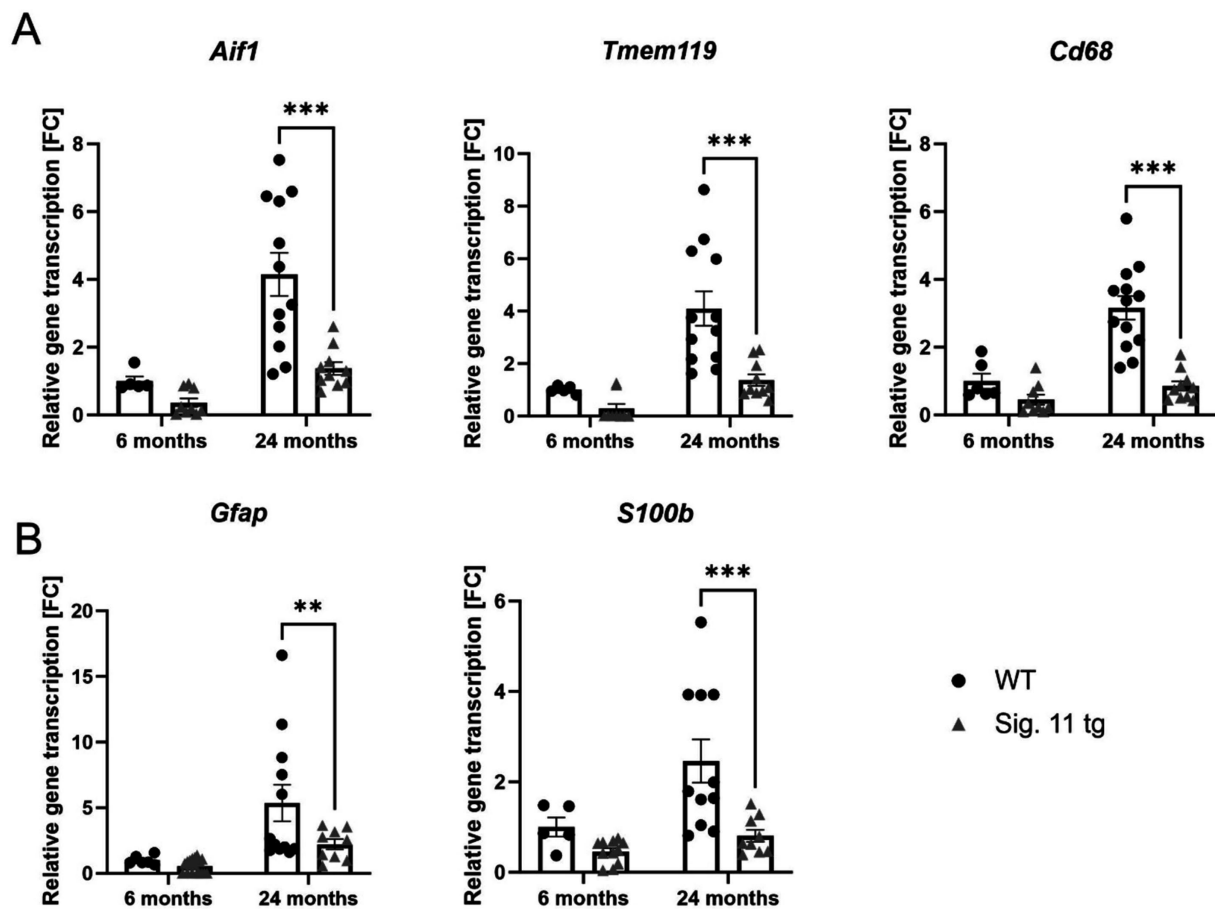
FIGURE 6
Decreased gene transcription of microglial and astrocytic markers in aged Siglec-11 transgenic compared to WT mice. Semi-quantitative real-time PCR (sqRT-PCR) of microglial and astrocytic markers in brain hemisphere homogenates of Siglec-11 transgenic (tg) and wildtype (WT) control mice. **(A)** Transcription of the microglial markers *Aif1* (allograft inflammatory factor 1) and *Tmem119* (transmembrane protein 119), along with the microglial activation marker *Cd68* showed decreased levels at 24-months of age in Siglec-11 tg mice compared to WT control mice. **(B)** Transcription of the astrocytic markers *Gfap* (glial fibrillary acidic protein) and *S100b* (S100 calcium-binding protein B) showed decreased levels of *S100b* at 24-months of age in Siglec-11 tg mice compared to WT control mice. Data were analyzed with two-way ANOVA and Fisher's LSD *post hoc* test and are shown as mean $\pm$ SEM. n = 5–18 mice per group. **$p \leq 0.01$, ***$p \leq 0.001$.

Siglec-11 tg mice compared to WT mice, which also exhibited lower *C1qc* gene transcription at 6 months of age.

Discussion

Sialic acid-binding immunoglobulin-type lectin (SIGLEC) receptors of microglial cells and tissue macrophages recognize intact sialylation, acting as innate immune checkpoints to regulate inflammation and oxidative stress in the central nervous system (Klaus et al., 2021; Liao et al., 2020).

Recent studies, have identified SIGLEC-11 as the most significant microglial gene associated with Alzheimer's disease (AD), following the categorization of AD and dementia-related genes based on their relevance to the disease process (Bellenguez et al., 2022). Genomic data suggest that in humans, both *SIGLEC11* and the closely related *SIGLEC16* gene likely originated through gene conversion from the non-functional pseudogene *SIGLEC16P* (Hayakawa et al., 2017; Wang et al., 2012). This event is believed to have led to the exclusive expression of SIGLEC-11 in human microglia. Notably, microglial SIGLEC-11 in the human brain

appears to exist solely as an alternative splice variant, which lacks the exon encoding the final (fifth) Ig-like C2-set domain within the protein's extracellular segment, a characteristic shared by the humanized Siglec-11 transgenic mice used in this study (Hane et al., 2021; Wang and Neumann, 2010).

Activation of microglial SIGLEC-11 by polysialic acid (polySia) attached to neural cell adhesion molecule (NCAM) on neighboring neurons suppressed lipopolysaccharide (LPS)-induced pro-inflammatory mediators, such as *Il-1ß,* in a murine neuron–microglia co-culture, demonstrating the neuroprotective effect of SIGLEC-11 (Wang and Neumann, 2010). Soluble polySia has also been explored therapeutically, targeting the SIGLEC-11 receptor in humanized Siglec-11 transgenic mice (Karlstetter et al., 2017; Liao et al., 2021). In an age-related macular degeneration animal model, intravitreal application of soluble polySia in humanized Siglec-11 transgenic mice reduced mononuclear phagocytes and vascular leakage, and prevented complement system activation (Karlstetter et al., 2017). In a Parkinson's disease model using the same humanized Siglec-11 tg mice, intraperitoneal administration of soluble polySia reduced microglial immunoreactivity and protected against dopaminergic neuronal degeneration in the substantia nigra (Liao et al., 2021).
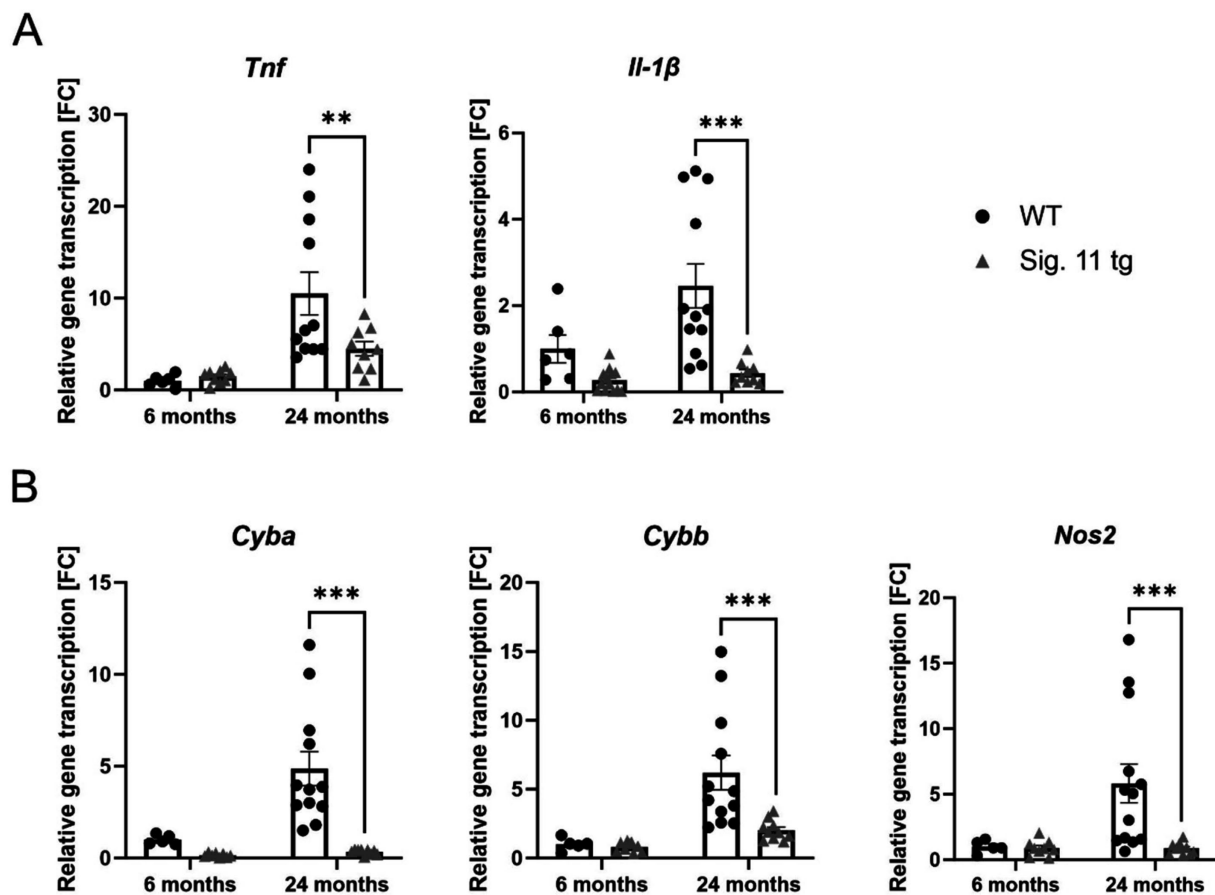
FIGURE 7

Decreased transcription of pro-inflammatory cytokines and oxidative stress markers in aged Siglec-11 transgenic compared to wildtype mice. Semi-quantitative real-time PCR (sqRT-PCR) of brain hemisphere homogenates of Siglec-11 transgenic (tg) and wildtype (WT) control mice. **(A)** Transcription of the pro-inflammatory cytokines *tumor necrosis factor-α* (*Tnf*) and *interleukin-1β* (*Il-1β*) were decreased in Siglec-11 tg mice in comparison to WT control mice at 24-months of age. **(B)** Transcription levels of *cytochrome b-245 alpha and beta* (*Cyba* and *Cybb*) and the *nitric oxide synthase 2* (*Nos2*) were decreased in 24-month-old Siglec-11 tg mice compared to WT mice. Data were analyzed with two-way ANOVA and Fisher's LSD *post hoc* test and are shown as mean $\pm$ SEM. n = 5–13 mice per group. **$p \leq 0.01$, ***$p \leq 0.001$.

This study focused on the role of SIGLEC-11 receptor in normal brain aging, comparing aged 24-month-old humanized Siglec-11 tg mice to wild-type (WT) mice. As a baseline, we examined mature 6-month-old adult mice. Additionally, we analyzed 1.5-month-old juvenile mice to investigate potential developmental effects but found no significant developmental differences between Siglec-11 tg and WT mice at that age.

Under steady-state conditions, microglia typically exhibit a quiescent immune profile and only become activated when stimulated, but increased microglial activation has been observed in aging brains across various species (Luo et al., 2010). Microglial density has also been shown to increase with age in CNS regions such as the hippocampus, visual and auditory cortices, and the retina (Damani et al., 2011; Mouton et al., 2002; Tremblay et al., 2012). Additionally, increased microglial clustering is seen in aging brains, especially near senile plaques in humans (Dickson et al., 1992) and in the brains of 24-month-old mice (Raj et al., 2017). Microglial activation is further evidenced by increased expression of the lysosomal CD68 microglial activation marker in aging mice brains (Halder and Milner, 2022).

In line with these observations, our study revealed a reduction in Iba1-positive microglial cell density and clustering in the hippocampus and substantia nigra of 24-month-old Siglec-11 tg compared to age-matched WT controls. We also noted reduced microglial phagolysosomal activation in the hippocampus of Siglec-11 tg mice compared to WT control mice at 24 months of age, as depicted by lower CD68 intensity per soma.

Dopaminergic neuronal loss in the substantia nigra *pars compacta* (SN*pc*) of aging C57BL/6 mice has been previously reported (Noda et al., 2020). Consistently, we observed a reduction in dopaminergic neuron density in aged 24-month-old WT control mice, whereas dopaminergic neurons were preserved in the SN*pc* of the Siglec-11 tg mice. This suggests that microglial SIGLEC-11 receptor protects against age-related neuronal loss in the substantia nigra.

The normal aging process is associated with numerous subtle and selective changes in the brain, often linked to cognitive decline (Burke and Barnes, 2006). Prominent changes include alterations in synaptic physiology, mitochondrial metabolism, and oxidative phosphorylation (Bishop et al., 2010; Castelli et al., 2019; Yankner et al., 2008). Our RNA sequencing and transcriptomic KEGG pathway analyses revealed oxidative phosphorylation as the most suppressed gene transcript pathway in 6-month-old Siglec-11 tg mice compared to WT controls. In contrast, pathways associated with apoptosis, inflammation, coagulation, and oxidative stress were enriched in WT mice compared to Siglec-11 tg mice at 6 months of age. By the age of 24 months, KEGG pathway analysis of Siglec-11 tg mice showed suppression of coagulation, complement
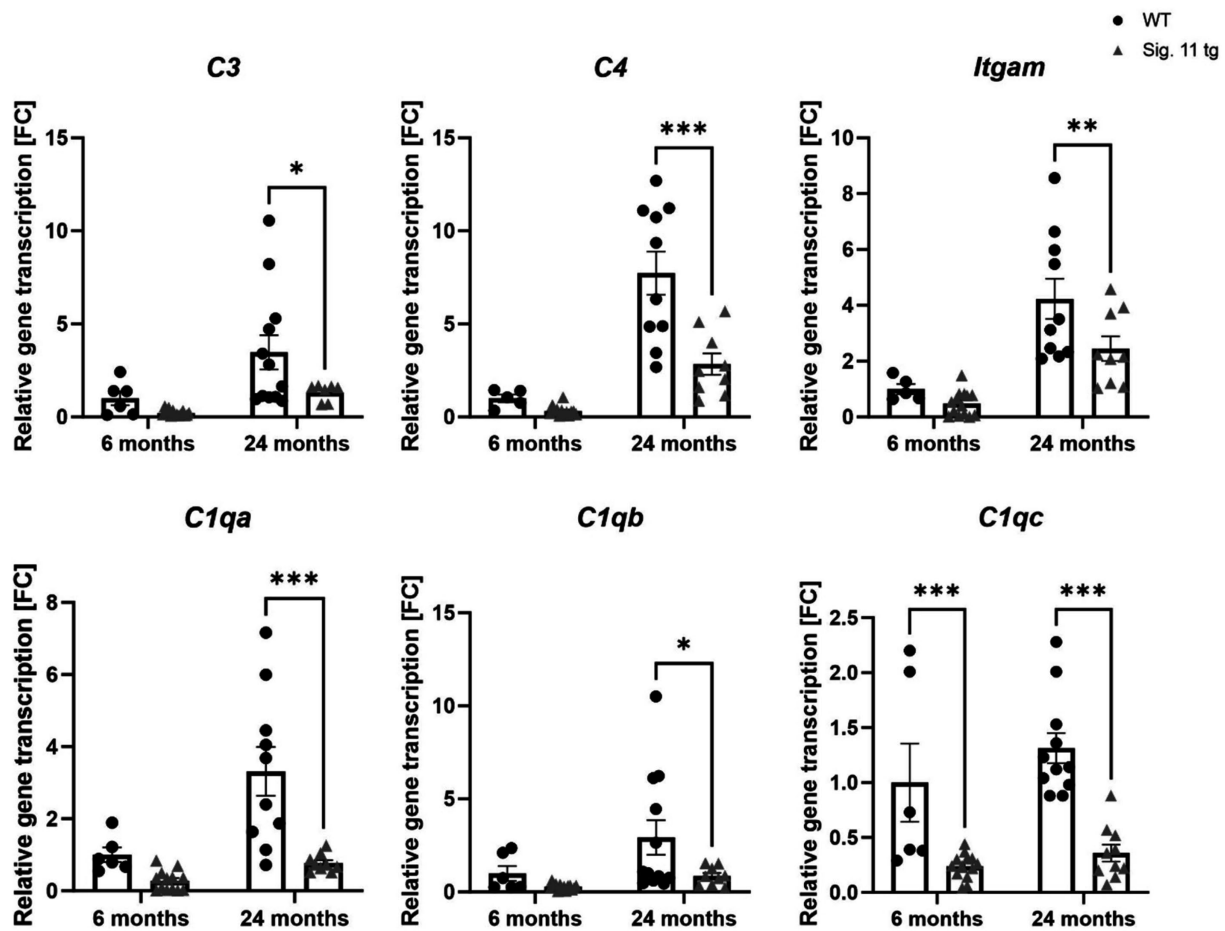
FIGURE 8
Decreased transcription of complement system associated factors in aged Siglec-11 transgenic compared to wildtype mice. Semi-quantitative real-time PCR (sqRT-PCR) of brain hemisphere homogenates of Siglec-11 transgenic (tg) and wildtype (WT) control mice. Transcription levels of complement components 3 and 4 (*C3* and *C4*), Integrin alpha M (*Itgam*), and complement C1q subcomponent subunits A and C (*C1qa* and *C1qc*) were decreased in 24-month-old Siglec-11 tg mice compared to WT mice. *C1qc* was also decreased in 6-month-old Siglec-11 tg mice compared to WT mice. Data were analyzed with two-way ANOVA and Fisher's LSD *post hoc* test and are shown as mean $\pm$ SEM. n = 5–14 mice per group. $*p \leq 0.05$, $**p \leq 0.01$, $***p \leq 0.001$.

cascade, and cytokine-cytokine receptor interaction pathways compared to WT mice. Here, the discrepancy between the enriched pathways at different age groups could be related to the whole genome transcriptome approach or the heterogeneous nature of the brain tissue, which was collected at different time points. The current study also suggests to use in future a cell-specific single-cell transcriptomic analysis of microglia isolated from different age groups at the same time point that should allow to much better illustrate the effect of age on microglial-specific pathways. Similar transcriptome studies also demonstrated that brain aging in mice is associated with an inflammatory response, oxidative stress, and synaptic alterations (Jiang et al., 2001; Lee et al., 2000). Our data also showed that *Snca*, which encodes the alpha-synuclein (α-synuclein) protein, was the top downregulated gene in 24-month-old Siglec-11 tg mice. Increased α-synuclein expression and its accumulation in the aging brain have been implicated in cognitive and motor dysfunction, particularly in Parkinson's disease (Xuan et al., 2011; Yang et al., 2020).

Previous studies have reported increased expression of *Cd68* and elevated levels of pro-inflammatory cytokines, such as *Tnf*, *Il-1ß*, *Il-6*, and *Il-10*, in aged microglia (Griffin et al., 2006; Wong et al., 2005; Antignano et al., 2023). Specifically, the Trem2/Dap12 signaling pathway has been identified as critical for inducing the activated, phagocytic microglial phenotype (Konishi and Kiyama, 2020). Moreover, a study examining the aging microglial signature demarcated the Fc Fragment of IgE receptor Ig (FCER1G) as a microglial biomarker associated with aging and neurodegeneration (Mukherjee et al., 2019). In aged 24-month-old Siglec-11 tg mice, we observed a lower inflammatory profile and reduced immune activation compared to WT controls, with decreased gene transcription of microglial markers *Aif1* and *Tmem119*, as well as inflammatory markers *Tnf* and *Il1ß*, as demonstrated by sqRT-PCR. Additionally, 24-month-old Siglec-11 tg mice exhibited lower gene transcription of the phagocytic marker *Cd68* compared to WT mice, reflecting a more youthful microglial transcript profile.

Oxidative stress is a hallmark of both cognitive aging and neurodegenerative diseases, as neurons are particularly vulnerable to oxidative damage (Ionescu-Tucker and Cotman, 2021). SIGLECs have been shown to prevent oxidative stress-related aging. For instance, Siglec-E knockout mice displayed a reduced maximum lifespan, signs of oxidative damage, and accelerated aging (Schwarz et al., 2015). In our study, we examined the effect of the human microglial SIGLEC-11 receptor on oxidative stress gene transcript markers in the aging brain. Our sqRT-PCR analysis demonstrated that brains of aged Siglec-11 tg mice had lower gene transcription of phagocytosis-associated oxidative

burst markers like *Cyba*, *Cybb*, and *Nos2* in comparison to WT controls. This further validated our RNA sequencing findings of suppressed oxidative phosphorylation pathways shown in the Siglec-11 tg mice. Moreover, we were able to validate our RNA sequencing findings of suppressed complement system pathways in the aged Siglec-11 tg mice by showing decreased gene transcription of complement markers *C3*, *C4*, and *Itgam* by sqRT-PCR. It is important to note that the decrease in inflammatory, complement, and oxidative stress gene markers observed in Siglec-11 tg mice also could be a consequence of reduced microglial numbers. However, the observed reduction in inflammation, with decreased microglial numbers, is clearly associated with a protective phenotype of Siglec-11 tg mice with increased neuronal density in the substantia nigra.

Lipid accumulation and droplet formation in microglia have been implicated in brain aging and neurodegeneration (Haney et al., 2024; Shimabukuro et al., 2016). Lipid droplets have typical autofluorescence properties that can be easily monitored by characteristic wavelength of confocal laser scanning microscopy. We determined the density of lipid-laden microglia and showed that Siglec-11 tg mice had less lipid-laden microglia in the substantia nigra at 6- and 24-months of age compared to WT controls.

In summary, aged 24-month-old humanized Siglec-11 tg mice exhibited a less aged brain phenotype compared to WT controls. They lacked the typical age-related increase in microglial density, CD68 upregulation, and microglial clustering. Additionally, mature Siglec-11 tg mice showed decreased lipid-laden microglial accumulation, suppression of oxidative stress and inflammatory pathways at 6 months of age, and suppression of complement and coagulative pathways at 24 months of age compared to WT controls. Particularly, gene transcripts of the pro-inflammatory cytokines *Tnf* and *Il-1β*, complement components *C3*, *C4,* and *Itgam*, and oxidative stress markers *Cyba*, *Cybb*, and *Nos2* were decreased in aged Siglec-11 tg mice. In addition, aged Siglec-11 tg mice presented less age-related neuronal loss in the substantia nigra at 24 months compared to WT mice. Collectively, these findings suggest that microglial SIGLEC-11 receptors play a crucial role in protecting the brain from "inflammaging."

Data availability statement

The datasets presented in this study can be found in online repositories. The names of the repository/repositories and accession number(s) can be found at: www.ncbi.nlm.nih.gov/geo, GSE282391.

Ethics statement

The animal studies were approved by Stabstelle Tierschutz University of Bonn. The studies were conducted in accordance with the local legislation and institutional requirements. Written informed consent was obtained from the owners for the participation of their animals in this study.

Author contributions

TA: Writing – original draft, Writing – review & editing, Conceptualization, Investigation, Methodology. NA: Writing – original draft, Writing – review & editing, Conceptualization, Investigation, Methodology. JW: Writing – review & editing, Formal analysis, Investigation, Methodology. GC-R: Writing – review & editing, Investigation, Methodology. CK: Writing – review & editing. BL-G: Writing – review & editing, Conceptualization, Investigation, Methodology, Project administration. HN: Writing – original draft, Writing – review & editing, Conceptualization, Funding acquisition, Project administration.

Funding

Acknowledgments

Conflict of interest

The authors declare that the research was conducted in the absence of any commercial or financial relationships that could be construed as a potential conflict of interest.

Generative AI statement

The authors declare that no Generative AI was used in the creation of this manuscript.

Publisher's note

All claims expressed in this article are solely those of the authors and do not necessarily represent those of their affiliated organizations, or those of the publisher, the editors and the reviewers. Any product that may be evaluated in this article, or claim that may be made by its manufacturer, is not guaranteed or endorsed by the publisher.

Supplementary material

The Supplementary material for this article can be found online at: https://www.frontiersin.org/articles/10.3389/fnins.2024.1504765/full#supplementary-material

References

Angata, T., Kerr, S. C., Greaves, D. R., Varki, N. M., Crocker, P. R., and Varki, A. (2002). Cloning and characterization of human Siglec-11. A recently evolved signaling molecule that can interact with SHP-1 and SHP-2 and is expressed by tissue macrophages, including brain microglia. *J. Biol. Chem.* 277, 24466–24474. doi: 10.1074/JBC.M202833200

Antignano, I., Liu, Y., Offermann, N., and Capasso, M. (2023). Aging microglia. *Cell. Mol. Life Sci.* 80:126. doi: 10.1007/S00018-023-04775-Y

Bellenguez, C., Küçükali, F., Jansen, I. E., Kleineidam, L., Moreno-Grau, S., Amin, N., et al. (2022). New insights into the genetic etiology of Alzheimer's disease and related dementias. *Nat. Genet.* 54, 412–436. doi: 10.1038/S41588-022-01024-Z

Bishop, N. A., Lu, T., and Yankner, B. A. (2010). Neural mechanisms of ageing and cognitive decline. *Nature* 464, 529–535. doi: 10.1038/NATURE08983

Bodea, L. G., Wang, Y., Linnartz-Gerlach, B., Kopatz, J., Sinkkonen, L., Musgrove, R., et al. (2014). Neurodegeneration by Activation of the Microglial Complement–Phagosome Pathway. *J Neurosci.* 34:8546. doi: 10.1523/JNEUROSCI.5002-13.2014

Burke, S. N., and Barnes, C. A. (2006). Neural plasticity in the ageing brain. *Nat. Rev. Neurosci.* 7, 30–40. doi: 10.1038/NRN1809

Bushnell, B., Rood, J., and Singer, E. (2017). BBMerge – accurate paired shotgun read merging via overlap. *PLoS One* 12:e0185056. doi: 10.1371/JOURNAL.PONE.0185056

Carlson, M. (2019). Bioconductor – org.Mm.eg.db. Available at: https://doi.org/10.18129/B9.bioc.org.Mm.eg.db (Accessed July 8, 2024).

Castelli, V., Benedetti, E., Antonosante, A., Catanesi, M., Pitari, G., Ippoliti, R., et al. (2019). Neuronal cells rearrangement during aging and neurodegenerative disease: metabolism, oxidative stress and organelles dynamic. *Front. Mol. Neurosci.* 12:132. doi: 10.3389/FNMOL.2019.00132

Damani, M. R., Zhao, L., Fontainhas, A. M., Amaral, J., Fariss, R. N., and Wong, W. T. (2011). Age-related alterations in the dynamic behavior of microglia. *Aging Cell* 10, 263–276. doi: 10.1111/J.1474-9726.2010.00660.X

Dickson, D. W., Crystal, H. A., Mattiace, L. A., Masur, D. M., Blau, A. D., Davies, P., et al. (1992). Identification of normal and pathological aging in prospectively studied non-demented elderly humans. *Neurobiol. Aging* 13, 179–189. doi: 10.1016/0197-4580(92)90027-U

Dobin, A., Davis, C. A., Schlesinger, F., Drenkow, J., Zaleski, C., Jha, S., et al. (2013). STAR: ultrafast universal RNA-seq aligner. *Bioinformatics* 29, 15–21. doi: 10.1093/BIOINFORMATICS/BTS635

Fan, H., Zhang, M., Wen, J., Wang, S., Yuan, M., Sun, H., et al. (2024). Microglia in brain aging: an overview of recent basic science and clinical research developments. *J. Biomed. Res.* 38, 122–136. doi: 10.7555/JBR.37.20220220

Griffin, R., Nally, R., Nolan, Y., McCartney, Y., Linden, J., and Lynch, M. A. (2006). The age-related attenuation in long-term potentiation is associated with microglial activation. *J. Neurochem.* 99, 1263–1272. doi: 10.1111/J.1471-4159.2006.04165.X

Halder, S. K., and Milner, R. (2022). Exaggerated hypoxic vascular breakdown in aged brain due to reduced microglial vasculo-protection. *Aging Cell* 21:e13720. doi: 10.1111/ACEL.13720

Hane, M., Chen, D. Y., and Varki, A. (2021). Human-specific microglial Siglec-11 transcript variant has the potential to affect polysialic acid-mediated brain functions at a distance. *Glycobiology* 31, 231–242. doi: 10.1093/GLYCOB/CWAA082

Haney, M. S., Pálovics, R., Munson, C. N., Long, C., Johansson, P. K., Yip, O., et al. (2024). APOE4/4 is linked to damaging lipid droplets in Alzheimer's disease microglia. *Nature* 628, 154–161. doi: 10.1038/s41586-024-07185-7

Hayakawa, T., Angata, T., Lewis, A. L., Mikkelsen, T. S., Varki, N. M., and Varki, A. (2005). A human-specific gene in microglia. *Science* 309, 754–755. doi: 10.1126/SCIENCE.1114321

Hayakawa, T., Khedri, Z., Schwarz, F., Landig, C., Liang, S. Y., Yu, H., et al. (2017). Coevolution of Siglec-11 and Siglec-16 via gene conversion in primates. *BMC Evol. Biol.* 17:228. doi: 10.1186/S12862-017-1075-Z

Howell, R. D., Dominguez-Lopez, S., Ocañas, S. R., Freeman, W. M., and Beckstead, M. J. (2020). Female mice are resilient to age-related decline of substantia nigra dopamine neuron firing parameters. *Neurobiol. Aging* 95, 195–204. doi: 10.1016/J.NEUROBIOLAGING.2020.07.025

Ionescu-Tucker, A., and Cotman, C. W. (2021). Emerging roles of oxidative stress in brain aging and Alzheimer's disease. *Neurobiol. Aging* 107, 86–95. doi: 10.1016/J.NEUROBIOLAGING.2021.07.014

Jiang, C. H., Tsien, J. Z., Schultz, P. G., and Hu, Y. (2001). The effects of aging on gene expression in the hypothalamus and cortex of mice. *Proc. Natl. Acad. Sci. USA* 98, 1930–1934. doi: 10.1073/PNAS.98.4.1930

Karlstetter, M., Kopatz, J., Aslanidis, A., Shahraz, A., Caramoy, A., Linnartz-Gerlach, B., et al. (2017). Polysialic acid blocks mononuclear phagocyte reactivity, inhibits complement activation, and protects from vascular damage in the retina. *EMBO Mol. Med.* 9, 154–166. doi: 10.15252/emmm.201606627

Khan, N., Kim, S. K., Gagneux, P., Dugan, L. L., and Varki, A. (2020). Maximum reproductive lifespan correlates with CD33rSIGLEC gene number: implications for NADPH oxidase-derived reactive oxygen species in aging. *FASEB J.* 34, 1928–1938. doi: 10.1096/FJ.201902116R

Klaus, C., Liao, H., Allendorf, D. H., Brown, G. C., and Neumann, H. (2021). Sialylation acts as a checkpoint for innate immune responses in the central nervous system. *Glia* 69, 1619–1636. doi: 10.1002/GLIA.23945

Konishi, H., and Kiyama, H. (2020). Non-pathological roles of microglial TREM2/DAP12: TREM2/DAP12 regulates the physiological functions of microglia from development to aging. *Neurochem. Int.* 141:104878. doi: 10.1016/J.NEUINT.2020.104878

Lee, C. K., Weindruch, R., and Prolla, T. A. (2000). Gene-expression profile of the ageing brain in mice. *Nat. Genet.* 25, 294–297. doi: 10.1038/77046

Lee, J., and Kim, H. J. (2022). Normal aging induces changes in the brain and neurodegeneration Progress: review of the structural, biochemical, metabolic, cellular, and molecular changes. *Front. Aging Neurosci.* 14:931536. doi: 10.3389/FNAGI.2022.931536

Liao, H., Klaus, C., and Neumann, H. (2020, 2020). Control of innate immunity by sialic acids in the nervous tissue. *Int. J. Mol. Sci.* 21:5494. doi: 10.3390/IJMS21155494

Liao, H., Winkler, J., Wißfeld, J., Shahraz, A., Klaus, C., and Neumann, H. (2021). Low molecular weight polysialic acid prevents lipopolysaccharide-induced inflammatory dopaminergic neurodegeneration in humanized SIGLEC11 transgenic mice. *Glia* 69, 2845–2862. doi: 10.1002/GLIA.24073

Liao, Y., Smyth, G. K., and Shi, W. (2014). featureCounts: an efficient general purpose program for assigning sequence reads to genomic features. *Bioinformatics* 30, 923–930. doi: 10.1093/BIOINFORMATICS/BTT656

Love, M. I., Huber, W., and Anders, S. (2014). Moderated estimation of fold change and dispersion for RNA-seq data with DESeq2. *Genome Biol.* 15:550. doi: 10.1186/S13059-014-0550-8

Luo, X. G., Ding, J. Q., and Chen, S. D. (2010). Microglia in the aging brain: relevance to neurodegeneration. *Mol. Neurodegener.* 5. doi: 10.1186/1750-1326-5-12

Macauley, M. S., Crocker, P. R., and Paulson, J. C. (2014). Siglec-mediated regulation of immune cell function in disease. *Nat. Rev. Immunol.* 14, 653–666. doi: 10.1038/NRI3737

Mootha, V. K., Lindgren, C. M., Eriksson, K. F., Subramanian, A., Sihag, S., Lehar, J., et al. (2003). PGC-1alpha-responsive genes involved in oxidative phosphorylation are coordinately downregulated in human diabetes. *Nat. Genet.* 34, 267–273. doi: 10.1038/NG1180

Mouton, P. R., Long, J. M., Lei, D. L., Howard, V., Jucker, M., Calhoun, M. E., et al. (2002). Age and gender effects on microglia and astrocyte numbers in brains of mice. *Brain Res.* 956, 30–35. doi: 10.1016/S0006-8993(02)03475-3

Mukherjee, S., Klaus, C., Pricop-Jeckstadt, M., Miller, J. A., and Struebing, F. L. (2019). A microglial signature directing human aging and neurodegeneration-related gene networks. *Front. Neurosci.* 13:2. doi: 10.3389/fnins.2019.00002

Noda, S., Sato, S., Fukuda, T., Tada, N., and Hattori, N. (2020). Aging-related motor function and dopaminergic neuronal loss in C57BL/6 mice. *Mol. Brain* 13, 46. doi: 10.1186/S13041-020-00585-6

Raj, D., Yin, Z., Breur, M., Doorduin, J., Holtman, I. R., Olah, M., et al. (2017). Increased white matter inflammation in aging- and Alzheimer's disease brain. *Front. Mol. Neurosci.* 10:206. doi: 10.3389/FNMOL.2017.00206

Rodrigue, K. M., and Kennedy, K. M. (2011). "The cognitive consequences of structural changes to the aging brain" in *Handbook of the psychology of aging*, Eds. K. W. Schaie and S. L. Willis (Academic press) 73–91.

RStudio Team. (2020). RStudio: Integrated development environment for R.RStudio. Available at: http://www.rstudio.com/

Schwarz, F., Pearce, O. M. T., Wang, X., Samraj, A. N., Läubli, H., Garcia, J. O., et al. (2015). Siglec receptors impact mammalian lifespan by modulating oxidative stress. *eLife* 4:6184. doi: 10.7554/ELIFE.06184

Shahraz, A., Kopatz, J., Mathy, R., Kappler, J., Winter, D., Kapoor, S., et al. (2015). Anti-inflammatory activity of low molecular weight polysialic acid on human macrophages. *Sci. Rep.* 5:16800. doi: 10.1038/srep16800

Shahraz, A., Wißfeld, J., Ginolhac, A., Mathews, M., Sinkkonen, L., and Neumann, H. (2021). Phagocytosis-related NADPH oxidase 2 subunit gp91phox contributes to neurodegeneration after repeated systemic challenge with lipopolysaccharides. *Glia*, 69, 137–150. doi: 10.1002/GLIA.23890

Shimabukuro, M. K., Langhi, L. G. P., Cordeiro, I., Brito, J. M., Batista, C. M. D. C., Mattson, M. P., et al. (2016). Lipid-laden cells differentially distributed in the aging brain are functionally active and correspond to distinct phenotypes. *Sci. Rep.* 6:3795. doi: 10.1038/SREP23795

Subramanian, A., Tamayo, P., Mootha, V. K., Mukherjee, S., Ebert, B. L., Gillette, M. A., et al. (2005). Gene set enrichment analysis: a knowledge-based approach for interpreting genome-wide expression profiles. *Proc. Natl. Acad. Sci. USA* 102, 15545–15550. doi: 10.1073/PNAS.0506580102

Tremblay, M. È., Zettel, M. L., Ison, J. R., Allen, P. D., and Majewska, A. K. (2012). Effects of aging and sensory loss on glial cells in mouse visual and auditory cortices. *Glia* 60, 541–558. doi: 10.1002/GLIA.22287

Wang, X., Chow, R., Deng, L., Anderson, D., Weidner, N., Godwin, A. K., et al. (2011). Expression of Siglec-11 by human and chimpanzee ovarian stromal cells, with uniquely human ligands: implications for human ovarian physiology and pathology. *Glycobiology* 21, 1038–1048. doi: 10.1093/GLYCOB/CWR039

Wang, X., Mitra, N., Cruz, P., Deng, L., Varki, N., Angata, T., et al. (2012). Evolution of Siglec-11 and Siglec-16 genes in hominins. *Mol. Biol. Evol.* 29, 2073–2086. doi: 10.1093/MOLBEV/MSS077

Wang, Y., and Neumann, H. (2010). Alleviation of neurotoxicity by microglial human Siglec-11. *J. Neurosci.* 30, 3482–3488. doi: 10.1523/JNEUROSCI.3940-09.2010

Wickham, H. (2016). ggplot2. Available at: https://doi.org/10.1007/978-3-319-24277-4 (Accessed July 8, 2024).

Wißfeld, J., Assale, T. A., Cuevas-Rios, G., Liao, H., and Neumann, H. (2024). Therapeutic potential to target sialylation and SIGLECs in neurodegenerative and psychiatric diseases. *Front. Neurol.* 15:874. doi: 10.3389/FNEUR.2024.1330874

Wong, A. M., Patel, N. V., Patel, N. K., Wei, M., Morgan, T. E., De Beer, M. C., et al. (2005). Macrosialin increases during normal brain aging are attenuated by caloric restriction. *Neurosci. Lett.* 390, 76–80. doi: 10.1016/J.NEULET.2005.07.058

Xuan, Q., Xu, S. L., Lu, D. H., Yu, S., Zhou, M., Uéda, K., et al. (2011). Increased expression of α-synuclein in aged human brain associated with neuromelanin accumulation. *J. Neural Transm.* 118, 1575–1583. doi: 10.1007/S00702-011-0636-3

Yang, W., Yu, W., Li, X., Li, X., and Yu, S. (2020). Alpha-synuclein differentially reduces surface expression of N-methyl-d-aspartate receptors in the aging human brain. *Neurobiol. Aging* 90, 24–32. doi: 10.1016/J.NEUROBIOLAGING.2020.02.015

Yankner, B. A., Lu, T., and Loerch, P. (2008). The aging brain. *Annu. Rev. Pathol.* 3, 41–66. doi: 10.1146/ANNUREV.PATHMECHDIS.2.010506.092044

Yu, G., Wang, L. G., Han, Y., and He, Q. Y. (2012). clusterProfiler: an R package for comparing biological themes among gene clusters. *Omics* 16, 284–287. doi: 10.1089/OMI.2011.0118

3.3 Publication 3: Decreased sialylation elicits complement-related microglia response and bipolar cell loss in the mouse retina

GLIA

WILEY

RESEARCH ARTICLE

Decreased sialylation elicits complement-related microglia response and bipolar cell loss in the mouse retina

German Cuevas-Rios[1] | Tawfik Abou Assale[1] | Jannis Wissfeld[1] | Annemarie Bungartz[1] | Julia Hofmann[2] | Thomas Langmann[2] | Harald Neumann[1]

[1]Institute of Reconstructive Neurobiology, Medical Faculty & University Hospital Bonn, University of Bonn, Bonn, Germany

[2]Experimental Immunology of the Eye, Department of Ophthalmology, University Hospital Cologne, Cologne, Germany

Correspondence

Harald Neumann, Institute of Reconstructive Neurobiology, Medical Faculty & University Hospital Bonn, University of Bonn, Venusberg-Campus 1, Bonn, Germany.
Email: harald.neumann@uni-bonn.de

Abstract

Sialylation plays an important role in self-recognition, as well as keeping the complement and innate immune systems in check. It is unclear whether the reduced sialylation seen during aging and in mice heterozygous for the null mutant of UDP-N-acetylglucosamine 2-epimerase/N-acetylmannosamine kinase (Gne+/−), an essential enzyme for sialic acid biosynthesis, contributes to retinal inflammation and degeneration. We found a reduction of polysialic acid and trisialic acid expression in several retinal layers in Gne+/− mice at 9 months of age compared to Gne+/+ wildtype (WT) mice, which was associated with a higher microglial expression of the lysosomal marker CD68. Furthermore, the total number of rod bipolar cells was reduced in 12 months old Gne+/− mice in comparison to WT mice, demonstrating loss of these retinal interneurons. Transcriptome analysis showed up-regulation of complement, inflammation, and apoptosis-related pathways in the retinas of Gne+/− mice. Particularly, increased gene transcript levels of the complement factors *C3* and *C4* and the pro-inflammatory cytokine *Il-1β* were observed by semi-quantitative real-time polymerase chain reaction (sqRT-PCR) in 9 months old Gne+/− mice compared to WT mice. The increased expression of CD68, loss of rod bipolar cells, and increased gene transcription of complement factor *C4*, were all prevented after crossing Gne+/− mice with complement factor *C3*-deficient animals. In conclusion, our data show that retinal hyposialylation in 9 and 12 months old Gne+/− mice was associated with complement-related inflammation and lysosomal microglia response, as well as rod bipolar cells loss, which was absent after genetic deletion of complement factor C3.

KEYWORDS

bipolar cells, complement, inflammation, microglia, retina, sialic acid, sialylation

1 | INTRODUCTION

Sialic acids are found at the terminal position of glycosylated proteins and lipids of the cell membrane, a condition referred here as sialylation.

Sialylated glycoproteins and glycolipids exert anti-inflammatory and antioxidative effects via binding to sialic-acid-binding immunoglobulin-like lectins (Siglec) receptors and regulatory complement factors (Klaus et al., 2021; Lünemann et al., 2021). Sialylation has been shown to

prevent the oxidative burst of microglia and macrophages, and reduce neurite loss in a macrophage-neuron co-culture after external stimuli such as neuronal cell debris (Shahraz et al., 2015). In addition, sialylation also inhibits alternative complement activation (Klaus et al., 2021; Lünemann et al., 2021). Here, sialylation acts through the inhibitory complement factor H via binding and inactivation of properdin, an activator of the alternative complement pathway (Shahraz et al., 2022).

In mammals, polysialic acid is a homopolymer of α2,8-linked sialic acid monomers, mainly found on cell membrane proteins in the nervous, immune and reproductive systems (Klaus et al., 2021; Lünemann et al., 2021). Polysialic acid is recognized by human Siglec receptors, triggering microglial and macrophage signaling, which can alleviate inflammatory neurotoxicity in vitro and in animal models (Klaus et al., 2021; Lünemann et al., 2021). The retina is enriched in polysialic acid, which is present across all of its layers, including the inner plexiform, the ganglion cell, and the outer nuclear layers (Karlstetter et al., 2017). To study the therapeutic effect of intravitreally applied soluble polysialic acid or polyglycolic/polylactic-conjugated polysialic acid on immune-related traits of the eye in vivo, retinal laser coagulation and bright light-induced retinal degeneration were performed in two independent transgenic mouse models expressing the human polysialic acid binding SIGLEC11 receptor (Karlstetter et al., 2017; Krishnan et al., 2023). Polysialic acid efficiently inhibited innate immune responses by blocking mononuclear phagocyte reactivity, inhibiting complement activation, and protecting against vascular damage in both animal models (Karlstetter et al., 2017; Krishnan et al., 2023). The polyglycolic/polylactic-conjugated polysialic acid is currently being tested in a phase II clinical trial in patients for geographic atrophy secondary to age-related macular degeneration (NCT05839041). Furthermore, it was shown that systemic application of polysialic acid inhibited the inflammatory neurodegeneration in a lipopolysaccharide-triggered Parkinson's disease animal model (Liao et al., 2021).

In the brain, where sialic acids may have protective functions, sialylation decreases with age. Particularly lower sialic acid levels have been reported in brain gangliosides of elderly human brains. The level of ganglioside-bound sialic acid was reduced in the human brain by about 65% at the age of 85 (Segler Stahl et al., 1983). To mimic the situation of reduced sialylation on the cell surface of the central nervous system during aging, mice deficient for one allele of the enzyme UDP-N-acetylglucamine 2-epimerase/N-acetylmonnosamine kinase (GNE) were studied (Klaus et al., 2020; Schwarzkopf et al., 2002). Complete *Gne* knock-out (Gne−/−) leads to embryonic lethality of mice, while Gne+/− animals only have slightly reduced levels (18.2% ± 2.9%) of sialylation in different regions of the brain at 12 months of age (Klaus et al., 2020). Interestingly, this reduced sialylation level in the brain of Gne+/− mice triggered loss of neurons starting at 6–9 months of age, which was rescued in complement factor *C3*-deficient (Gne+/−C3−/−) mice (Klaus et al., 2020). The aging human retina is particularly susceptible to complement-mediated inflammatory processes as seen in age-related macular degeneration (Gemenetzi & Lotery, 2016; Johnson et al., 2000, 2001), and to loss of certain neuronal subpopulations such as

bipolar cells (Aggarwal et al., 2007). Therefore, we comprehensively analyzed the retina of middle-aged Gne+/− mice, at 9 and 12 months of age, to elucidate any effects of reduced sialylation.

We found a reduction in oligo/polysialylation and increased expression of the lysosomal microglial marker CD68, increased gene transcription of immune-related complement factors 3 (*C3*) and 4 (*C4*), interleukin-1β (*Il-1β*), and activation of the complement, inflammation and apoptosis pathways, as well as loss of rod bipolar cells in middle-aged Gne+/− mice. Crossing the Gne+/− genotype with *C3*-deficient mice demonstrated that retinal changes triggered by the genetically reduced sialylation were prevented by deletion of *C3*.

2 | MATERIALS AND METHODS

2.1 | Mice and tissue collection

Mice heterozygous for null mutant of the bifunctional enzyme UDP-GlcNAc 2-epimerase/ManNAc kinase (referred here as Gne+/−, or Gne+/−C3+/+ mice) were kindly provided by Rüdiger Horstkorte (Schwarzkopf et al., 2002), and backcrossed for at least 10 generations with C57BL/6J mice. In addition, mice homozygous for the C3 targeted mutation were obtained as B6; 129S4-C3[tm1Crr]/J from Jackson Laboratory via Charles River (referred here as C3−/−), and also backcrossed for at least 10 generations in C57BL/6J mice. For this project, mice at an age of 9 and 12 months with the following four different genotypes were utilized: Gne+/+C3+/+ (wildtype; WT), Gne+/−C3+/+, Gne+/+C3−/−, and Gne+/−C3−/− mice. Additional retinas of 3-months-old mice were utilized to analyze sialylation at an early time point. All animals were housed at a 12 h dark/night cycle in a temperature-control facility with ad libitum water and food. All experiments were conducted randomly with male and female mice and in compliance with the animal care committees and the legal regulations. All experiments have been approved by the boards of the University Hospital of Bonn and by the local government. All possible efforts were made to minimize the number of animals and their suffering. For tissue collection, mice were euthanized and then perfused transcardially with ice-cold phosphate buffer saline (PBS) for 3 min. Both eyes were enucleated and were used either as retina homogenates for RNA isolation, or for immunohistochemistry of eye cryosections or retinal whole-mounts.

2.2 | Semi-quantitative real-time polymerase chain reaction (sqRT-PCR)

Retinal whole-mounts were dissected, homogenized in QIAzol Lysis reagent (Qiagen), and stored at −80°C until further processing. Next, chloroform was used to separate the RNA phase and isopropanol to precipitate the RNA. Afterwards, the suspension was washed with 70% ethanol and the final pellet was resuspended in ultra-pure DEPC treated water. RNA concentration and quality were measured using a

NanoDrop 2000c spectrophotometer (Thermo Scientific, Germany). The reverse transcription of the obtained RNA material was performed with SuperScript III First-Strand Synthesis System (Invitrogen, Germany) and a mixture of random hexanucleotides (Invitrogen, Germany) according to the manufacturer's protocol. Semi-quantitative real-time polymerase chain reaction (sqRT-PCR) for the designed oligonucleotides listed in the Supplementary Table 1 was performed using the SYBR GreenER qPCR SuperMix Universal (Invitrogen, Germany) on the Mastercycler epigradient S (Eppendorf, Germany). The housekeeping gene glyceraldehyde-3-phosphate dehydrogenase (GAPDH) was used as internal control for all mouse-retina samples. Results were analyzed with the Master cycler ep realplex software (Eppendorf, Germany) and the values were normalized to respective mouse-sample GAPDH values and to WT animals. The delta delta CT (cycle threshold) method was used to quantify relative gene transcription.

2.3 | RNA sequencing, differential gene expression, and pathway analysis

Total retinal RNA for RNA sequencing (RNAseq) was extracted as described above from 9 months old mice, in order to identify transcriptional changes in the retinal phenotype that might precede any neurodegenerative phenotypes. Library preparation (QuantSeq 3′ mRNA-Seq Library Prep Kit, Lexogen) with an input of 100 ng total RNA, quality control (Tapestation 2200, Fa. Agilent) and RNA sequencing were performed at the NGS Core Facility, University Hospital of Bonn, with 2×10^7 single-end reads per sample on NovaSeq 6000 (Illumina). Quality control was performed on raw reads using FastQC (v0.11.8) and MultiQC (1.7), and samples that had an unusual high guanine/cytosine (GC) content (>2 Standard Deviation) were excluded in the raw reads. Adapters were trimmed from the reads using Bbmerge/BBDUK (pmid: 29073143). Reads were then aligned to the mouse reference genome mm10 (GRCm38) with the ensemble gene annotation version 101 using STAR [v2.7.3a] (Dobin et al., 2013) with standard parameters. Read count generation was performed using featureCounts/Subread [v2.0.0] (Liao et al., 2014) ignoring multimapping reads. Quality control was performed again as described earlier. Differential expression analysis was performed with R [v4.3.1] in RStudio [v2023.6.2, build 531] (RStudio Team, 2020) using DESeq2 [v1.42.0] (Love et al., 2014) with the individual groups as contrasts. Transcript annotations were retrieved using the Bioconductor package org.Mm.eg.db [v3.11.4] (Carlson, 2019), and plots were created using ggplot2 [v3.3.3] (Wickham, 2016). Pathway enrichment analyses were performed using clusterProfiler [v3.16.1] (Yu et al., 2012) and GSEA Desktop [v4.2.2] (Mootha et al., 2003; Subramanian et al., 2005) with log2FC ≥ 1 and adjusted p-value <.05. Gene transcripts of all four groups (Gne+/+C3+/+, Gne+/−C3+/+, Gne+/+C3−/−, and Gne+/−C3−/−) were used, if not otherwise indicated in the results part, for the different analyses to extract the differential gene expression (DEG), enriched pathways, and hallmarks for the groups of interest.

2.4 | Immunohistochemistry of mouse retina

Retina frozen cryosections were used to analyze sialylation, expression of glial markers (microglia, Müller cells, and astrocytes), complement factor C1q, and the cell density of different retinal neurons. For that, eyes were fixed with 4% paraformaldehyde (PFA), then embedded and frozen in O.C.T. Compound Tissue Tek (Sakura/Fisher Scientific, Germany). Then, eyes were cut in sagittal sections of 20 μm with a cryostat (Microm, HM 560, Thermo Scientific, Germany), starting from the lateral side of the eye and passing through the optic nerve head, which served later as reference-structure for microscope retinal imaging and analysis. After being dried and washed with PBS, the sections were incubated in blocking solution; 5% normal goat serum (NGS), 10% bovine serum albumin (BSA), and 0.1%–0.3% Triton X-100, for 1 h at room temperature (RT). Then, three retinal sections per mouse were incubated overnight at 4°C in primary antibodies diluted in blocking solution. For sialylation status analysis of the retinal layers, antibody against polysialic acid, typically attached to neural cell adhesion molecule (PSA-NCAM; clone: 2-2B; 1:500; MAB5324, Millipore) and antibody against trisialic acid typically found on gangliosides (A2B5, 1:500; 433110, Invitrogen) were used. For the analysis of microglia distribution and activation in the retinal layers, we used antibodies against ionized calcium-binding adapter molecule 1 (Iba1), also known as allograft inflammatory factor 1 (Aif-1; 1:500, Wako, 019-19741), and the lysosomal molecule CD68 (1:500, Bio-Rad, MCA1957). For Müller cells and astrocytes, we used an antibody against glial fibrillar acidic protein (GFAP; 1:1000, Agilent/Dako, Z0334), as well as anti-glutamine synthetase (1:500, Invitrogen, PA5-28940) for better visualization of Müller cells in a co-staining with polysialic acid. For complement opsonization analysis, an antibody directed against the complement factor C1q was used (1:200, Abcam, ab182451). To identify and quantify retinal neurons, the following primary antibodies were utilized: for cone photoreceptors anti-cone arrestin (1:500, Merk/Millipore, AB15282), for rods outer segments rhodopsin (Rho 4D2; 1:1000, Abcam, ab98887), for rod bipolar cells the protein kinase C-alpha (PKCα, H-7; 1:250, Santa Cruz Biotechnology, sc-8393), and for ganglion cells the brain-specific homeobox/POU domain protein 3A (Brn3a; 1:2000, Merk/ Sigma-Aldrich, AB5945). In order to visualize all the retinal nuclei, including nuclei in the outer nuclear layer (ONL; photoreceptors cell body layer), the nuclear marker 4′,6-diamidino-2-phenylindole (DAPI: 1:10,000, Sigma-Aldrich, Germany) was used. As a negative control, one retina-section per mouse was incubated with secondary antibodies and used to subtract the background for the fluorescence intensity analysis. After washing with PBS (4× 5 min), the following secondary antibodies diluted in blocking solution were used to incubate the retina sections for 2 h at RT: Alexa Fluor 647 conjugated goat anti-mouse (1:500, Jackson ImmunoResearch, 115-606-072) for PSA-NCAM, A2B5, and PKCα; Alexa Fluor 647 conjugated goat anti-rabbit (1:500–1:1000, Jackson ImmunoResearch, 111-606-144) for C1q, cone arrestin, GFAP, and Iba1; Alexa Fluor 488 conjugated goat anti-rat (1:500, Invitrogen, A-11006) for CD68; Alexa Fluor

488 conjugated goat anti-rabbit (1:500, Invitrogen, A11008) for glutamine synthetase; Alexa Fluor 488 conjugated goat anti-mouse (1:500, Invitrogen A11001) for rhodopsin; Cy3 conjugated goat anti-rabbit (1:500, Jackson ImmunoResearch, 111-167-003) for Brn3a. Then, the tissue was washed and stained for nuclei with DAPI (1:10,000, Sigma-Aldrich, Germany) for 1 min. All incubation and washing steps were performed in a dark wet chamber. The stained sections were covered with a glass coverslip and Aqua/Polymount (Polysciences Inc., Germany).

Retinal whole-mounts were dissected from the eyes after PFA fixation and stained to analyze microglia density and morphology. After washing with PBS, retinas were incubated with blocking solution; 5% NGS, 0.2% BSA, and 0.3% Triton X-100 overnight at 4°C. Then, retinas were incubated for 24 h at 4°C with primary antibodies directed against Iba1 (1:500, Wako, 019-19741), and against the lysosomal marker CD68 (1:500, Bio-Rad, MCA1957) diluted in the above-mentioned blocking solution. After washing with PBS, secondary antibodies for Iba1, Alexa Fluor 647 goat anti-rabbit (1:800; Jackson ImmunoResearch, 111-606-144), and for CD68, Cy3 goat anti-rat (1:800, Jackson ImmunoResearch, 112-166-072), diluted in washing solution (PBS + 0.3% Triton X-100) were used to incubate the retinas for 2 h at RT. The tissue was washed again with PBS and stained for nuclei with DAPI (1:10,000, Sigma-Aldrich, Germany) for 1 min. All incubation and washing steps were performed on a nutating mixer (VWR, USA). Finally, the stained tissue was placed onto microscope slides (Epredia, Germany), flattened and mounted with Aqua/Polymount (Polysciences Inc., Germany) and a glass coverslip.

2.5 | Confocal microscopy

All images were collected by a Leica SP8 resonant scanning confocal microscope and the LAS-X software (Leica Biosystems, Germany) with a 40× objective lens, except for retinal cryosections stained for C1q that were collected with a 63× objective lens. The images were taken covering the entire retina thickness, by using z-stacks at 2 μm intervals, except for the C1q staining, that were imaged at 1 μm intervals, with 10 optical sections. A total of six images were taken per mouse retina from the central, middle, and peripheral areas from the left and right sides of the retina cryosection for all stainings. Additional images were collected from negative control stainings that were used to subtract the background signal for the fluorescence intensity analysis. Single images were converted to maximum projections of z-stacks (10 optical sections) for all stained retinal sections, except for those stained for cone arrestin, which were overlaid with just eight optical sections, and for PKCα with three optical sections. The images were saved as tag image file format (TIFF) multichannel with the LAS-X software (Leica Biosystems, Germany, v3.5.5). Then, images from retinal whole-mounts stained for Iba1 and CD68 were taken from the outer plexiform layer (OPL). Six z-stacks images of 10 optical sections, at 1 μm intervals were taken per mouse retina from central, middle and peripheral areas from two contralateral retinal sides, with a total of six images per mouse.

2.6 | Image analysis

Image analysis was performed with ImageJ software (v2.1.0/1.53c, NIH, USA) by measuring the fluorescence integrated density (mean gray value by the area) after subtraction of the mean background fluorescence signal, obtained from the negative control images. For all staining analyses, the mean fluorescence intensity and cell density of each mouse were normalized to the mean of the WT mice group. The nuclei stained with DAPI were used to identify the retinal layers; ganglion cell layer (GCL), inner plexiform layer (IPL), inner nuclear layer (INL), outer plexiform layer (OPL), and outer nuclear layer (ONL). The expression of polysialic and trisialic acids (stained with the antibodies PSA-NCAM and A2B5, respectively) was determined in the whole retinal thickness, as well as in individual retinal layers (data not shown). Similarly, the expression of the microglial markers Iba1 and the lysosomal marker CD68, as well as the expression of the Müller cells and astrocyte marker GFAP was quantified in all retinal layers. For the analysis of Iba1/CD68 and GFAP fluorescence intensity, the area spanning from GCL to IPL were selected and considered together, since the cell bodies of the glial cells were often situated between both layers. The quantification of C1q was performed only in the OPL due to the highest staining signal of this complement component in this layer compared to the other retinal layers, which showed a weak C1q signal. Microglial cell density was calculated in the OPL in retinal whole-mounts using maximum projections z-stacks images, and by counting manually the somas of Iba1 positive cells. The skeleton of microglial cells was analyzed in retinal whole-mounts using the plug-in MotiQ in ImageJ (Hansen et al., 2022). At least eight microglial cells per mouse-retina in three different images were randomly selected with the ImageJ polygon tool, including microglia soma and its processes in the selection. After being cropped and saved as single cell image, a two-dimensional (2D) reconstruction was performed and different parameters were measured such as ramification index, spanned area (or total area cover by the cell), number of branches, number of tips, number of junctions, and the tree length. Lower values of the skeleton parameters would indicate that microglia turn from highly ramified to more amoeboid shape (Stence et al., 2001; Young & Morrison, 2018). Images of the retinal cryosections stained for cone arrestin (cone photoreceptors), PKCα (rod bipolar cells), and Brn3a (ganglion cells) were utilized to calculate the cell density of the different retinal neurons dividing the number of positive cells by the selected area using DAPI signal as reference to identify the corresponding neuronal area. The thickness or width of the ONL which contains the photoreceptors cell bodies was measured to investigate indirectly possible photoreceptors loss. As described before, the images of retinal cryosections stained for nuclei with DAPI were taken from the central, middle, and peripheral retina, using the optic nerve head as reference to ensure that the images were taken consistently in all mice and to decrease discrepancies in the retina thickness values. The ONL width was measured with the freehand line tool of ImageJ in three different regions per image in all the nine images of each mouse, with a total of 27 measurement points per mouse.

2.7 | Statistical analysis

All the experiments' data are presented as mean ±, or, + SEM (standard error of the mean; if not stated otherwise). For all analysis, the results were normalized to the mean of the WT mice within each age-group to calculate the relative values. Extreme outliers were removed after being identified with Grubbs' test using the outlier calculator of GraphPad QuickCalcs. Statistical comparisons between two groups were performed by unpaired Student's t-test, or by Welch ANOVA with Welch's correction for more than two mouse groups. Both, statistical analysis and graphs were created using GraphPad Prism (v8.0.2). Finally, statistically significant differences were depicted as *p < .05; **p < .01; ***p < .001; ****p < .0001.

3 | RESULTS

3.1 | Reduced expression of trisialic and polysialic acids in the retinas of Gne+/− mice

Heterozygous Gne+/− mice have been previously used as model system to study reduced levels of sialylation in the aging brain (Klaus et al., 2020). Here, we focused on the retina of Gne+/− mice. First, we confirmed reduced gene transcription of the *Gne* gene in the retinas of Gne+/− animals that only have one intact allele of this gene. In detail, the analysis of retinal homogenates showed a significant decrease (p = .02) of the relative *Gne* mRNA levels from 1.02 ± 0.08 fold change (FC) in wildtype (WT; Gne+/+) control mice to 0.73 ± 0.03 FC in heterozygous Gne+/− mice (Supplementary Figure 1). Next, we studied the oligo- and polysialylation status of the retina by immunostaining with antibodies directed against trisialic acid (A2B5 antibody), often found on gangliosides (Figure 1a,b), and against polysialic acid (clone: 2-2B antibody), typically attached to neural cell adhesion molecules (NCAM; Figure 1c,d). The stainings of trisialic acid and polysialic acid showed a higher signal intensity in the ganglion cell layer (GCL) and in the plexiform layers (IPL and OPL), and a lower signal intensity in the nuclear layers (ONL and INL). However, while trisialic acid showed higher staining intensity in photoreceptor outer segments (POS), polysialic acid staining was weaker. We next performed a co-staining with PSA-NCAM and glutamine synthetase (Supplementary Figure 2) to investigate whether the staining pattern of polysialic acid is associated with a retinal cell type, particularly with Müller cells, since the polysialic acid staining seems to
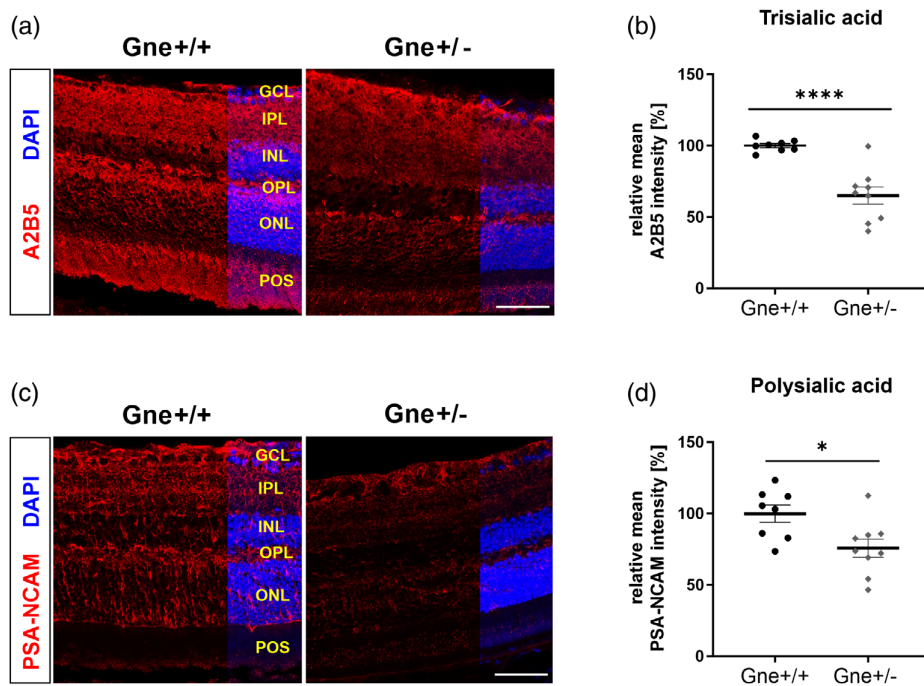
FIGURE 1 Reduced retinal levels of sialic acids in Gne+/− mice. (a) Representative images of retinal cryosections co-stained for trisialic acid of gangliosides (A2B5, red) and with the nuclear marker DAPI (blue). (b) Quantification of the fluorescence intensity of A2B5-immunostaining in mouse retina showed a significant decrease of trisialic acid at 9 months of age in Gne+/− mice; n = 8–9. (c) Representative images of retinal cryosections co-stained for polysialic acid of neuronal cell adhesion molecule (PSA-NCAM; red) and the nuclear marker DAPI (blue). (d) The fluorescence intensity analysis of PSA-NCAM-immunostaining in mouse retina revealed reduced polysialic acid expression at 9 months of age in Gne+/− mice; n = 8–9. Both scale bars: 50 μm. GCL, ganglion cell layer; INL, inner nuclear layer; IPL, inner plexiform layer; ONL, outer nuclear layer; OPL, outer plexiform layer; POS, photoreceptors outer segments. All data shown as mean ± SEM; normalized to wildtype mice; *p ≤ .05; ****p ≤ .0001.

(a)

(b)

FIGURE 2　Increased retinal lysosomal CD68 expression of microglia in Gne+/− mice. (a) Representative images of retinal cryosections of 12 months old Gne+/+ and Gne+/− mice stained with antibodies for the microglia markers, the ionized calcium binding adaptor molecule 1 (Iba1; red), CD68 (green), and the nuclear marker DAPI (blue). (b) Analysis of the fluorescence intensity showed only a tendency for higher expression levels of Iba1 in 12 months Gne+/− mice in the inner nuclear layer (INL; $p = .050$), while CD68 was increased in both 9 and 12 months Gne+/− mice in most of the retinal layers; $n = 7$–10. Scale bar, 50 μm. GCL, ganglion cell layer; INL, inner nuclear layer; IPL, inner plexiform layer; ONL, outer nuclear layer; OPL, outer plexiform layer. All data shown as mean + SEM; normalized to wildtype mice; ns = not significant, *$p \leq .05$; **$p \leq .010$.

follow the Müller cells arrangement. The images show that polysialic acid co-localizes partially with Müller cells, especially around the GCL. However, polysialic acid can also be seen delimitating other retinal structures in all layers (Supplementary Figure 2). Analysis of the retinal images revealed that the expression level of trisialic and polysialic acid was reduced in the retina of Gne+/− compared to the WT control mice at 9 months of age (Figure 1a,c). Quantification of the fluorescence intensity revealed a significant reduction ($p < .0001$) in trisialic acid expression from 100 ± 1.45% in WT to 64.9 ± 6.07% in Gne+/− mice at 9 months of age (Figure 1b). Also, retinas of 9 months Gne+/− mice showed a decrease of 24.2 ± 6.41% ($p = .01$) of the relative expression intensity of polysialic acid compared to WT mice. (Figure 1d). No significant reduction of trisialic acid and polysialic acid was present in the retinas of Gne+/− mice at 3 months of age (Supplementary Figure 3), suggesting that reduced retinal sialylation is developing over time in middle-aged mice.

Thus, retinas of heterozygous Gne+/− mice exhibited reduced *Gne* transcription levels accompanied with a significant decreased of trisialic and polysialic acids at 9 months of age.

3.2 | Increased expression of microglial lysosomal marker, and mild gliosis in the ganglion cell layer and inner plexiform layer in the retinas of Gne+/− mice

Since sialylation might act as a check point for the innate immune system in the retina (Klaus et al., 2021; Lünemann et al., 2021), we investigated microglial activation markers across the retinal layers in cryosections by staining with antibodies directed against the microglial proteins Iba1 and CD68 (Figure 2a). Analysis of the Iba1 positive cells revealed that most microglial cells were located in the GCL, as well as in the inner and outer plexiform layers, while only few microglial cells were found in the ONL or in the subretinal space, in both

genotypes (Figure 2a). Analysis of the fluorescence intensity showed similar Iba1 intensities in most of the retinal layers between the Gne +/− and Gne+/+ WT mice at 9 and 12 months of age, except for the INL, which showed a trend for an increased Iba1 intensity in Gne+/− mice at 12 months ($p = .050$). On the other hand, the expression of the microglial CD68 was higher in almost all retinal layers in Gne+/− compared to Gne+/+ mice at 9 and 12 months of age. Prominently, the outer plexiform layer displayed a relative increase ($p = .014$) in fluorescence intensity of CD68 from 100 ± 14.8% in WT animals to 144.17 ± 7.48% in Gne+/− mice at 9 months of age (Figure 2b). Next, we determined the relative density of Iba1 positive microglial cells using retinal whole-mounts co-stained with antibodies directed against Iba1 and CD68 (Supplementary Figure 4A). The results revealed comparable cell densities between Gne+/− and WT mice at 9 and 12 months of age (Supplementary Figure 4B). To elucidate any morphological changes of microglia in response to hyposialylation, we also analyzed the shape and ramification of microglia with the software ImageJ and the MotiQ plug in (Supplementary Figure 4C). Data showed highly ramified microglia and no visible changes in the morphological parameters between the 9-month-old Gne+/− and the WT mice (Supplementary Figure 4D).

Activation of retinal astrocytes, Müller cells, and overall gliosis, have been associated with inflammation and several other retinal pathologies (Guttenplan et al., 2020; Iandiev et al., 2006; Inman & Horner, 2007; Nadal-Nicolás et al., 2018; Yang et al., 2019). Therefore, we investigated retinal Müller cells and astrocytes with an antibody directed against glial fibrillary acidic protein (GFAP; Supplementary Figure 5A). The staining signal of GFAP was mainly found in the ganglion cell layer and extended with a gradual decrease of intensity towards the outer plexiform layer. In some samples, GFAP expression was also observed in the outer nuclear layer (Supplementary Figure 5A). The analysis of the mean fluorescence intensity showed increased GFAP intensity in the ganglion cell layer/inner plexiform layer (GCL/IPL) in Gne+/− mice. In detail, relative GFAP signal in the GCL/IPL was increased ($p = .03$) at 9 months of age from 100 ± 8.85% in WT to 123.37 ± 4.47% in Gne+/− mice (Supplementary Figure 5B).

Overall, the expression of the lysosomal microglial marker CD68 was increased in several layers and the Müller cells/astrocytic gliosis marker GFAP was detected at slightly higher levels in the retinal GCL/IPL of heterozygous Gne+/− mice.

3.3 | Bipolar cell loss in retinas of 12-months-old Gne+/− mice, but no change in C1q expression

Hyposialylation is reported to be associated with neuronal and synaptic loss in the substantia nigra and hippocampus, particularly at 9 and 12 months of age (Klaus et al., 2020). Therefore, we investigated the thickness of the photoreceptor outer nuclear layer (ONL) after staining with the nuclear marker DAPI to determine any obvious changes in neuronal density of the photoreceptors layer (Figure 3a). In addition, we analyzed the cellular density of the retinal basic circuitry with

specific antibodies against rod photoreceptors outer segments (rhodopsin; Supplementary Figure 6A), cone photoreceptors (cone arrestin; Figure 3c), rod bipolar cells (PKCα; Figure 3e), and ganglion cells (Brn3a; Figure 3g).

Analysis of the ONL thickness revealed no significant changes in Gne+/− mice compared to the WT mice at 9 and 12 months of age (Figure 3b). In line with this finding, analysis of fluorescence intensity showed no differences of rhodopsin levels in 9 and 12 months Gne+/− mice compared to WT animals (Supplementary Figure 6B). Similarly, the relative cell density of cone photoreceptors was comparable between Gne+/− and Gne+/+ mice at 9 and 12 months of age (Figure 3d). The analysis of PKCα positive cells showed no rod bipolar cell density changes in 9-months old Gne+/− mice, whereas at 12 months of age the relative density of rod bipolar cells was decreased ($p = .02$) from 100 ± 1.42% in WT Gne+/+ to 92.54 ± 2.58% in Gne+/− mice (Figure 3f). The ganglion cell density was not affected at 9 months or at 12 months of age (Figure 3h).

Degenerating neurons are often opsonized by complement factors before they are cleared by microglial phagocytosis (Hong et al., 2016; Werneburg et al., 2020). Therefore, we analyzed C1q deposition in the retinas of 9- and 12-months old mice. Analysis revealed a clear C1q signal in the outer plexiform layer (OPL), and only a weak signal in the GCL, in both Gne+/− and WT control mice (Supplementary Figure 7A). Hence, the quantification of the fluorescence intensity was performed in the OPL (Supplementary Figure 7B). The results showed a comparable expression level of C1q between the Gne+/− mice and the WT animals at both, 9 and 12 months of age (Supplementary Figure 7B).

Taken together, these data demonstrated loss of rod bipolar cells at 12 months of age, while no change in the expression of C1q was observed between Gne+/− and Gne+/+ mice.

3.4 | Inflammatory transcriptome profile of Gne +/− mouse retina

To better understand the mechanisms of microglia activation and loss of rod bipolar cells in this model of hyposialylation, we performed bulk RNAseq analysis of retinas from 9 months old Gne +/− and WT control mice. Our main intention was to identify the early transcriptional changes that often occur before protein changes and cellular loss. Although the principal component analysis (PCA) did not show a clear separation between the Gne+/− and the WT (Gne+/+) control mice group (Supplementary Figure 8A), the differentially expressed genes (DEG) confirmed a substantially reduced transcripts of the *Gne* gene in the Gne+/− mice (p adj. 5.93e−19). Furthermore, several novel interesting gene transcripts were differentially expressed between both groups (Supplementary Figure 8B). Particularly, transcripts of the protein-coding genes crystallin alpha B (*Cryab*) and beta-crystallin B1 (*Crybb1*) were up-regulated in the Gne+/− mice, which are encoding crystallin proteins essential to preserve the lens transparency and refractivity. In addition, the HORMA domain containing
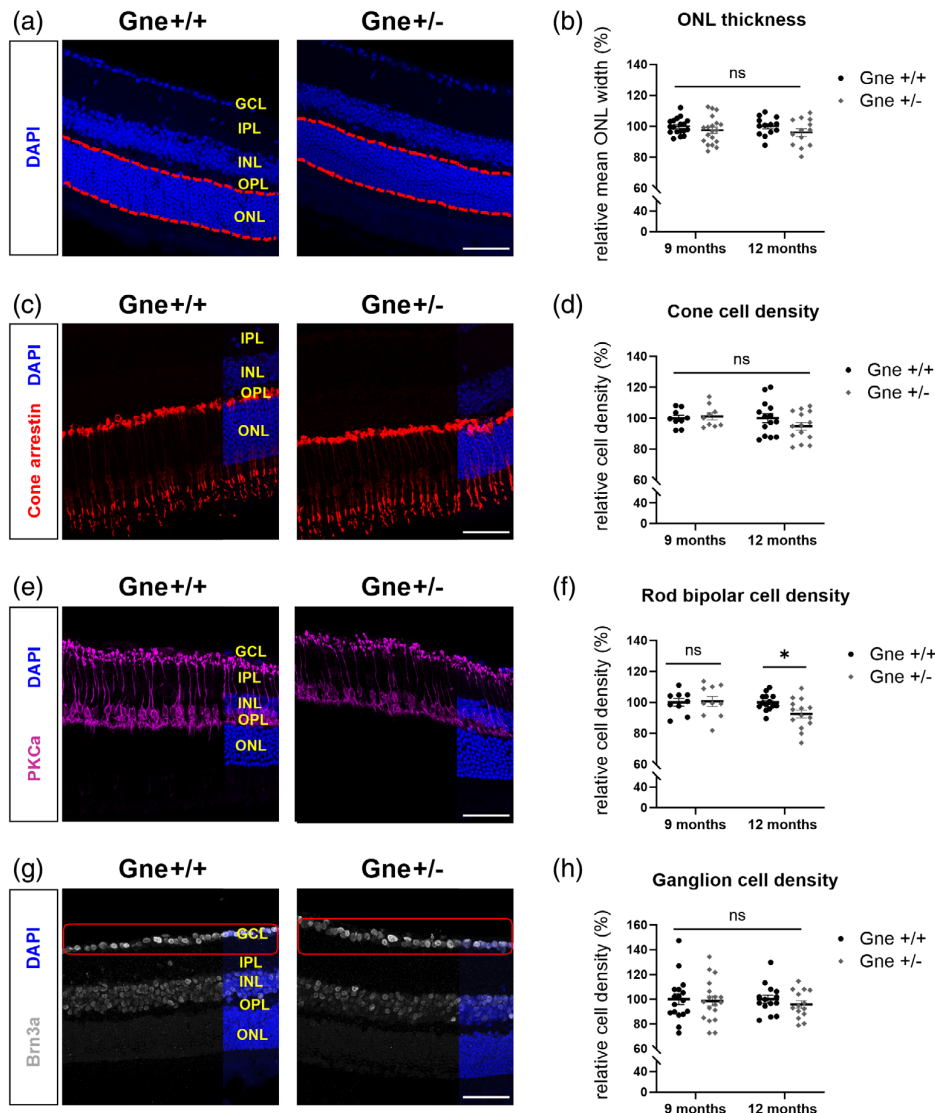
FIGURE 3 Bipolar cells loss in retinas of Gne+/− mice. (a) Representative images of staining with the nuclear marker DAPI (blue) on retinal cryosections of 12 months old Gne+/− and Gne+/+ mice. (b) The analysis of the width of outer nuclear layer (ONL; red dotted line) exhibited no significant changes in 9 and 12 months old Gne+/− mice compared to Gne+/+ mice; $n = 13$–19. (c) Images of retinal cryosections of 12 months old mice stained with the antibody cone arrestin (red). (d) The quantification of cone arrestin positive cells showed similar cell density in 9 and 12 months Gne+/− mice in comparison to Gne+/+ mice; $n = 9$–14. (e) Images of bipolar cells stained with the antibody for the protein kinase C-alpha (PKCα; magenta) in retinal cryosections of 12 months old Gne mice. (f) The analysis of cell density revealed a reduction of rod bipolar cell number in Gne+/− at 12 months of age compared to Gne+/+ mice; $n = 9$–14. (g) Representative images of staining in retinal cryosections with the antibody brain specific homeobox/POU domain protein 3A (Brn3a; gray) in 12 months Gne mice. (h) The cell counting of Brn3a positive cells displayed no difference of ganglion cells at 12 months between Gne+/− and Gne+/+ mice; $n = 14$–18. All scale bars; 50 μm. GCL, ganglion cell layer; INL, inner nuclear layer; IPL, inner plexiform layer; ONL, outer nuclear layer; OPL, outer plexiform layer. All data shown as mean ± SEM; normalized to wildtype mice; ns = not significant, *$p \leq .05$.

2 (*Hormad2*) gene transcription that is crucial for the meiotic prophase was also upregulated (Kogo et al., 2012) (Supplementary Figure 8B).

In addition, we performed gene set enrichment analysis (GSEA). Interestingly, several hallmark gene sets were up-regulated in Gne +/− mice. Particularly, UV responses, angiogenesis, epithelial/mesenchymal transi-tion, Il6/JAK/STAT3, TNFA signaling via NFKB, apoptosis, p53 pathway, KRAS signaling, coagulation, and complement gene sets (Figure 4a).

Subsequently, we verified several gene transcripts identified by GSEA in Gne+/− mice using sqRT-PCR, particularly the complement system, inflammation, apoptosis, and epithelial/mesenchymal, as well as those related to microglia, oxidative stress, and retina-associated functions. Accordingly, we investigated the gene transcript levels of the microglial markers, the allograft inflammatory factor 1 (*Aif1*), CD68 antigen (*Cd68*) and transmembrane protein 119 (*Tmem119*),
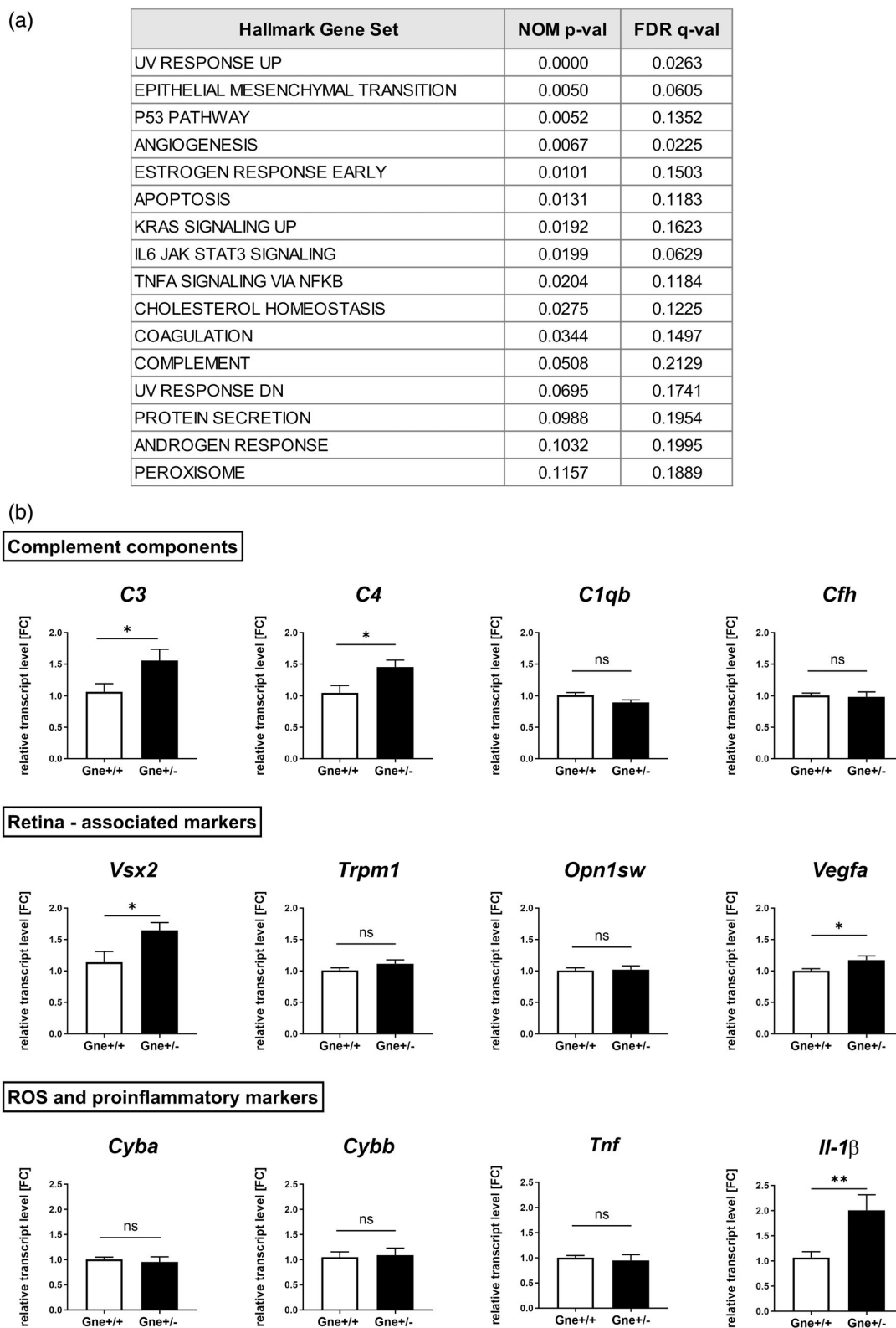
(a)

Hallmark Gene Set	NOM p-val	FDR q-val
UV RESPONSE UP	0.0000	0.0263
EPITHELIAL MESENCHYMAL TRANSITION	0.0050	0.0605
P53 PATHWAY	0.0052	0.1352
ANGIOGENESIS	0.0067	0.0225
ESTROGEN RESPONSE EARLY	0.0101	0.1503
APOPTOSIS	0.0131	0.1183
KRAS SIGNALING UP	0.0192	0.1623
IL6 JAK STAT3 SIGNALING	0.0199	0.0629
TNFA SIGNALING VIA NFKB	0.0204	0.1184
CHOLESTEROL HOMEOSTASIS	0.0275	0.1225
COAGULATION	0.0344	0.1497
COMPLEMENT	0.0508	0.2129
UV RESPONSE DN	0.0695	0.1741
PROTEIN SECRETION	0.0988	0.1954
ANDROGEN RESPONSE	0.1032	0.1995
PEROXISOME	0.1157	0.1889

(b)

Complement components

Retina - associated markers

ROS and proinflammatory markers

FIGURE 4   Legend on next page.

complement component 3 (*C3*), complement component 4 (*C4*), complement component 1q (*C1qb*) and complement regulatory factor h (*Cfh*). Additionally, we analyzed the pro-inflammatory cytokines interleukin-1 beta (*Il-1β*), and the tumor necrosis factor alpha (*Tnf*), and the oxidative stress markers cytochrome b-245 alpha chain (*Cyba*) and beta chain (*Cybb*, Figure 4b). The sqRT-PCR results showed an upregulation in the mRNA levels of *C3* ($p = .03$), *C4* ($p = .02$), and *Il-1β* ($p = .01$) in 9 months Gne+/− mice retinas compared to Gne+/+ WT mice (Figure 4b). Furthermore, we observed elevated gene transcript levels of retina-associated markers the visual system homeobox 2 (*Vsx2*; $p = .022$) and vascular endothelial growth factor A (*Vegfa*: $p = .04$) in Gne+/− mice (Figure 4b). No changes were observed in the microglial markers, in the oxidative stress markers, *Cyba* and *Cybb*, in *Tnf* levels, or in the complement receptor 3 (*Itgam*; Supplementary Figure 9). In line, transcriptional levels of analyzed genes associated with apoptosis and epithelial/mesenchymal hallmarks were unaffected (Supplementary Figure 9).

Overall, the transcriptome data show a mild pro-inflammatory *Il-1β* phenotype and activation of the complement system factors *C3* and *C4* along with increased retina-associated *Vsx2* and angiogenesis-related *Vegfa* in hyposialylated mouse retinas.

3.5 | Increased CD68 expression in microglia was prevented after deletion of complement factor 3

Previous data elucidated the relevance of the complement system in microglial activation and neuronal loss in brains of Gne+/− mice. In this context, the complement system can be targeted by deletion of the key complement factor C3 (Klaus et al., 2020). Therefore, we next analyzed retinal cryosections of Gne+/− 12 months old mice (referred henceforth as Gne+/−C3+/+ for clarity) crossed with *C3*-deficient mice to decipher the role of the complement system in retinal inflammation and neurodegeneration associated with hyposialylation. The fluorescence intensity of the microglial markers Iba1 and CD68 was reduced in Gne+/− mice crossed with *C3*-deficient mice (Gne+/−C3−/−) in all retinal layers compared to Gne+/−C3+/+ mice (Figure 5a,b). In the ONL the Iba1 intensity was increased in Gne+/−C3+/+ mice to $120.33 \pm 7.89\%$ compared to WT animals, while it was decreased in Gne+/−C3−/− mice to $46.70 \pm 3.58\%$ ($p = <.0001$). In addition, the intensity of the CD68 in the ONL of Gne+/−C3+/+ mice retina was

$128.52 \pm 8.96\%$, whereas in Gne+/−C3−/− it was reduced to $68.21 \pm 16.51\%$ ($p = .01$). Similar results were observed in the rest of the retinal layers. No differences in the fluorescence intensities of Iba1 and CD68 were found between *C3*-deficient mice crossed either with Gne+/− or with WT mice (Gne+/−C3−/− and Gne+/+C3−/−), indicating that despite reduced sialylation microglial response was reduced in *C3*-deficiency (Figure 5b).

Thus, *C3*-deficiency overall suppressed the microglial activation markers Iba1 and CD68 in hyposialylated retinas of 12 months Gne+/−C3+/+ mice.

3.6 | Bipolar cells loss in Gne+/− mice was prevented after deletion of complement factor 3

We also examined whether the loss of rod bipolar cells could be prevented by deleting the critical complement component C3. Therefore, we investigated rod bipolar cell density in Gne+/− mice crossed with C3−/− mice (Gne+/−C3−/−; Figure 6a,b). Surprisingly, the deletion of *C3* had a substantial effect on rod bipolar cells with increased density in both, Gne+/+C3−/− and Gne+/−C3−/− mice compared to the mice with intact complement *C3* (Gne+/+C3+/+ and Gne+/−C3+/+). Accordingly, the loss of rod bipolar cells observed in retinas of 12 months Gne+/−C3+/+ mice compared to WT animals was no longer visible after deletion of *C3*. In detail, Gne+/−C3−/− mice showed substantially more rod bipolar cells compared to Gne+/−C3+/+ mice ($110.13 \pm 3.96\%$ vs. $92.54 \pm 2.58\%$, $p = .001$), indicating an overall protective role of *C3*-deficiency on rod bipolar cells (Figure 6b).

Taken together, these results demonstrate that *C3*-deficiency has an overall protective effect on rod bipolar cell survival in hyposialylated retinas of 12-month-old Gne+/−C3+/+ mice.

3.7 | Several transcriptome changes in Gne+/− mice were prevented after deletion of complement factor 3

Next, we focused on transcriptomic changes in 9 months old mice that were crossed with *C3*-deficient mice (Gne+/−C3−/− and Gne+/+C3−/−) in comparison to the Gne+/−C3+/+ and

---

FIGURE 4 Up-regulation of several hallmark gene sets, and increased gene transcription of complement factors, retina-associated markers, and interleukin-1 beta in Gne+/− mice retinas. (a) Top upregulated hallmarks in Gne+/− mice retinas compared to WT controls, identified with the gene set enrichment analysis (GSEA) software in the 9-months old mice. (b) Transcriptional analysis of mouse retinas by semi-quantitative real-time polymerase chain reaction (sqRT-PCR) showed a significant elevation of the complement component 3 (*C3*) and complement component 4 (*C4*) gene transcripts. In contrast, the transcript levels of complement component 1, q subcomponent, beta polypeptide (*C1qb*), and complement factor h (*Cfh*) displayed no differences in Gne+/− mice at 9 months of age. The gene transcript levels of the visual system homeobox 2 (*Vsx2*) and vascular endothelial growth factor A (*Vegfa*) were increased, while the levels of transient receptor potential cation channel, subfamily M, member 1 (*Trpm1*) and opsin 1, short wave-sensitive (*Opn1sw*) were unaffected in 9 months old Gne+/− mice. The quantification of the transcript levels of cytochrome b-245 alpha chain (*Cyba*), cytochrome b-245 beta chain (*Cybb*), and tumor necrosis factor alpha (*Tnf*) showed similar expression in Gne+/− and Gne+/+ wildtype mice. However, the gene expression of interleukin-1 beta (*Il-1β*) was elevated at 9 months in Gne+/− mice; $n = 10$–13. FC, fold change; FDR *q*-val, false discovery rate *q* value; NOM *p*-val, nominal *p* value; ROS, reactive oxygen species. All data shown as mean + SEM; normalized to wildtype mice; ns = not significant, $*p \leq .05$; $**p \leq .01$.
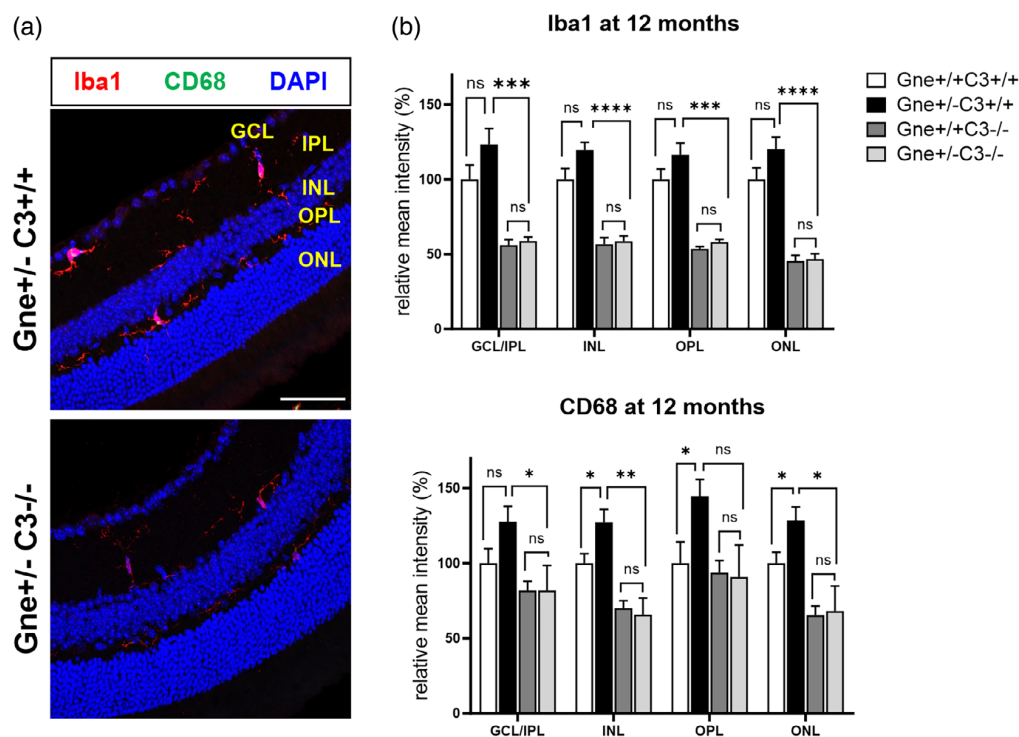
FIGURE 5 Reversal of increased retinal microglial CD68 expression in Gne+/− mice after deletion of complement C3. (a) Representative images of retinal cryosections of 12 months old Gne+/−C3+/+ and Gne+/−C3−/− mice stained with the ionized calcium binding adaptor molecule 1 (Iba1; red) and CD68 (green) antibodies, and the nuclear marker DAPI (blue). (b) Analysis of the fluorescence intensity revealed reduced intensity of Iba1 and CD68 in most of the retinal layers of 12 months Gne+/−C3−/− mice compared to Gne+/−C3+/+ mice; $n = 7$. Scale bar, 50 μm. GCL, ganglion cell layer; INL, inner nuclear layer; IPL, inner plexiform layer; ONL, outer nuclear layer; OPL, outer plexiform layer. Welch ANOVA with Welch's correction. All data shown as mean + SEM; normalized to Gne wildtype mice (Gne+/+C3+/+); ns = not significant, *$p \leq .05$; **$p \leq .01$; ***$p \leq .001$; ****$p \leq .0001$.
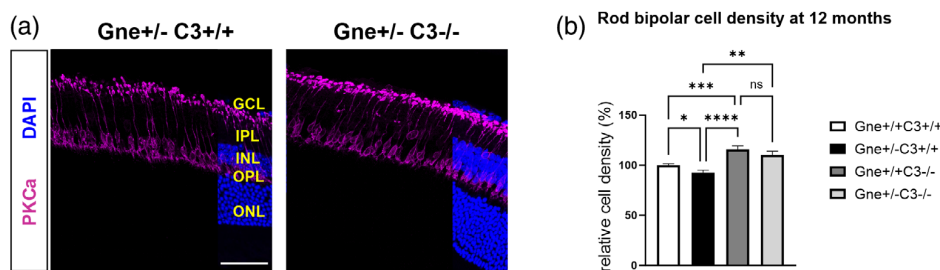

FIGURE 6 Reversal of retinal bipolar cell loss of Gne+/− mice after deletion of complement C3. (a) Representative images of retinal cryosections of 12 months Gne+/−C3+/+ and Gne+/−C3−/− mice co-stained with the antibody for the protein kinase C-alpha (PKCα; magenta) for rod bipolar cells and the nuclear marker DAPI (blue). (b) The analysis of the cell density showed prevention of the rod bipolar cell loss observed in 12 months Gne+/−C3+/+ mice by deletion of complement C3 (Gne+/−C3−/−); $n = 12$–14. Scale bar, 50 μm. GCL, ganglion cell layer; INL, inner nuclear layer; IPL, inner plexiform layer; ONL, outer nuclear layer; OPL, outer plexiform layer. Welch ANOVA with Welch's correction. Data shown as mean + SEM; normalized to Gne wildtype mice (Gne+/+C3+/+); ns = not significant, *$p \leq .05$; **$p \leq .01$; ***$p \leq .001$; ****$p \leq .0001$.

Gne+/+C3+/+ WT mice. The deficiency of C3 was verified by genotyping of mice and by qRT-PCR analysis of mouse retina (Figure 7). The PCA plot from the RNAseq analysis only showed a clear separation between both mouse groups having intact C3 (C3+/+) from the groups with deletion of C3 (C3−/−), while no obvious separation was visible between the mice heterozygous for Gne (Gne+/−) and wildtype mice (Gne+/+; Supplementary Figure 10A). The DEG analysis between Gne+/−C3+/+ and Gne+/−C3−/− mice demonstrated several differentially expressed genes after deletion of C3 (Supplementary Figure 10B). To further unravel the effect of the C3 knock-out on the Gne+/−C3+/+ transcriptome, the top 50 up-regulated and down-regulated genes were identified in the GSEA
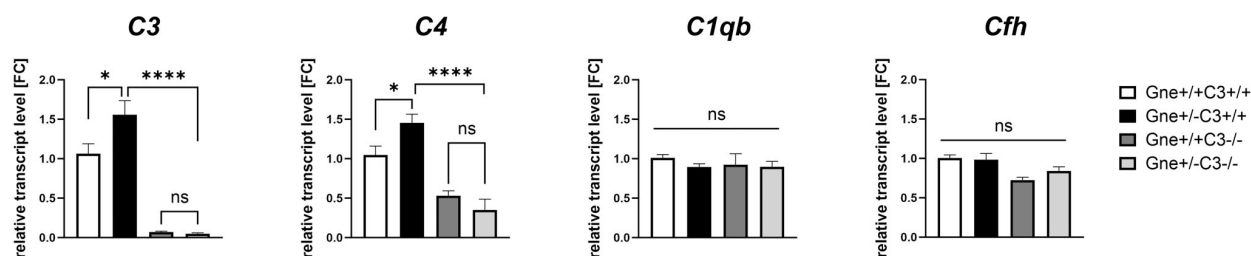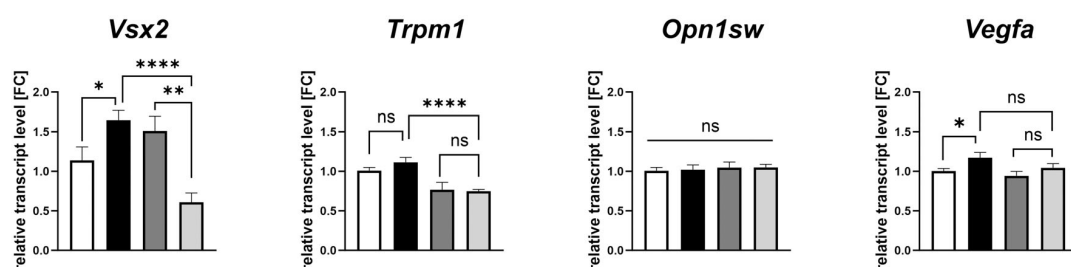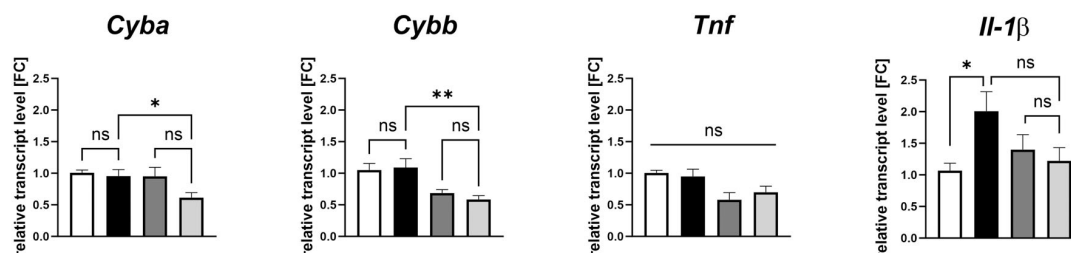
FIGURE 7 Reversal of transcriptome changes of Gne+/− mice retinas after deletion of complement C3. Nine months old Gne+/+C3−/− and Gne+/−C3−/− mice showed almost undetectable gene transcription of component 3 (*C3*). Elevated transcript levels of complement component 4 (*C4*), and of the visual system homeobox 2 (*Vsx2*) were prevented in Gne+/− mice crossed with *C3*-deficient mice (Gne+/−C3−/−). The increased gene transcription of interleukin-1 beta (*Il-1β*) in Gne+/− displayed a slight trend for reverted levels in Gne+/−C3−/− mice ($p = .054$), while the vascular endothelial growth factor A (*Vegfa*) showed not significant decreased in Gne+/+C3−/− compared to Gne+/−C3+/+ mice. Transcriptional levels of the transient receptor potential cation channel, subfamily M, member 1 (*Trpm1*), the cytochrome b-245 alpha chain (*Cyba*), and the cytochrome b-245 beta chain (*Cybb*) exhibited a significant decrease in Gne+/−C3−/− mice compared to Gne+/−C3+/+ mice at 9 months of age. Gene transcript levels of the complement component 1, q subcomponent, beta polypeptide (*C1qb*), complement factor h (*Cfh*), opsin 1, short wave sensitive (*Opn1sw*), and the tumor necrosis factor alpha (*Tnf*) were unchanged; $n = 6$–13. FC, fold change; ROS, reactive oxygen species. Welch ANOVA with Welch's correction. All data shown as mean + SEM; normalized to wildtype mice (Gne+/+C3+/+); ns = not significant, *$p \leq .05$; **$p \leq .01$; ****$p \leq .0001$.

comparison between Gne+/−C3+/+ mice and the rest of genotype groups and displayed as a heatmap (Supplementary Figure 11).

The heatmap revealed several highly expressed immune related genes in Gne+/−C3+/+ mice retinas, such as *H2-EB1*, *P2ry10b*, *Lcp1*, as well as genes involved in collagen synthesis, which were downregulated back to wildtype control levels in *C3* knock-out groups. The heat map also confirms the downregulation of *Gne* transcription in mice heterozygous for the null *Gne* mutation (Gne+/−C3+/+ and Gne+/−C3−/−). Notably, the downregulation of *Derl3* gene involved

in eliminating misfolded glycoproteins, which was shown in the Gne+/−C3+/+ mouse retinas, was also reverted in the C3−/− mice. Overall, the majority of changes in gene retinal transcription of Gne+/−C3+/+ mice were partially prevented with the deletion of complement factor *C3* (Supplementary Figure 11).

The observed increase of *C4* in the retinas of 9-month-old Gne+/−C3+/+ mice was reversed in Gne+/−C3−/− mice (FC: 1.454 ± 0.11 vs. 0.352 ± 0.14, $p = <.0001$, Figure 7). However, gene transcription of *C1qb* and *Cfh* was similar in all genotype groups,

including the *C3*-deficient mice (Figure 7). Regarding the *Il-1β* elevation in Gne+/−C3+/+ mice, the transcript levels tended to be reversed by *C3*-deficiency to the wildtype animal levels (FC: 2.007 ± 0.31 vs. 1.223 ± 0.21, *p* = .054, Figure 7). Notably, no significant differences were detected in the transcript levels of *C3*, *C4*, and *Il-1β* between Gne+/+C3−/− and Gne+/−C3−/− mice. Concerning retina-associated markers, the increased *Vsx2* gene expression in Gne+/−C3+/+ mice was reduced in Gne+/−C3−/− mice (FC: 1.647 ± 0.12 vs. 0.607 ± 0.12, *p* = <.0001, Figure 7), while the Gne+/−C3−/− mice showed no significant reversal of *Vegfa* transcript levels compared to Gne+/−C3+/+ mice (Figure 7). On the other hand, *Trpm1* transcript levels in the Gne+/−C3−/− mice were lower compared with Gne+/−C3+/+ mice (FC: 0.750 ± 0.02 vs. 1.115 ± 0.06, *p* = <.0001, Figure 7). Finally, *Opn1sw* and *Tnf* gene expression was unchanged in all mouse groups (Figure 7). Notably, transcription levels of the oxidative stress markers, *Cyba* and *Cybb*, showed lower values in Gne+/−C3−/− compared to Gne+/−C3+/+ mice (*Cyba*: *p* = .018 and *Cybb*: *p* = .007, respectively; Figure 7).

These data indicate a reversal of the increased transcription levels of *C4* by deficiency of *C3* in Gne+/−C3+/+ mice, accompanied by a slight reduction of transcripts associated with inflammation and retina-associated markers.

4 | DISCUSSION

Reduced sialylation in the central nervous system (CNS) is a typical feature of aging, leading to inflammation and complement-mediated loss of synapses and neurons (Klaus et al., 2020). Here, we used heterozygous *Gne*-deficient mice (Gne+/−) to simulate decreased levels of sialylation in the retina. Our results show a reduced expression of protein-bound polysialic acid by 24.2 ± 6.41% and a more pronounced reduced expression of ganglioside-bound trisialic acid by 35.1 ± 6.07% in the retinas of Gne+/− mice at 9 months of age. This reduced sialylation was apparently acquired in adult mice, since no significant loss of polysialic acid and trisialic acid was observed in 3 months old mice. Data are in line with the previously reported slight reduction of polysialic acid and trisialic acid levels in the brain of Gne+/− mice (Klaus et al., 2020), as well as the observation of an overall reduction of membrane-bound sialic acid in different organs of adult Gne+/− mice reported by Gagiannis et al. (2007).

Sialylation has several biological and structural functions in the CNS. Sialylation is also a check-point for complement activation and microglial responses via binding to complement regulatory proteins and Siglec receptors (sialic-acid-binding immunoglobulin-like lectins). Microglial cells as part of the innate immune system are important for maintaining retinal homeostasis. However, overactivity of microglia is associated with multiple retinal diseases such as age-related macular degeneration (AMD), retinitis pigmentosa, and glaucoma (Bosco et al., 2015; Gupta et al., 2003; Karlstetter et al., 2015). Interestingly, we did not observe any differences in the microglial number, morphology and distribution across the retinal layers of Gne+/− mice. However, our data show that reduced sialylation in Gne+/− mice leads to

an increased staining intensity of the microglial lysophagosomal marker CD68 in several retinal layers at 9 and 12 months of age. The gene transcript levels of CD68 were not elevated at 9 months of age in Gne+/− mice, suggesting a post-transcriptional upregulation of CD68 in microglia. Such an increased protein expression of CD68 has been interpreted in several studies as a microglia activation process in the retina and around the optic nerve (Santos et al., 2008; Yuan & Neufeld, 2001). In summary, we suggest that there is a non-proliferative phagolysosomal reactivity of microglia in response to decreased sialylation levels in the mouse retina.

In line with increased expression of CD68 in microglial cells, we observed elevated gene transcription of the pro-inflammatory cytokine *Il-1β* in the retinas of Gne+/− mice at 9 months of age. Several studies have reported that in the retina *Il-1β* is mainly expressed by infiltrating macrophages and by activated resident microglia (Eandi et al., 2016; Jiao et al., 2015; Natoli et al., 2017; Rivera et al., 2013). In vitro studies showed up-regulation of *Il-1β* upon treatment or challenge with lipofuscin (Zhang et al., 2015), oxidative stress (Kauppinen et al., 2012), and complement proteins (Asgari et al., 2013; Laudisi et al., 2013). In vivo, light-induced retinal degeneration was associated with robust and early stage up-regulation of *Il-1β* (Jiao et al., 2015), as also presented in a laser-induced model of choroidal neovascularization (Balser et al., 2019). Importantly, inhibition of *Il-1β* prior to the photo-oxidative damage prevented microglial activation and macrophage infiltration, and the associated photoreceptors death (Natoli et al., 2017). In addition, cultured human and mouse mononuclear phagocytes expressed *Il-1β* and triggered cone photoreceptors degeneration in explants of retinal tissue (Eandi et al., 2016). In line with the above-mentioned studies, our data suggest that up-regulation of the pro-inflammatory cytokine *Il-1β* is a response to reduced retinal hyposialylation and might be a deleterious factor for the retinal tissue.

Increased expression of glial fibrillary acid protein (GFAP) is one indicator of a macroglial cell response to retinal damage, often associated with the production of proinflammatory cytokines (Nakazawa et al., 2006; Natoli et al., 2016). Our results showed an increased expression of GFAP in the ganglion cell layer in the retina of Gne+/− mice at 9 months of age, suggesting possible response of astrocytes and Müller cells to the retinal hyposialylation. Increased expression of macroglial markers, regarded as gliosis, has been associated with retinal inflammation and loss of ganglion cells in mouse models of glaucoma and with photoreceptors death in retinal detachment rat models (Guttenplan et al., 2020; Inman & Horner, 2007; Nakazawa et al., 2006).

Timely and locally restricted activation of microglia is crucial for retinal homeostasis. However, chronic or dysregulated immune responses can lead to synaptic and neuronal removal (Clayton et al., 2017; Friker et al., 2020; Hanisch & Kettenmann, 2007). Therefore, we investigated neuronal loss of different cells of the basic visual circuit of the retina, specifically rod and cone cells, rod bipolar cells, ganglion cells, as well as the thickness of the photoreceptor outer nuclear layer. The outer nuclear layer width, which contains the cell body of photoreceptors, and the ganglion cell number were not affected in Gne+/− mice. However, our data showed loss of rod bipolar cells at 12 months of age in Gne+/− mice. Notably, loss of

rod bipolar cells has been described during aging in the human retina (Aggarwal et al., 2007). The number of rod bipolar cells in humans starts to decline from 35 to 62 years of age, and the cell loss worsens from the seventh decade onwards (Aggarwal et al., 2007). Our data from Gne+/− mice suggest that reduced retinal sialylation could potentially trigger the loss of rod bipolar cells. Thus, it would be interesting to decipher whether the loss of rod bipolar cells in aging humans is associated with reduced retinal sialylation.

In vitro studies have reported that desialylated neurons were phagocytosed by macrophages and microglia in a complement-receptor 3-dependent manner, while sialylation prevented any complement-mediated clearance via mononuclear phagocytes (Linnartz et al., 2012; Linnartz-Gerlach et al., 2016). In line with this, Wang and colleagues showed that C1q binding to desialylated synapses induced by sevoflurane exposure leads to synapses removal by microglia in the brains of new born mice (Wang et al., 2024). Notably, loss of rod bipolar cells was associated with increased transcription of the complement factor 3 (*C3*), and complement factor 4 (*C4*) in the hyposialylated retinas of Gne+/− mice, indicating that the complement system might be critical for the removal of the rod bipolar cells. However, the exact mechanism leading to loss of rod bipolar cells in the hyposialylated retinas is unknown. We cannot exclude the possibility of involvement of reactive oxygen species from phagocytes, which are well known to lead to neuronal damage (Boje & Arora, 1992; Kreutzberg, 1996; Zeng et al., 2005). Nevertheless, our results did not show any alteration in the transcription of two components of the phagocytic oxidase system, the cytochrome b alpha (*Cyba*), and cytochrome b beta (*Cybb*) chain in Gne+/− mice.

The volcano plot from the RNAseq analysis showed upregulation of the *Cryab* and *Crybb1* gene transcripts in the retinas of Gne+/− mice, which encode the transcription of the crystallin proteins essential to preserve the lens transparency and refractivity. Mutation in these genes are associated to congenital cataract in humans and mice (Cohen et al., 2007; Cui et al., 2017; Willoughby et al., 2005). In addition, *Cryab* also plays a major role in anti-apoptotic pathways under stressful stimuli throughout the nervous system (Zhang et al., 2019). *Cryab* is also known to play an anti-inflammatory role by regulating pro-inflammatory macrophages in the nervous system (Hagen et al., 2024; Lim et al., 2021), as well as preventing microglia activation in the retina in a mouse model of endotoxin-induced uveitis (Wang et al., 2021).

We followed up on the concept that the loss of rod bipolar cells in Gne+/− mice might be mediated by the complement system and therefore, we studied retinas of Gne+/− mice crossed with complement *C3*-deficient mice (Gne+/−C3−/−). Our results demonstrated that the deficiency of *C3* decreased the expression of the microglial markers Iba1 and CD68 and reduced transcript levels of *C4* and *Il-1β*, thus preventing any up-regulation of these makers and genes in the Gne+/−C3+/+ mice. Particularly, the microglial markers Iba1 and CD68 were decreased in Gne+/−C3−/− mice compared to Gne+/−C3+/+, but also compared to Gne+/+C3+/+ (wildtype) mice at 12 months of age. Interestingly, the loss of rod bipolar cells in Gne+/−C3+/+ mice was prevented after deficiency of *C3*, but rod bipolar cell number was even higher in *C3*-deficient mice for both *Gne*

genotypes (Gne+/−C3−/− and Gne+/+C3−/−) compared to both, Gne+/−C3+/+ and WT mice (Gne+/+C3+/+). This higher rod bipolar density in 12 months *C3*-deficient mice suggests that complement C3 is apparently involved in deleterious effects for retinas of middle-aged mice. In contrast to the data published by Hoh Kam and colleagues, which denoted the detrimental effects of C3 and/or factor H deficiency on the retinal health of 12-months-old mice, our study did not show any apparent phenotype without further genetic intervention (Hoh Kam et al., 2013). Furthermore, Hoh Kam and colleagues did not investigate retinal bipolar cells or other retinal neurons (Hoh Kam et al., 2013). On the contrary, our findings are consistent with those presented by Gharagozloo et al., that observed high expression of C3 in retinal astrocytes in post-mortem human retinas of patients with loss of retinal ganglion cells (RGC) related to multiple sclerosis (Gharagozloo et al., 2021). The results of Gharagozloo and colleagues were validated using a mouse model of experimental autoimmune encephalomyelitis (EAE) with optic neuritis, in which developmental depletion of C3 led to less RGC loss and lower optic nerve injury (Gharagozloo et al., 2021). Consistently, our data also align with the results of Jiao and colleagues, who showed that mice exposed to photo-oxidative retinal damaged displayed lower reactivity of glial cells and less photoreceptors removal by macrophages in mice with genetic deletion of C3 (Jiao et al., 2020).

Increased expression of C3 has been reported in different diseases or conditions typically associated to inflammation and tissue damage. For instance, in a population cohort study, it was found that increased levels of C3 were associated to higher risk of diabetic complications such as retinopathy, neuropathy, and nephropathy (Rasmussen et al., 2018). In the same line, another study in human patients reported that changes in the N-glycosylation of C3 were observed in severe albuminuria, hypertension, and non-proliferative retinopathy in patients with type 1 diabetes and suggesting glycosylation analysis of C3 as an approach to analyze progression and severity of the disease (Šoić et al., 2023). On the other hand, an experimental study with mice in a retinal degeneration model induced by administration of sodium iodate (NaIO3) showed an increase expression and deposition of the complement components C1s, C3, CFH and CFB alongside other proinflammatory cytokines such as Il-1β. The authors suggest that macrophages, microglia, and Müller cells are the source of the local inflammation (Enzbrenner et al., 2021).

Interestingly, several key hallmark gene sets (including UV response, epithelial-mesenchymal transition, and p53 pathway) identified in the GSEA are associated with AMD. First, components of the up-regulated hallmark UV response have been associated to the development of AMD, specifically in the context of solar radiation (Prüss-üstün et al., 2006; Sui et al., 2013; Taylor et al., 1990). In line, by targeting some components of epithelial-mesenchymal transition using compounds such as retinoic acid receptor-γ (RAR-γ) or Kallistatin (KAL), fibrosis and oxidative stress associated to AMD can be attenuated (Kimura et al., 2015; Shen et al., 2023; Tuo et al., 2015). Second, alterations in the epithelial-mesenchymal transition have been suggested as drivers of retinal pigment epithelium (RPE) alterations in AMD (Yao et al., 2022). Third, the p53 pathway has been

linked to alterations of the RPE cells related to AMD, and also with responses to retinal blue light damage. Under these circumstances, blockade or modulation of the p53 pathway reduced choroidal neovascularization and retinal senescence in different AMD models (Bhattacharya et al., 2012; Fietz et al., 2023; Son et al., 2020; Song et al., 2024; Wolfrum et al., 2022).

Furthermore, the *Cryab* and *Crybb*1 genes were shown to be up-regulated in the volcano plot of the DEG analysis. Alterations in the crystallins have not only been associated with the development of cataracts, but also with RPE alterations connected to retinal degeneration as seen in AMD. Particularly, crystallins were shown to play protective roles against oxidative stress or microglia-mediated neutrophil activation in RPE cells (Boyce et al., 2022; Christopher et al., 2014; Ghosh et al., 2018; Kannan et al., 2016; Kurzawa-Akanbi et al., 2022).

A limitation of our study is the fact that complete *Gne* knock-out (Gne−/−) leads to embryonic lethality of mice (Schwarzkopf et al., 2002), and that the hyposialylation level in Gne+/− mice is not tightly controllable. Accordingly, a conditional knock-out of the *Gne* gene in specific retinal cells might be better suited to see a more pronounced retinal phenotype. However, we still assume that our mouse model with moderate hyposialyation reflects the natural course of aging. Yet, more studies on sialylation levels in human retinal tissue are necessary to prove such an aging process associated with inflammation.

In addition, we do not know whether the mild retinal phenotype observed in the Gne+/− mice is a local response in the eye or whether the observed changes are related to systemic hyposialylation in our mouse model. Similarly, the effects of the *C3* deficiency on the prevention of the retinal phenotype in Gne+/− mice could be influenced by systemic changes related to the *C3* knockout mouse. Therefore, future analyses are needed to investigate in depth the mechanisms that lead to changes in hyposialylated retinas and the role of the complement system in retinal inflammation and degeneration in the context of hyposialylation.

In conclusion, the findings of our study confirm that sialylation acts as check-point for the immune system by modulating microglia activation and complement activation in the mouse retina. In addition, our data suggest that sialylation should be considered as a potential therapeutic target in the treatment of degenerative and inflammatory diseases of the aging retina.

AUTHOR CONTRIBUTIONS

ACKNOWLEDGMENTS

CONFLICT OF INTEREST STATEMENT

The other authors declare that the research was conducted in the absence of any commercial or financial relationships that could be construed as a potential conflict of interest.

DATA AVAILABILITY STATEMENT

The data that support the findings of this study are available from the corresponding author upon reasonable request. RNAseq raw data are available in NCBI's Gene Expression Omnibus (GEO), under the accession number GSE275072 (https://www.ncbi.nlm.nih.gov).

ORCID

German Cuevas-Rios 🅙 https://orcid.org/0009-0008-1801-2479
Harald Neumann 🅙 https://orcid.org/0000-0002-5071-5202

REFERENCES

Aggarwal, P., Nag, T. C., & Wadhwa, S. (2007). Age-related decrease in rod bipolar cell density of the human retina: An immunohistochemical study. *Journal of Biosciences*, *32*(2), 293–298. https://doi.org/10.1007/s12038-007-0029-9

Asgari, E., Le Friec, G., Yamamoto, H., Perucha, E., Sacks, S. S., Köhl, J., Cook, H. T., & Kemper, C. (2013). C3a modulates IL-1β secretion in human monocytes by regulating ATP efflux and subsequent NLRP3 inflammasome activation. *Blood*, *122*(20), 3473–3481. https://doi.org/10.1182/blood-2013-05-502229

Balser, C., Wolf, A., Herb, M., & Langmann, T. (2019). Co-inhibition of PGF and VEGF blocks their expression in mononuclear phagocytes and limits neovascularization and leakage in the murine retina. *Journal of Neuroinflammation*, *16*(1), 26. https://doi.org/10.1186/s12974-019-1419-2

Bhattacharya, S., Chaum, E., Johnson, D. A., & Johnson, L. R. (2012). Age-related susceptibility to apoptosis in human retinal pigment epithelial cells is triggered by disruption of p53-Mdm2 association. *Investigative Ophthalmology & Visual Science*, *53*(13), 8350–8366. https://doi.org/10.1167/iovs.12-10495

Boje, K. M., & Arora, P. K. (1992). Microglial-produced nitric oxide and reactive nitrogen oxides mediate neuronal cell death. *Brain Research*, *587*(2), 250–256. https://doi.org/10.1016/0006-8993(92)91004-X

Bosco, A., Romero, C. O., Breen, K. T., Chagovetz, A. A., Steele, M. R., Ambati, B. K., & Vetter, M. L. (2015). Neurodegeneration severity can be predicted from early microglia alterations monitored in vivo in a mouse model of chronic glaucoma. *DMM Disease Models and Mechanisms*, *8*(5), 443–455. https://doi.org/10.1242/dmm.018788

Boyce, M., Xin, Y., Chowdhury, O., Shang, P., Liu, H., Koontz, V., Strizhakova, A., Nemani, M., Hose, S., Zigler, J. S., Campbell, M., Sinha, D., Handa, J. T., Kaarniranta, K., Qian, J., & Ghosh, S. (2022). Microglia–neutrophil interactions drive dry AMD-like pathology in a mouse model. *Cells*, *11*(22), 3535. https://doi.org/10.3390/cells11223535

Carlson, M. (2019). *org.Mm.eg.db: Genome wide annotation for Mouse*. R Package Version 3.8.2.

Christopher, K. L., Pedler, M. G., Shieh, B., Ammar, D. A., Petrash, J. M., & Mueller, N. H. (2014). Alpha-crystallin-mediated protection of lens cells against heat and oxidative stress-induced cell death. *Biochimica et Biophysica Acta—Molecular Cell Research*, 1843(2), 309–315. https://doi.org/10.1016/j.bbamcr.2013.11.010

Clayton, K. A., Van Enoo, A. A., & Ikezu, T. (2017). Alzheimer's disease: The role of microglia in brain homeostasis and proteopathy. *Frontiers in Neuroscience*, 11(DEC), 680. https://doi.org/10.3389/fnins.2017.00680

Cohen, D., Bar-Yosef, U., Levy, J., Gradstein, L., Belfair, N., Ofir, R., Joshua, S., Lifshitz, T., Carmi, R., & Birk, O. S. (2007). Homozygous CRYBB1 deletion mutation underlies autosomal recessive congenital cataract. *Investigative Ophthalmology and Visual Science*, 48(5), 2208–2213. https://doi.org/10.1167/iovs.06-1019

Cui, X. J., Lv, F. Y., Li, F. H., Zeng, K., & Abdelrahman, K. A. (2017). Correlations of single nucleotide polymorphisms of CRYAA and CRYAB genes with the risk and clinicopathological features of children suffering from congenital cataract. *Medicine (United States)*, 96(25), e7158. https://doi.org/10.1097/MD.0000000000007158

Dobin, A., Davis, C. A., Schlesinger, F., Drenkow, J., Zaleski, C., Jha, S., Batut, P., Chaisson, M., & Gingeras, T. R. (2013). STAR: Ultrafast universal RNA-seq aligner. *Bioinformatics*, 29(1), 15–21. https://doi.org/10.1093/bioinformatics/bts635

Eandi, C. M., Messance, H. C., Augustin, S., Dominguez, E., Lavalette, S., Forster, V., Hu, S. J., Siquieros, L., Craft, C. M., Sahel, J. A., Tadayoni, R., Paques, M., Guillonneau, X., & Sennlaub, F. (2016). Subretinal mononuclear phagocytes induce cone segment loss via IL-1β. *eLife*, 5(JULY), e16490. https://doi.org/10.7554/eLife.16490

Enzbrenner, A., Zulliger, R., Biber, J., Pousa, A. M. Q., Schäfer, N., Stucki, C., Giroud, N., Berrera, M., Kortvely, E., Schmucki, R., Badi, L., Grosche, A., Pauly, D., & Enzmann, V. (2021). Sodium iodate-induced degeneration results in local complement changes and inflammatory processes in murine retina. *International Journal of Molecular Sciences*, 22(17), 9218. https://doi.org/10.3390/ijms22179218

Fietz, A., Corsi, F., Hurst, J., & Schnichels, S. (2023). Blue light damage and p53: Unravelling the role of p53 in oxidative-stress-induced retinal apoptosis. *Antioxidants*, 12(12), 2072. https://doi.org/10.3390/antiox12122072

Friker, L. L., Scheiblich, H., Hochheiser, I. V., Brinkschulte, R., Riedel, D., Latz, E., Geyer, M., & Heneka, M. T. (2020). β-Amyloid clustering around ASC fibrils boosts its toxicity in microglia. *Cell Reports*, 30(11), 3743–3754.e6. https://doi.org/10.1016/j.celrep.2020.02.025

Gagiannis, D., Orthmann, A., Danßmann, I., Schwarzkopf, M., Weidemann, W., & Horstkorte, R. (2007). Reduced sialylation status in UDP-N-acetylglucosamine-2-epimerase/N-acetylmannosamine kinase (GNE)-deficient mice. *Glycoconjugate Journal*, 24(2–3), 125–130. https://doi.org/10.1007/s10719-006-9019-7

Gemenetzi, M., & Lotery, A. J. (2016). Complement pathway biomarkers and age-related macular degeneration. *Eye (Basingstoke)*, 30(1), 1–14. https://doi.org/10.1038/eye.2015.203

Gharagozloo, M., Smith, M. D., Jin, J., Garton, T., Taylor, M., Chao, A., Meyers, K., Kornberg, M. D., Zack, D. J., Ohayon, J., Calabresi, B. A., Reich, D. S., Eberhart, C. G., Pardo, C. A., Kemper, C., Whartenby, K. A., & Calabresi, P. A. (2021). Complement component 3 from astrocytes mediates retinal ganglion cell loss during neuroinflammation. *Acta Neuropathologica*, 142(5), 899–915. https://doi.org/10.1007/s00401-021-02366-4

Ghosh, S., Shang, P., Terasaki, H., Stepicheva, N., Hose, S., Yazdankhah, M., Weiss, J., Sakamoto, T., Bhutto, I. A., Xia, S., Zigler, J. S., Kannan, R., Qian, J., Handa, J. T., & Sinha, D. (2018). A role for βA3/A1-crystallin in type 2 EMT of RPE cells occurring in dry age-related macular degeneration. *Investigative Ophthalmology and Visual Science*, 59(4), AMD104–AMD113. https://doi.org/10.1167/iovs.18-24132

Gupta, N., Brown, K. E., & Milam, A. H. (2003). Activated microglia in human retinitis pigmentosa, late-onset retinal degeneration, and age-related macular degeneration. *Experimental Eye Research*, 76(4), 463–471. https://doi.org/10.1016/S0014-4835(02)00332-9

Guttenplan, K. A., Stafford, B. K., El-Danaf, R. N., Adler, D. I., Münch, A. E., Weigel, M. K., Huberman, A. D., & Liddelow, S. A. (2020). Neurotoxic reactive astrocytes drive neuronal death after retinal injury. *Cell Reports*, 31(12), 107776. https://doi.org/10.1016/j.celrep.2020.107776

Hagen, K. M., Gordon, P., Frederick, A., Palmer, A. L., Edalat, P., Zonta, Y. R., Scott, L., Flancia, M., Reid, J. K., Joel, M., & Ousman, S. S. (2024). CRYAB plays a role in terminating the presence of proinflammatory macrophages in the older, injured mouse peripheral nervous system. *Neurobiology of Aging*, 133, 1–15. https://doi.org/10.1016/j.neurobiolaging.2023.10.004

Hanisch, U. K., & Kettenmann, H. (2007). Microglia: Active sensor and versatile effector cells in the normal and pathologic brain. *Nature Neuroscience*, 10(11), 1387–1394. https://doi.org/10.1038/nn1997

Hansen, J. N., Brückner, M., Pietrowski, M. J., Jikeli, J. F., Plescher, M., Beckert, H., Schnaars, M., Fülle, L., Reitmeier, K., Langmann, T., Förster, I., Boche, D., Petzold, G. C., & Halle, A. (2022). MotiQ: An open-source toolbox to quantify the cell motility and morphology of microglia. *Molecular Biology of the Cell*, 33(11), ar99. https://doi.org/10.1091/mbc.E21-11-0585

Hoh Kam, J., Lenassi, E., Malik, T. H., Pickering, M. C., & Jeffery, G. (2013). Complement component C3 plays a critical role in protecting the aging retina in a murine model of age-related macular degeneration. *American Journal of Pathology*, 183(2), 480–492. https://doi.org/10.1016/j.ajpath.2013.04.008

Hong, S., Beja-Glasser, V. F., Nfonoyim, B. M., Frouin, A., Li, S., Ramakrishnan, S., Merry, K. M., Shi, Q., Rosenthal, A., Barres, B. A., Lemere, C. A., Selkoe, D. J., & Stevens, B. (2016). Complement and microglia mediate early synapse loss in Alzheimer mouse models. *Science*, 352(6286), 712–716. https://doi.org/10.1126/science.aad8373

Iandiev, I., Biedermann, B., Bringmann, A., Reichel, M. B., Reichenbach, A., & Pannicke, T. (2006). Atypical gliosis in Müller cells of the slowly degenerating rds mutant mouse retina. *Experimental Eye Research*, 82(3), 449–457. https://doi.org/10.1016/j.exer.2005.07.018

Inman, D. M., & Horner, P. J. (2007). Reactive nonproliferative gliosis predominates in a chronic mouse model of glaucoma. *Glia*, 55(9), 942–953. https://doi.org/10.1002/glia.20516

Jiao, H., Natoli, R., Valter, K., Provis, J. M., & Rutar, M. (2015). Spatiotemporal cadence of macrophage polarisation in a model of light-induced retinal degeneration. *PLoS One*, 10(12), e0143952. https://doi.org/10.1371/journal.pone.0143952

Jiao, H., Provis, J. M., Natoli, R., & Rutar, M. (2020). Ablation of C3 modulates macrophage reactivity in the outer retina during photo-oxidative damage. *Molecular Vision*, 26, 679–690. /pmc/articles/PMC7553722/.

Johnson, L. V., Leitner, W. P., Staples, M. K., & Anderson, D. H. (2001). Complement activation and inflammatory processes in drusen formation and age related macular degeneration. *Experimental Eye Research*, 73(6), 887–896. https://doi.org/10.1006/exer.2001.1094

Johnson, L. V., Ozaki, S., Staples, M. K., Erickson, P. A., & Anderson, D. H. (2000). A potential role for immune complex pathogenesis in drusen formation. *Experimental Eye Research*, 70(4), 441–449. https://doi.org/10.1006/exer.1999.0798

Kannan, R., Sreekumar, P. G., & Hinton, D. R. (2016). Alpha crystallins in the retinal pigment epithelium and implications for the pathogenesis and treatment of age-related macular degeneration. *Biochimica et Biophysica Acta—General Subjects*, 1860(1), 258–268. https://doi.org/10.1016/j.bbagen.2015.05.016

Karlstetter, M., Kopatz, J., Aslanidis, A., Shahraz, A., Caramoy, A., Linnartz-Gerlach, B., Lin, Y., Lückoff, A., Fauser, S., Düker, K., Claude, J., Wang, Y., Ackermann, J., Schmidt, T., Hornung, V., Skerka, C., Langmann, T., & Neumann, H. (2017). Polysialic acid blocks mononuclear phagocyte reactivity, inhibits complement activation, and protects from vascular damage in the retina. *EMBO Molecular Medicine*, 9(2), 154–166. https://doi.org/10.15252/emmm.201606627

Karlstetter, M., Scholz, R., Rutar, M., Wong, W. T., Provis, J. M., & Langmann, T. (2015). Retinal microglia: Just bystander or target for

therapy? *Progress in Retinal and Eye Research*, 45, 30–57. https://doi.org/10.1016/j.preteyeres.2014.11.004

Kauppinen, A., Niskanen, H., Suuronen, T., Kinnunen, K., Salminen, A., & Kaarniranta, K. (2012). Oxidative stress activates NLRP3 inflammasomes in ARPE-19 cells-implications for age-related macular degeneration (AMD). *Immunology Letters*, 147(1–2), 29–33. https://doi.org/10.1016/j.imlet.2012.05.005

Kimura, K., Orita, T., Liu, Y., Yang, Y., Tokuda, K., Kurakazu, T., Noda, T., Yanai, R., Morishige, N., Takeda, A., Ishibashi, T., & Sonoda, K. H. (2015). Attenuation of EMT in RPE cells and subretinal fibrosis by an RAR-γ agonist. *Journal of Molecular Medicine*, 93(7), 749–758. https://doi.org/10.1007/s00109-015-1289-8

Klaus, C., Hansen, J. N., Ginolhac, A., Gérard, D., Gnanapragassam, V. S., Horstkorte, R., Rossdam, C., Buettner, F. F. R., Sauter, T., Sinkkonen, L., Neumann, H., & Linnartz-Gerlach, B. (2020). Reduced sialylation triggers homeostatic synapse and neuronal loss in middle-aged mice. *Neurobiology of Aging*, 88, 91–107. https://doi.org/10.1016/j.neurobiolaging.2020.01.008

Klaus, C., Liao, H., Allendorf, D. H., Brown, G. C., & Neumann, H. (2021). Sialylation acts as a checkpoint for innate immune responses in the central nervous system. *Glia*, 69(7), 1619–1636. https://doi.org/10.1002/glia.23945

Kogo, H., Tsutsumi, M., Inagaki, H., Ohye, T., Kiyonari, H., & Kurahashi, H. (2012). HORMAD2 is essential for synapsis surveillance during meiotic prophase via the recruitment of ATR activity. *Genes to Cells*, 17(11), 897–912. https://doi.org/10.1111/gtc.12005

Kreutzberg, G. W. (1996). Microglia: A sensor for pathological events in the CNS. *Trends in Neurosciences*, 19(8), 312–318. https://doi.org/10.1016/0166-2236(96)10049-7

Krishnan, A., Sendra, V. G., Patel, D., Lad, A., Greene, M. K., Smyth, P., Gallaher, S. A., Herron, Ú. M., Scott, C. J., Genead, M., & Tolentino, M. (2023). PolySialic acid-nanoparticles inhibit macrophage mediated inflammation through Siglec agonism: A potential treatment for age related macular degeneration. *Frontiers in Immunology*, 14, 1237016. https://doi.org/10.3389/fimmu.2023.1237016

Kurzawa-Akanbi, M., Whitfield, P., Burté, F., Bertelli, P. M., Pathak, V., Doherty, M., Hilgen, B., Gliaudelytè, L., Platt, M., Queen, R., Coxhead, J., Porter, A., Öberg, M., Fabrikova, D., Davey, T., Beh, C. S., Georgiou, M., Collin, J., Boczonadi, V., ... Lako, M. (2022). Retinal pigment epithelium extracellular vesicles are potent inducers of age-related macular degeneration disease phenotype in the outer retina. *Journal of Extracellular Vesicles*, 11(12), 12295. https://doi.org/10.1002/jev2.12295

Laudisi, F., Spreafico, R., Evrard, M., Hughes, T. R., Mandriani, B., Kandasamy, M., Morgan, B. P., Sivasankar, B., & Mortellaro, A. (2013). Cutting edge: The NLRP3 Inflammasome links complement-mediated inflammation and IL-1β release. *The Journal of Immunology*, 191(3), 1006–1010. https://doi.org/10.4049/jimmunol.1300489

Liao, H., Winkler, J., Wißfeld, J., Shahraz, A., Klaus, C., & Neumann, H. (2021). Low molecular weight polysialic acid prevents lipopolysaccharide-induced inflammatory dopaminergic neurodegeneration in humanized SIGLEC11 transgenic mice. *Glia*, 69(12), 2845–2862. https://doi.org/10.1002/glia.24073

Liao, Y., Smyth, G. K., & Shi, W. (2014). FeatureCounts: An efficient general purpose program for assigning sequence reads to genomic features. *Bioinformatics*, 30(7), 923–930. https://doi.org/10.1093/bioinformatics/btt656

Lim, E. M. F., Hoghooghi, V., Hagen, K. M., Kapoor, K., Frederick, A., Finlay, T. M., & Ousman, S. S. (2021). Presence and activation of pro-inflammatory macrophages are associated with CRYAB expression in vitro and after peripheral nerve injury. *Journal of Neuroinflammation*, 18(1), 82. https://doi.org/10.1186/s12974-021-02108-z

Linnartz, B., Kopatz, J., Tenner, A. J., & Neumann, H. (2012). Sialic acid on the neuronal glycocalyx prevents complement c1 binding and complement receptor-3-mediated removal by microglia. *Journal of Neuroscience*, 32(3), 946–952. https://doi.org/10.1523/JNEUROSCI.3830-11.2012

Linnartz-Gerlach, B., Schuy, C., Shahraz, A., Tenner, A. J., & Neumann, H. (2016). Sialylation of neurites inhibits complement-mediated macrophage removal in a human macrophage-neuron co-culture system. *Glia*, 64(1), 35–47. https://doi.org/10.1002/glia.22901

Love, M. I., Huber, W., & Anders, S. (2014). Moderated estimation of fold change and dispersion for RNA-seq data with DESeq2. *Genome Biology*, 15(12), 1–21. https://doi.org/10.1186/s13059-014-0550-8

Lünemann, J. D., von Gunten, S., & Neumann, H. (2021). Targeting sialylation to treat central nervous system diseases. *Trends in Pharmacological Sciences*, 42(12), 998–1008. https://doi.org/10.1016/j.tips.2021.09.002

Mootha, V. K., Lindgren, C. M., Eriksson, K. F., Subramanian, A., Sihag, S., Lehar, J., Puigserver, P., Carlsson, E., Ridderstråle, M., Laurila, E., Houstis, N., Daly, M. J., Patterson, N., Mesirov, J. P., Golub, T. R., Tamayo, P., Spiegelman, B., Lander, E. S., Hirschhorn, J. N., ... Groop, L. C. (2003). PGC-1α-responsive genes involved in oxidative phosphorylation are coordinately downregulated in human diabetes. *Nature Genetics*, 34(3), 267–273. https://doi.org/10.1038/ng1180

Nadal-Nicolás, F. M., Vidal-Sanz, M., & Agudo-Barriuso, M. (2018). The aging rat retina: From function to anatomy. *Neurobiology of Aging*, 61, 146–168. https://doi.org/10.1016/j.neurobiolaging.2017.09.021

Nakazawa, T., Matsubara, A., Noda, K., Hisatomi, T., She, H., Skondra, D., Miyahara, S., Sobrin, L., Thomas, K. L., Chen, D. F., Grosskreutz, C. L., Hafezi-Moghadam, A., & Miller, J. W. (2006). Characterization of cytokine responses to retinal detachment in rats. *Molecular Vision*, 12(13), 867–878.

Natoli, R., Fernando, N., Madigan, M., Chu-Tan, J. A., Valter, K., Provis, J., & Rutar, M. (2017). Microglia-derived IL-1β promotes chemokine expression by Müller cells and RPE in focal retinal degeneration. *Molecular Neurodegeneration*, 12(1), 31. https://doi.org/10.1186/s13024-017-0175-y

Natoli, R., Jiao, H., Barnett, N. L., Fernando, N., Valter, K., Provis, J. M., & Rutar, M. (2016). A model of progressive photo-oxidative degeneration and inflammation in the pigmented C57BL/6J mouse retina. *Experimental Eye Research*, 147, 114–127. https://doi.org/10.1016/j.exer.2016.04.015

Prüss-üstün, A., Zeeb, H., Mathers, C., & Repacholi, M. (2006). Solar ultraviolet radiation: Global burden of disease from solar ultraviolet radiation. *World Health*, 55(13), 987–999. http://bases.bireme.br/cgi-bin/wxislind.exe/iah/online/?IsisScript=iah/iah.xis&src=google&base=REPIDISCA&lang=p&nextAction=lnk&exprSearch=176351&indexSearch=ID

Rasmussen, K. L., Nordestgaard, B. G., & Nielsen, S. F. (2018). Complement C3 and risk of diabetic microvascular disease: A cohort study of 95202 individuals from the general population. *Clinical Chemistry*, 64(7), 1113–1124. https://doi.org/10.1373/clinchem.2018.287581

Rivera, J. C., Sitaras, N., Noueihed, B., Hamel, D., Madaan, A., Zhou, T., Honoré, J. C., Quiniou, C., Joyal, J. S., Hardy, P., Sennlaub, F., Lubell, W., & Chemtob, S. (2013). Microglia and interleukin-1β in ischemic retinopathy elicit microvascular degeneration through neuronal semaphorin-3A. *Arteriosclerosis, Thrombosis, and Vascular Biology*, 33(8), 1881–1891. https://doi.org/10.1161/ATVBAHA.113.301331

RStudio Team. (2020). *RStudio: Integrated development environment for R.* RStudio. http://www.rstudio.com/

Santos, A. M., Calvente, R., Tassi, M., Carrasco, M. C., Martín-Oliva, D., Marín-Teva, J. L., Navascués, J., & Cuadros, M. A. (2008). Embryonic and postnatal development of microglial cells in the mouse retina. *Journal of Comparative Neurology*, 506(2), 224–239. https://doi.org/10.1002/cne.21538

Schwarzkopf, M., Knobeloch, K. P., Rohde, E., Hinderlich, S., Wiechens, N., Lucka, L., Horak, I., Reutter, W., & Horstkorte, R. (2002). Sialylation is essential for early development in mice. *Proceedings of the National Academy of Sciences of the United States of America*, 99(8), 5267–5270. https://doi.org/10.1073/pnas.072066199

Segler Stahl, K., Webster, J. C., & Brunngraber, E. G. (1983). Changes in the concentration and composition of human brain gangliosides with aging. *Gerontology*, 29(3), 161–168. https://doi.org/10.1159/000213109

Shahraz, A., Kopatz, J., Mathy, R., Kappler, J., Winter, D., Kapoor, S., Schütza, V., Scheper, T., Gieselmann, V., & Neumann, H. (2015). Anti-inflammatory activity of low molecular weight polysialic acid on human macrophages. *Scientific Reports*, *5*, 1–17. https://doi.org/10.1038/srep16800

Shahraz, A., Lin, Y., Mbroh, J., Winkler, J., Liao, H., Lackmann, M., Bungartz, A., Zipfel, P. F., Skerka, C., & Neumann, H. (2022). Low molecular weight polysialic acid binds to properdin and reduces the activity of the alternative complement pathway. *Scientific Reports*, *12*(1), 5818. https://doi.org/10.1038/s41598-022-09407-2

Shen, G., Li, Y., Zeng, Y., Hong, F., Zhang, J., Wang, Y., Zhang, C., Xiang, W., Wang, J., Fang, Z., Qi, W., Yang, X., Gao, G., & Zhou, T. (2023). Kallistatin deficiency induces the oxidative stress-related epithelial-mesenchymal transition of retinal pigment epithelial cells: A novel protagonist in age-related macular degeneration. *Investigative Ophthalmology and Visual Science*, *64*(12), 15. https://doi.org/10.1167/iovs.64.12.15

Šoić, D., Štambuk, J., Tijardović, M., Keser, T., Lauc, G., Bulum, T., Lovrenčić, M. V., Rebrina, S. V., Tomić, M., Novokmet, M., Smirčić-Duvnjak, L., & Gornik, O. (2023). Human complement component C3 N-glycome changes in type 1 diabetes complications. *Frontiers in Endocrinology*, *14*, 1101154. https://doi.org/10.3389/fendo.2023.1101154

Son, Y., Lim, D., Park, S., Song, I. S., Kim, J. H., Shin, S., Jang, H., Liu, K. H., Song, O. Y., Kang, G. Y., Cho, W., Seok, Y., Na, M. K., Chung, H., & Oh, S. (2020). Ilimaquinone inhibits neovascular age-related macular degeneration through modulation of Wnt/β-catenin and p53 pathways. *Pharmacological Research*, *161*, 105146. https://doi.org/10.1016/j.phrs.2020.105146

Song, Y., Wei, D., Wang, Q., Guo, J., Zhu, Y., Shang, E., & Duan, J. (2024). Luteoloside mitigates premature age-related macular degeneration by suppressing p53-p21-Rb1 axis: Insights from transcriptomic analysis, serum metabolomics and gut microbiota analysis. *Journal of Pharmaceutical and Biomedical Analysis*, *248*, 116296. https://doi.org/10.1016/j.jpba.2024.116296

Stence, N., Waite, M., & Dailey, M. E. (2001). Dynamics of microglial activation: A confocal time-lapse analysis in hippocampal slices. *Glia*, *33*(3), 256–266. https://doi.org/10.1002/1098-1136(200103)33:3<256::AID-GLIA1024>3.0.CO;2-J

Subramanian, A., Tamayo, P., Mootha, V. K., Mukherjee, S., Ebert, B. L., Gillette, M. A., Paulovich, A., Pomeroy, S. L., Golub, T. R., Lander, E. S., & Mesirov, J. P. (2005). Gene set enrichment analysis: A knowledge-based approach for interpreting genome-wide expression profiles. *Proceedings of the National Academy of Sciences of the United States of America*, *102*(43), 15545–15550. https://doi.org/10.1073/pnas.0506580102

Sui, G. Y., Liu, G. C., Liu, G. Y., Gao, Y. Y., Deng, Y., Wang, W. Y., Tong, S. H., & Wang, L. (2013). Is sunlight exposure a risk factor for age-related macular degeneration? A systematic review and meta-analysis. *British Journal of Ophthalmology*, *97*(4), 389–394. https://doi.org/10.1136/bjophthalmol-2012-302281

Taylor, H. R., Munoz, B., West, S., Bressler, N. M., Bressler, S. B., & Rosenthal, F. S. (1990). Visible light and risk of age-related macular degeneration. *Transactions of the American ophthalmological society*, *88*, 163–178. /pmc/articles/PMC1298584/?report=abstract.

Tuo, J., Wang, Y., Cheng, R., Li, Y., Chen, M., Qiu, F., Qian, H., Shen, D., Penalva, R., Xu, H., Ma, J. X., & Chan, C. C. (2015). Wnt signaling in age-related macular degeneration: Human macular tissue and mouse model. *Journal of Translational Medicine*, *13*(1), 330. https://doi.org/10.1186/s12967-015-0683-x

Wang, F., Jiang, Z., Lou, B., Duan, F., Qiu, S., Cheng, Z., Ma, X., Yang, Y., & Lin, X. (2021). αB-Crystallin alleviates endotoxin-induced retinal inflammation and inhibits microglial activation and autophagy. *Frontiers in Immunology*, *12*, 641999. https://doi.org/10.3389/fimmu.2021.641999

Wang, G., Liu, H. Y., Meng, X. W., Chen, Y., Zhao, W. M., Li, W. T., Xu, H. B., Peng, K., & Ji, F. H. (2024). Complement C1q-mediated microglial synaptic elimination by enhancing desialylation underlies sevoflurane-induced developmental neurotoxicity. *Cell & Bioscience*, *14*(1), 42. https://doi.org/10.1186/s13578-024-01223-7

Werneburg, S., Jung, J., Kunjamma, R. B., Ha, S. K., Luciano, N. J., Willis, C. M., Gao, G., Biscola, N. P., Havton, L. A., Crocker, S. J., Popko, B., Reich, D. S., & Schafer, D. P. (2020). Targeted complement inhibition at synapses prevents microglial synaptic engulfment and synapse loss in demyelinating disease. *Immunity*, *52*(1), 167–182.e7. https://doi.org/10.1016/j.immuni.2019.12.004

Wickham, M. (2016). *ggplot2: Elegant graphics for data analysis*. Springer-Verlag.

Willoughby, C. E., Shafiq, A., Ferrini, W., Chan, L. L. Y., Billingsley, G., Priston, M., Mok, C., Chandna, A., Kaye, S., & Héon, E. (2005). CRYBB1 mutation associated with congenital cataract and microcornea. *Molecular Vision*, *11*(March), 587–593.

Wolfrum, P., Fietz, A., Schnichels, S., & Hurst, J. (2022). The function of p53 and its role in Alzheimer's and Parkinson's disease compared to age-related macular degeneration. *Frontiers in Neuroscience*, *16*, 1029473. https://doi.org/10.3389/fnins.2022.1029473

Yang, Y., Liu, W., Sun, K., Jiang, L., & Zhu, X. (2019). Tmem30a deficiency leads to retinal rod bipolar cell degeneration. *Journal of Neurochemistry*, *148*(3), 400–412. https://doi.org/10.1111/jnc.14643

Yao, P. L., Parmar, V. M., Choudhary, M., & Malek, G. (2022). NURR1 expression regulates retinal pigment epithelial-mesenchymal transition and age-related macular degeneration phenotypes. *Proceedings of the National Academy of Sciences of the United States of America*, *119*(28), e2202256119. https://doi.org/10.1073/pnas.2202256119

Young, K., & Morrison, H. (2018). Quantifying microglia morphology from photomicrographs of immunohistochemistry prepared tissue using imagej. *Journal of Visualized Experiments*, *2018*(136), 57648. https://doi.org/10.3791/57648

Yu, G., Wang, L. G., Han, Y., & He, Q. Y. (2012). ClusterProfiler: An R package for comparing biological themes among gene clusters. *OMICS: A Journal of Integrative Biology*, *16*(5), 284–287. https://doi.org/10.1089/omi.2011.0118

Yuan, L., & Neufeld, A. H. (2001). Activated microglia in the human glaucomatous optic nerve head. *Journal of Neuroscience Research*, *64*(5), 523–532. https://doi.org/10.1002/jnr.1104

Zeng, H. Y., Zhu, X. A., Zhang, C., Yang, L. P., Wu, L. M., & Tso, M. O. M. (2005). Identification of sequential events and factors associated with microglial activation, migration, and cytotoxicity in retinal degeneration in rd mice. *Investigative Ophthalmology and Visual Science*, *46*(8), 2992–2999. https://doi.org/10.1167/iovs.05-0118

Zhang, J., Bai, Y., Huang, L., Qi, Y., Zhang, Q., Li, S., Wu, Y., & Li, X. (2015). Protective effect of autophagy on human retinal pigment epithelial cells against lipofuscin fluorophore A2E: Implications for age-related macular degeneration. *Cell Death & Disease*, *6*(11), e1972. https://doi.org/10.1038/CDDIS.2015.330

Zhang, J. F., Liu, J., Wu, J. L., Li, W. F., Chen, Z. W., & Yang, L. S. (2019). Progression of the role of CRYAB in signaling pathways and cancers. *Onco-Targets and therapy*, *12*, 4129–4139. https://doi.org/10.2147/OTT.S201799

SUPPORTING INFORMATION

Additional supporting information can be found online in the Supporting Information section at the end of this article.

4. Discussion with references

4.1 Effect of 6'-Sialyllactose on neomycin-induced ototoxicity

The first study of this project evaluated the potential of 6'-sialyllactose (6SL) as a preventative therapy to neomycin-induced ototoxicity in a mouse model. The hair cell degeneration and loss of auditory sensory neurons is a chronic process of sensorineural hearing loss (Yang et al., 2015). There are multiple causes of acquired sensorineural hearing loss, such as aging, noise exposure, and drugs including antibiotics such as aminoglycosides, which are still in use in industrialized countries despite their nephrotoxic and ototoxic side effects (Krause et al., 2016; Lee et al., 2018). Aminoglycosides have been utilized in several animal models to induce acute hearing loss, where deafness occurs due to cochlear hair cell loss in the typical basal-to-apical progression (Yang et al., 2015). Moreover, newborn mice treated with aminoglycosides exhibit cochlear inflammation and oxidative burst in the inner ear (Sun et al., 2014). Our study demonstrated that mice exposed to neomycin exhibit hearing loss, as indicated by elevated auditory brain stem responses (ABR) thresholds, and lead to cochlear inflammation, as indicated by spiral ganglia macrophage activation. As evident from the ABR thresholds, 6SL treatment prevented hearing impairment at lower frequencies, although higher frequency cochlear regions remained vulnerable to damage. Furthermore, 6SL treatment reduced cochlear macrophage density and activation, in addition to the expression of pro-inflammatory cytokines, suggesting an anti-inflammatory effect. This well aligns with the aminoglycoside-induced cochlear damage proposed mechanism, where hearing loss progresses from the higher frequency basal cochlear regions, and spreads apically, to the lower frequency regions (Huth et al., 2011). The ameliorated hearing loss we observed in our study was limited to the lower frequencies, possibly because the basal region of the higher frequencies was too severely damaged to be prevented by therapeutic intervention. One limitation of our study was the inability to fully interpret the ABR wave I amplitude data, as we could not quantify cochlear hair cells due to insufficient histological preservation of the complete hair cell lining from the basal to the apical regions. *In vitro*, 6SL demonstrated anti-inflammatory and anti-oxidative effects on human macrophages and showed neuroprotective effects against macrophage-mediated neurite loss. In conclusion, our findings support the therapeutic potential of 6SL

in ameliorating neomycin-induced hearing loss, with the stipulation that its efficacy possibly depends on the severity of cochlear damage and the timing of intervention.

4.2 Neuroprotective role of SIGLEC-11

The second study investigated the role of the SIGLEC-11 receptor in microglial cells, particularly in the context of normal brain aging and neuroprotection. Brain aging is a long-lasting process characterized by persistent inflammation, microglial activation, and oxidative stress, all of which can contribute to neuronal damage and loss (Lee et al., 2022; Luo et al., 2010). SIGLEC-11 is a human-specific microglial cell surface receptor that binds sialylated glycomolecules, exerting inhibitory effects on microglial inflammatory signaling (Angata et al., 2002; Khan et al., 2020; Wang et al., 2011, 2010). Although its precise role in neurodegeneration is yet to be better understood, *SIGLEC11* gene has been highlighted as a key microglial gene with a potential link to Alzheimer's disease (Bellenguez et al., 2022). Our study investigated humanized Siglec-11 transgenic (tg) mice (Karlstetter et al., 2017; Liao et al., 2021), revealing that these mice exhibit less age-related microglial activation and neuronal degeneration compared to wild-type (WT) controls. In particular, aged Siglec-11 tg mice showed reduced microglial density, clustering, and phagocytic activation in the hippocampus and substantia nigra. Additionally, Siglec-11 tg mice exhibited preserved dopaminergic neurons in the substantia nigra, indicating neuroprotection. Gene expression analyses demonstrated that Siglec-11 tg mice had suppressed inflammatory, oxidative stress, and complement system pathways at both 6 and 24 months of age, with significant reductions in pro-inflammatory cytokines and oxidative stress markers, which are typically elevated in aging brains (Bishop et al., 2010). While the observed reduction in inflammatory, complement, and oxidative stress markers in Siglec-11 tg mice may be the result of decreased microglial numbers, this decrease in inflammation, coupled with reduced microglia, is associated with a protective phenotype, as evidenced by the preserved neuronal density in the substantia nigra. A limitation to this study was performing a whole-genome transcriptome, which could explain the discrepancy we saw in the enriched pathways across the age groups. In future, it could be beneficial to perform single-cell transcriptomic analysis of microglia from various age groups at the same time point to better capture age-related changes in microglial pathways. The current findings point to a crucial role for SIGLEC-11 in mitigating age-

related neuroinflammation and oxidative stress, potentially offering a therapeutic target for neurodegenerative diseases.

4.3 Reduced sialylation impact on retinal degeneration

The third study utilized heterozygous Gne-deficient mice (Gne+/−), which have an overall reduction of membrane-bound sialic acid, and serve as a model for aging-related changes in the central nervous system (CNS), to investigate the effect of decreased sialylation on the retina (Gagiannis et al., 2007; Klaus et al., 2020). We hypothesized that the reduced sialylation level could lead to retinal microglial overactivation, a phenotype associated with several retinal diseases, such as age-related macular degeneration (AMD) (Bosco et al., 2015; Gupta et al., 2003; Karlstetter et al., 2015). In line with previous studies of sialylation deficits in other organs and brain tissue (Gagiannis et al., 2007; Klaus et al., 2020), our results showed a reduction in sialylation markers, such as polysialic acid and ganglioside-bound sialic acid, in the retinas of Gne+/- mice, observed primarily at 9 months of age. Despite no apparent differences in retinal microglial density, morphology, or distribution, 9 and 12 months old Gne+/- mice showed heightened retinal microglial activation in comparison to WT mice, indicated by increased CD68 protein staining expression. This was coupled with elevated gene expression of the pro-inflammatory cytokine *Il-1β* in 9 months old Gne+/- mice, further supporting the idea that hyposialylation triggers inflammatory responses within the retina, as multiple studies demonstrated the upregulation of *Il-1β* due to retinal damage (Balser et al., 2019; Jiao et al., 2015). Moreover, our data demonstrated an upregulation of the glial fibrillary acid protein (GFAP) gliosis marker expression in 9 months old Gne+/- mice retina, indicating possible astrocytic and Müller cell to decreased sialylation. Although the ganglion cell numbers and outer nuclear layer remained unaffected, there was a notable loss of rod bipolar cells in 12 months old Gne+/− mice, which could reflect sialylation-mediated vulnerability to neurodegeneration. In line with previous studies that showed complement dependent phagocytosis of desialylated neurons (Linnartz-Gerlach et al., 2016; Linnartz et al., 2012), we observed increased gene transcripts of complement factor 3 and 4 (C3 & C4). Interestingly, RNA sequencing of Gne+/- mice retina revealed an upregulation of the *Cryab* and *Crybb1* genes, compared to WT mice. Both genes are linked to congenital cataracts (Cohen et al., 2007; Cui et al., 2017; Willoughby et al., 2005), while Cryab also plays a

key protective role against apoptosis and inflammation in the nervous system, including regulating macrophage activity and preventing inflammatory retinal microglial activation (Hagen et al., 2024; Lim et al., 2021; Wang et al., 2021; Zhang et al., 2019). Crossing Gne+/- mice with complement C3-deficient mice (Gne+/-C3-/-) prevented the inflammatory profile we observed in Gne+/- mice retina, as indicated by reverting the elevation of Iba1 and CD68 microglial markers, and reverting the *Il-1β* and *C4* transcript levels, back to levels compared to WT mice. Moreover, the loss of rod bipolar cells observed in Gne+/- was prevented in complement C3 knock-out mice. Our gene set enrichment analysis (GSEA) revealed several enriched pathways that has been linked to AMD, including UV response, epithelial-mesenchymal transition, and p53 pathway (Fietz et al., 2023; Sui et al., 2013; Yao et al., 2022). Although the mild hyposialylation seen in Gne+/- mice better reflects the natural course of aging, a more severe reduction in sialylation, possibly achieved by a complete conditional retinal *Gne* knock-out, could help deeper unravel the effects of hyposialylation on retinal inflammation and neurodegeneration. Taken together, our data indicate a critical role of the compliment system in mediating the effects of reduced sialylation on retinal inflammation and the loss of rod bipolar cells.

4.4 References

Angata, T., Kerr, S. C., Greaves, D. R., Varki, N. M., Crocker, P. R., & Varki, A. (2002). Cloning and characterization of human Siglec-11. A recently evolved signaling molecule that can interact with SHP-1 and SHP-2 and is expressed by tissue macrophages, including brain microglia. *The Journal of Biological Chemistry*, *277*(27), 24466–24474. https://doi.org/10.1074/JBC.M202833200

Balser, C., Wolf, A., Herb, M., & Langmann, T. (2019). Co-inhibition of PGF and VEGF blocks their expression in mononuclear phagocytes and limits neovascularization and leakage in the murine retina. *Journal of Neuroinflammation*, *16*(1). https://doi.org/10.1186/S12974-019-1419-2

Bellenguez, C., Küçükali, F., Jansen, I. E., Kleineidam, L., Moreno-Grau, S., Amin, N., Naj, A. C., Campos-Martin, R., Grenier-Boley, B., Andrade, V., Holmans, P. A., Boland, A., Damotte, V., van der Lee, S. J., Costa, M. R., Kuulasmaa, T., Yang, Q., de Rojas, I., Bis, J. C., … Lambert, J. C. (2022). New insights into the genetic etiology of

Alzheimer's disease and related dementias. *Nature Genetics*, *54*(4), 412. https://doi.org/10.1038/S41588-022-01024-Z

Bishop, N. A., Lu, T., & Yankner, B. A. (2010). Neural mechanisms of ageing and cognitive decline. *Nature*, *464*(7288), 529–535. https://doi.org/10.1038/NATURE08983

Bosco, A., Romero, C. O., Breen, K. T., Chagovetz, A. A., Steele, M. R., Ambati, B. K., & Vetter, M. L. (2015). Neurodegeneration severity can be predicted from early microglia alterations monitored in vivo in a mouse model of chronic glaucoma. *DMM Disease Models and Mechanisms*, *8*(5), 443–455. https://doi.org/10.1242/DMM.018788/-/DC1

Cohen, D., Bar-Yosef, U., Levy, J., Gradstein, L., Belfair, N., Ofir, R., Joshua, S., Lifshitz, T., Carmi, R., & Birk, O. S. (2007). Homozygous CRYBB1 deletion mutation underlies autosomal recessive congenital cataract. *Investigative Ophthalmology & Visual Science*, *48*(5), 2208–2213. https://doi.org/10.1167/IOVS.06-1019

Cui, X. J., Lv, F. Y., Li, F. H., Zeng, K., & Abdelrahman, K. A. (2017). Correlations of single nucleotide polymorphisms of CRYAA and CRYAB genes with the risk and clinicopathological features of children suffering from congenital cataract. *Medicine*, *96*(25). https://doi.org/10.1097/MD.0000000000007158

Fietz, A., Corsi, F., Hurst, J., & Schnichels, S. (2023). Blue Light Damage and p53: Unravelling the Role of p53 in Oxidative-Stress-Induced Retinal Apoptosis. *Antioxidants (Basel, Switzerland)*, *12*(12). https://doi.org/10.3390/ANTIOX12122072

Gagiannis, D., Orthmann, A., Danßmann, I., Schwarzkopf, M., Weidemann, W., & Horstkorte, R. (2007). Reduced sialylation status in UDP-N-acetylglucosamine-2-epimerase/N- acetylmannosamine kinase (GNE)-deficient mice. *Glycoconjugate Journal*, *24*(2–3), 125–130. https://doi.org/10.1007/s10719-006-9019-7

Gupta, N., Brown, K. E., & Milam, A. H. (2003). Activated microglia in human retinitis pigmentosa, late-onset retinal degeneration, and age-related macular degeneration. *Experimental Eye Research*, *76*(4), 463–471. https://doi.org/10.1016/S0014-4835(02)00332-9

Hagen, K. M., Gordon, P., Frederick, A., Palmer, A. L., Edalat, P., Zonta, Y. R., Scott, L., Flancia, M., Reid, J. K., Joel, M., & Ousman, S. S. (2024). CRYAB plays a role in terminating the presence of pro-inflammatory macrophages in the older, injured mouse peripheral nervous system. *Neurobiology of Aging*, *133*, 1–15.

https://doi.org/10.1016/J.NEUROBIOLAGING.2023.10.004

Huth, M. E., Ricci, A. J., & Cheng, A. G. (2011). Mechanisms of aminoglycoside ototoxicity and targets of hair cell protection. *International Journal of Otolaryngology*, *2011*, 1–19. https://doi.org/10.1155/2011/937861

Jiao, H., Natoli, R., Valter, K., Provis, J. M., & Rutar, M. (2015). Spatiotemporal Cadence of Macrophage Polarisation in a Model of Light-Induced Retinal Degeneration. *PLoS ONE*, *10*(12), e0143952. https://doi.org/10.1371/JOURNAL.PONE.0143952

Karlstetter, M., Kopatz, J., Aslanidis, A., Shahraz, A., Caramoy, A., Linnartz-Gerlach, B., Lin, Y., Lückoff, A., Fauser, S., Düker, K., Claude, J., Wang, Y., Ackermann, J., Schmidt, T., Hornung, V., Skerka, C., Langmann, T., & Neumann, H. (2017). Polysialic acid blocks mononuclear phagocyte reactivity, inhibits complement activation, and protects from vascular damage in the retina. *EMBO Molecular Medicine*, *9*(2), 154–166. https://doi.org/10.15252/emmm.201606627

Karlstetter, M., Scholz, R., Rutar, M., Wong, W. T., Provis, J. M., & Langmann, T. (2015). Retinal microglia: just bystander or target for therapy? *Progress in Retinal and Eye Research*, *45*, 30–57. https://doi.org/10.1016/J.PRETEYERES.2014.11.004

Khan, N., Kim, S. K., Gagneux, P., Dugan, L. L., & Varki, A. (2020). Maximum reproductive lifespan correlates with CD33rSIGLEC gene number: Implications for NADPH oxidase-derived reactive oxygen species in aging. *FASEB Journal : Official Publication of the Federation of American Societies for Experimental Biology*, *34*(2), 1928–1938. https://doi.org/10.1096/FJ.201902116R

Klaus, C., Hansen, J. N., Ginolhac, A., Gérard, D., Gnanapragassam, V. S., Horstkorte, R., Rossdam, C., Buettner, F. F. R., Sauter, T., Sinkkonen, L., Neumann, H., & Linnartz-Gerlach, B. (2020). Reduced sialylation triggers homeostatic synapse and neuronal loss in middle-aged mice. *Neurobiology of Aging*, *88*, 91–107. https://doi.org/10.1016/J.NEUROBIOLAGING.2020.01.008

Krause, K. M., Serio, A. W., Kane, T. R., & Connolly, L. E. (2016). Aminoglycosides: An Overview. *Cold Spring Harbor Perspectives in Medicine*, *6*(6). https://doi.org/10.1101/CSHPERSPECT.A027029

Lee, J., & Kim, H. J. (2022). Normal Aging Induces Changes in the Brain and Neurodegeneration Progress: Review of the Structural, Biochemical, Metabolic, Cellular, and Molecular Changes. *Frontiers in Aging Neuroscience*, *14*.

https://doi.org/10.3389/FNAGI.2022.931536

Lee, M. Y., & Park, Y.-H. (2018). Potential of Gene and Cell Therapy for Inner Ear Hair Cells. *BioMed Research International*, *2018*, 1–11. https://doi.org/10.1155/2018/8137614

Liao, H., Winkler, J., Wißfeld, J., Shahraz, A., Klaus, C., & Neumann, H. (2021). Low molecular weight polysialic acid prevents lipopolysaccharide-induced inflammatory dopaminergic neurodegeneration in humanized SIGLEC11 transgenic mice. *Glia*, *69*(12), 2845–2862. https://doi.org/10.1002/GLIA.24073

Lim, E. M. F., Hoghooghi, V., Hagen, K. M., Kapoor, K., Frederick, A., Finlay, T. M., & Ousman, S. S. (2021). Presence and activation of pro-inflammatory macrophages are associated with CRYAB expression in vitro and after peripheral nerve injury. *Journal of Neuroinflammation*, *18*(1). https://doi.org/10.1186/S12974-021-02108-Z

Linnartz-Gerlach, B., Schuy, C., Shahraz, A., Tenner, A. J., & Neumann, H. (2016). Sialylation of neurites inhibits complement-mediated macrophage removal in a human macrophage-neuron Co-Culture System. *GLIA*, *64*(1), 35–47. https://doi.org/10.1002/glia.22901

Linnartz, B., Kopatz, J., Tenner, A. J., & Neumann, H. (2012). Sialic acid on the neuronal glycocalyx prevents complement c1 binding and complement receptor-3-mediated removal by microglia. *Journal of Neuroscience*, *32*(3), 946–952. https://doi.org/10.1523/JNEUROSCI.3830-11.2012

Luo, X. G., Ding, J. Q., & Chen, S. Di. (2010). Microglia in the aging brain: relevance to neurodegeneration. *Molecular Neurodegeneration*, *5*(1). https://doi.org/10.1186/1750-1326-5-12

Sui, G. Y., Liu, G. C., Liu, G. Y., Gao, Y. Y., Deng, Y., Wang, W. Y., Tong, S. H., & Wang, L. (2013). Is sunlight exposure a risk factor for age-related macular degeneration? A systematic review and meta-analysis. *The British Journal of Ophthalmology*, *97*(4), 389–394. https://doi.org/10.1136/BJOPHTHALMOL-2012-302281

Sun, S., Yu, H., Yu, H., Honglin, M., Ni, W., Zhang, Y., Guo, L., He, Y., Xue, Z., Ni, Y., Li, J., Feng, Y., Chen, Y., Shao, R., Chai, R., & Li, H. (2014). Inhibition of the Activation and Recruitment of Microglia-Like Cells Protects Against Neomycin-Induced Ototoxicity. *Molecular Neurobiology*, *51*(1), 252–267. https://doi.org/10.1007/s12035-014-8712-y

Wang, F., Jiang, Z., Lou, B., Duan, F., Qiu, S., Cheng, Z., Ma, X., Yang, Y., & Lin, X. (2021). αB-Crystallin Alleviates Endotoxin-Induced Retinal Inflammation and Inhibits Microglial Activation and Autophagy. *Frontiers in Immunology*, *12*. https://doi.org/10.3389/FIMMU.2021.641999

Wang, X., Chow, R., Deng, L., Anderson, D., Weidner, N., Godwin, A. K., Bewtra, C., Zlotnik, A., Bui, J., Varki, A., & Varki, N. (2011). Expression of Siglec-11 by human and chimpanzee ovarian stromal cells, with uniquely human ligands: implications for human ovarian physiology and pathology. *Glycobiology*, *21*(8), 1038–1048. https://doi.org/10.1093/GLYCOB/CWR039

Wang, Y., & Neumann, H. (2010). Alleviation of neurotoxicity by microglial human Siglec-11. *The Journal of Neuroscience : The Official Journal of the Society for Neuroscience*, *30*(9), 3482–3488. https://doi.org/10.1523/JNEUROSCI.3940-09.2010

Willoughby, C. E., Shafiq, A., Ferrini, W., Chan, L. L. Y., Billingsley, G., Priston, M., Mok, C., Chandna, A., Kaye, S., & Héon, E. (2005). CRYBB1 mutation associated with congenital cataract and microcornea. *Molecular Vision*, *11*, 587–593. https://europepmc.org/article/med/16110300

Yang, C.-H., Schrepfer, T., Schacht, J., Coffin, A. B., & Steyger, P. S. (2015). *Age-related hearing impairment and the triad of acquired hearing loss*. https://doi.org/10.3389/fncel.2015.00276

Yao, P. L., Parmar, V. M., Choudhary, M., & Malek, G. (2022). NURR1 expression regulates retinal pigment epithelial-mesenchymal transition and age-related macular degeneration phenotypes. *Proceedings of the National Academy of Sciences of the United States of America*, *119*(28). https://doi.org/10.1073/PNAS.2202256119

Zhang, J. F., Liu, J., Wu, J. L., Li, W. F., Chen, Z. W., & Yang, L. S. (2019). Progression of the role of CRYAB in signaling pathways and cancers. *OncoTargets and Therapy*, *12*, 4129–4139. https://doi.org/10.2147/OTT.S201799

5. Acknowledgement

I would like to thank Professor Harald Neumann for the opportunity to conduct this research, and for his continuous support and guidance throughout this journey. I would also like to thank Dr. Christine Klaus, Dr. Negin Afrang, and Dr. German Cuevas-Rios for their continual support and contributions throughout my PhD, as well as all current and past members of AG Neumann, without whom this work would not have been possible. Finally, I would like to convey my heartfelt thanks to my family and friends for their unconditional support and encouragement.